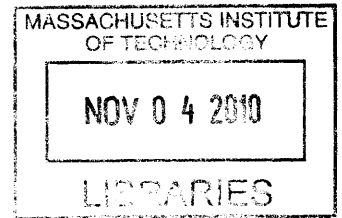


# Analysis and Design of an In-Pipe System for Water Leak Detection

by

Dimitris M. Chatzigeorgiou



Submitted to the Department of Mechanical Engineering  
in partial fulfillment of the requirements for the degree of

**ARCHIVES**

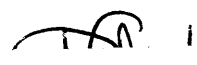
Master of Science in Mechanical Engineering

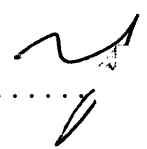

at the

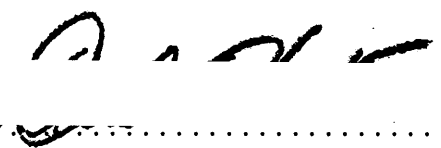
MASSACHUSETTS INSTITUTE OF TECHNOLOGY

September 2010

© Massachusetts Institute of Technology 2010. All rights reserved.

Author .....   
Department of Mechanical Engineering  
August 27, 2010

Certified by .....  .....   
Kamal Youcef-Toumi  
Professor of Mechanical Engineering  
Thesis Supervisor

Accepted by .....   
David E. Hardt  
Chairman, Department Committee on Graduate Students



# Analysis and Design of an In-Pipe System for Water Leak Detection

by

Dimitris M. Chatzigeorgiou

Submitted to the Department of Mechanical Engineering  
on August 27, 2010, in partial fulfillment of the  
requirements for the degree of  
Master of Science in Mechanical Engineering

## Abstract

Leaks are a major factor for unaccounted water losses in almost every water distribution network. Pipeline leak may result, for example, from bad workmanship or from any destructive cause, due to sudden changes of pressure, corrosion, cracks, defects in pipes or lack of maintenance. The problem of leak becomes even more serious when it is concerned with the vital supply of fresh water to the community. In addition to waste of resources, contaminants may infiltrate into the water supply. The possibility of environmental health disasters due to delay in detection of water pipeline leaks have spurred research into the development of methods for pipeline leak and contamination detection.

This thesis is on the analysis and design of a *floating mobile sensor for leak detection in water distribution pipes*. This work covers the study of two modules, namely a "*floating body*" along with its "*sensing module*".

The *Mobility Module* or the floating body was carefully studied and designed using advanced CFD techniques to make the body as non-invasive to the flow as possible and to avoid signal corruption. In addition, experiments were carried out to investigate the effectiveness of using in-pipe measurements for leak detection in plastic pipes. Specifically, acoustic signals due to simulated leaks were measured and studied for designing a detection system to be deployed inside water networks of 100mm pipe size.

Thesis Supervisor: Kamal Youcef-Toumi  
Title: Professor of Mechanical Engineering





## Acknowledgments

At this point I would like to thank my advisor, Professor Kamal Youcef-Toumi, for his valuable advice and patience throughout the duration of this work. His energy and enthusiasm in research had motivated me and made my research life smooth and exciting. I would also like to thank him for giving me the chance to participate in three “*Clean Water and Clean Energy*” workshops, one of them held in Dhahran, Saudi Arabia and was a wonderful experience.

Secondly, I wish to thank all my lab buddies, Dan Burns, Mauricio Gutierrez, Kwang Yong Lim, Vijay Shilpiekandula, and Sang-il Lee for making me feel comfortable and part of the group from day one. Additionally I would like to thank Prof. Sanjay Sarma, Dr. Atia Khalifa, Dr. Ajay Deshpande, Sumeet Kumar and Dr. Stephen Ho for their help and great advice throughout this work.

Next, I would like to thank my good friends here in Boston, who stood by me in good and bad during those two years at MIT and gave meaning to my after-lab-life every single day from day one to day seven-hundred-twenty-nine. Buddies, I wouldn't have managed to finish this work without you.

My deepest gratitude goes to my family for their unflagging love and support throughout my life; this thesis is simply impossible without them. Miss you all back there in Greece.

I would also like to thank the Onassis Public Benefit Foundation for their support and for believing in me from the very beginning of this work.

I would finally like to thank the King Fahd University of Petroleum and Minerals (KFUPM) in Dhahran, Saudi Arabia, for funding the research reported in this thesis through the *Center for Clean Water and Clean Energy* at MIT and KFUPM.

This thesis is dedicated with all my heart to my newborn niece. She is now six months old and is adorable. I had the chance to meet her last month in Greece. My whole family is excited about her. I am looking forward to seeing her again...



# Contents

<b>1</b>	<b>Introduction</b>	<b>19</b>
1.1	Problem Definition . . . . .	19
1.2	Motivation . . . . .	19
1.3	Thesis Objectives . . . . .	20
1.4	Structure of the Thesis . . . . .	22
<b>2</b>	<b>Background</b>	<b>23</b>
2.1	Introduction . . . . .	23
2.2	Water Losses . . . . .	23
2.3	Leak Detection Techniques . . . . .	24
2.3.1	Overview . . . . .	24
2.3.2	Summary and Evaluation . . . . .	30
2.4	Inspection Robots . . . . .	32
2.5	System Functional Requirements . . . . .	36
2.6	Chapter Summary . . . . .	37
<b>3</b>	<b>Sensing Module - Instrumentation</b>	<b>39</b>
3.1	Introduction . . . . .	39
3.2	Sensor Overview and Characteristics . . . . .	39
3.2.1	Hydrophone . . . . .	39
3.2.2	Dynamic Pressure Sensor (DPS) . . . . .	42
3.3	Instrumentation Characteristics . . . . .	42
3.3.1	Amplifier . . . . .	42

3.3.2	Data Acquisition (DAQ) Hardware . . . . .	44
3.3.3	Connection Overview . . . . .	46
3.3.4	Data Acquisition (DAQ) Software . . . . .	46
3.4	Chapter Summary . . . . .	47
<b>4</b>	<b>Sensing Module - Experimentation</b>	<b>49</b>
4.1	Introduction . . . . .	49
4.2	Experimental Setup Overview . . . . .	49
4.3	Simulating Leaks . . . . .	51
4.4	Experimentation Objectives . . . . .	53
4.5	Chapter Summary . . . . .	55
<b>5</b>	<b>Sensing Module - Experimental Results</b>	<b>57</b>
5.1	Introduction . . . . .	57
5.2	Hydrophone vs DPS . . . . .	57
5.3	Effect of Leak Flow Rate . . . . .	59
5.3.1	Leak as a PVC Valve . . . . .	62
5.3.2	Leak as a Circular Hole . . . . .	62
5.4	Effect of Medium Surrounding Pipe . . . . .	67
5.5	Effect of Pipe Flow . . . . .	70
5.6	Effect of Sensor Position . . . . .	71
5.7	Chapter Summary . . . . .	76
<b>6</b>	<b>Mobility Module - Design Characteristics</b>	<b>77</b>
6.1	Introduction . . . . .	77
6.2	Functional Requirements . . . . .	77
6.3	Mobility Module Design . . . . .	78
6.3.1	Design Overview . . . . .	78
6.3.2	Earlier Versions Overview . . . . .	81
6.4	Chapter Summary . . . . .	82

<b>7</b>	<b>Mobility Module - Analysis</b>	<b>89</b>
7.1	Introduction . . . . .	89
7.2	Analysis . . . . .	89
7.2.1	Size Limitations . . . . .	89
7.2.2	Degrees of Freedom . . . . .	91
7.2.3	Motion . . . . .	92
7.3	Flow Considerations in Design (CFD) . . . . .	94
7.3.1	CFD Meshing . . . . .	96
7.3.2	CFD Problem Setup . . . . .	98
7.3.3	CFD Results . . . . .	98
7.4	Chapter Summary . . . . .	100
<b>8</b>	<b>Mobility Module - Experimental Results</b>	<b>103</b>
8.1	Introduction . . . . .	103
8.2	Stability . . . . .	103
8.3	Floating . . . . .	105
8.4	Chapter Summary . . . . .	105
<b>9</b>	<b>Conclusions and Closing Remarks</b>	<b>111</b>
9.1	Thesis Summary and Contribution . . . . .	111
9.2	Recommendations for Future Work . . . . .	113
<b>A</b>	<b>LabVIEW Code</b>	<b>115</b>
<b>B</b>	<b>MATLAB Code - Signal Postprocessing</b>	<b>123</b>
<b>C</b>	<b>MATLAB Code - Filters</b>	<b>129</b>



# List of Figures

1-1	Schematic of the mobile floating sensor concept. The pipeline is buried underground and the “yellow” mobile sensor is floating, while at the same time communicating with the “outer world” and sensing for leaks.	21
1-2	The four different subsystems of the floating mobile sensor.	22
2-1	Leak detection in water pipelines using the <i>Sewerin Aquaphone A100</i> . [Picture from <a href="http://www.sewerin.com">www.sewerin.com</a> ]	26
2-2	Typical Leak Noise Correlators. Sensor A, Sensor B and Correlator device. [Courtesy of Dantec Measurement Technology]	27
2-3	Tracer Gas technique sketch.	28
2-4	The <i>RADIODETECTION RD1000</i> Portable Ground Penetrating Radar System.	29
2-5	Some state-of-the-art leak inspection robots.	33
2-6	Top Left: Un-tethered Autonomous <i>Kurt I</i> , Top Right: <i>CISBOT</i> , Bottom: <i>GRISLEE</i>	33
2-7	A typical leak detection survey with the <i>Smartball</i> .	35
2-8	Sketch of the <i>Sahara</i> leak detection system.	35
3-1	The hydrophone 8103 from B&K. Picture taken from <a href="http://www.bksv.com">http://www.bksv.com</a>	40
3-2	The receiving frequency response of the hydrophone sensor 8103 from B&K. Graph taken from <a href="http://www.bksv.com">http://www.bksv.com</a>	41
3-3	The <i>WB-1372 DeltaTron Power Supply</i> from B&K. Picture taken from <a href="http://www.bksv.com">http://www.bksv.com</a>	41

3-4	The <i>Charge to DeltaTron</i> converter type 2647 from <i>B&amp;K</i> . Picture taken from <a href="http://www.bksv.com">http://www.bksv.com</a> . . . . .	41
3-5	The Dynamic Pressure Sensor 106B52 from <i>PCB Piezotronics</i> . Picture taken from <a href="http://www.pcb.com">http://www.pcb.com</a> . . . . .	42
3-6	A sketch describing all the subsystems within the dynamic pressure sensor 106B52 from PCB Piezotronics. Picture taken from <a href="http://www.pcb.com">http://www.pcb.com</a>	43
3-7	The 482A21 <i>Sensor Signal Conditioner</i> from <i>PCB Piezotronics</i> . Picture taken from <a href="http://www.pcb.com">http://www.pcb.com</a> . . . . .	43
3-8	The SR560 amplifier from <i>Stanford Research Systems</i> . . . . .	44
3-9	The <i>National Instruments</i> 9234 24bit analog input module. Picture taken from <a href="http://www.ni.com">http://www.ni.com</a> . . . . .	45
3-10	The <i>National Instruments</i> 9113 chassis. Picture taken from <a href="http://www.ni.com">http://www.ni.com</a>	45
3-11	The <i>National Instruments</i> 9022 real-time controller. Picture taken from <a href="http://www.ni.com">http://www.ni.com</a> . . . . .	45
3-12	The user interface in LabVIEW for DAQ. . . . .	47
4-1	Test loop in the lab consisting mostly of 100mm ID pipe sections . . .	50
4-2	The solid model of the test loop. . . . .	50
4-3	The solid model of the sensor-holder used to hold and move the hydrophone along the pipe. The sensor holder part is sketched in brown color. . . . .	51
4-4	The actual sensor-holder while moving the hydrophone along the pipe. Magnets on both sides are used to move the sensor. . . . .	52
4-5	The DPS is mounted flush on the pipe body. The hydrophone is mounted on the sensor holder and is moving with the use of magnets from the outside. The 1/8" valve simulating a leak is also shown in the picture. . . . .	52
4-6	The 1/8" valve simulating a leak. . . . .	53
4-7	The circular hole simulating a leak. . . . .	54



5-1 Signals captured by [a] DPS and [b] hydrophone for the case of a 10lit/min leak. Pressure in the pipe is 45psi. The time signal as well as the frequency spectrum of each case are shown. . . . . 58

5-2 Signals captured by [a] DPS and [b] hydrophone for the case of a 14lit/min leak. Pressure in the pipe is 38psi. The time signal as well as the frequency spectrum of each case are shown. . . . . 60

5-3 Signals captured by [a] DPS and [b] hydrophone for the case of a 6lit/min leak. Pressure in the pipe is 50psi. The time signal as well as the frequency spectrum of each case are shown. . . . . 61

5-4 The frequency spectra for the signals captured by the DPS for different leak flow rates. The sensor is placed at the leak position. . . . . 63

5-5 The frequency spectra for the signals captured by the hydrophone for different leak flow rates. The sensor is placed at the leak position. . . 63

5-6 Leak signals for 1mm up to 6mm leak sizes. The frequency spectrum for each case is presented. Leak is open to air. . . . . 65

5-7 The test section for the “sand” experiments. A tank filled with sand was used. Leak jet was hitting the sand at the bottom. . . . . 68

5-8 The frequency spectra of the leak signals captured in air/sand/water. Green/Air, Orange/Sand and Red/Water. Power of the signal in sand and water is more than the same power for the signal in air. Moreover the frequency spectra is “wider” for those two cases in comparison to the “air experiments”. . . . . 68

5-9 Effect of having pipe flow on frequency spectrum - sensor used: hydrophone . . . . . 72

5-10 Effect of pipe flow rate on leak signal for constant leak flow rate of 8lit/min - sensor used: DPS . . . . . 73

5-11 Effect of pipe flow rate on captured signal; pipe flow 8lit/min - sensor used: DPS . . . . . 73

5-12 Calculated power of leak signal with and without pipe flow - sensor used: hydrophone . . . . . 74

5-13	Frequency spectra for signals captured for $4mm$ leak; Pipe is surrounded by water and the hydrophone was placed at different positions upstream and downstream of the leak location. . . . .	75
6-1	The design of the mobility module. [Left] Front View. [Right] Side view. . . . .	79
6-2	A zoom in the mobility module's solid model. Explanation on different parts is sketched. . . . .	79
6-3	The 3D solid model of the mobility module. Model is shown inside a $100mm$ pipe section. . . . .	80
6-4	The 3D printed prototype of the leg. Material is ABS plastic. . . . .	82
6-5	The 3D printed prototype of the upper part of the external hull. Material is ABS plastic. . . . .	83
6-6	The 3D printed prototype of the lower part of the external hull. Material is ABS plastic. . . . .	84
6-7	The 3D printed parts of the mobility module. Material is ABS plastic. . . . .	85
6-8	The assembled mobility module. . . . .	85
6-9	The prototype # 3. . . . .	86
6-10	The prototype # 4. The module inside the pipe is shown in the left figure. The details of the leg are presented in the right figure. . . . .	87
6-11	The prototype # 6. . . . .	87
7-1	A 2D sketch of a cylindrical mobility module inside a bended pipe. . . . .	90
7-2	Maximum allowed thickness $H_{max}$ of the mobility module for a given length $L$ . . . . .	91
7-3	The design of the mobility module. [Left] Front view. [Right] Side view. . . . .	92
7-4	Body is floating within the pipe with speed $V_m$ , while water speed is $V_w$ . . . . .	93
7-5	Body can be considered to be stationary in this case and water is flowing at a lower speed, namely $V_{rel} = V_w - V_m$ . Notice that in this frame of reference the pipe wall is also moving with $V_m$ . . . . .	93

7-6	The response of the system's velocity for the following values: $V_w = 1m/s$ , $m = 1kg$ , $C_D = 0.4$ , $A = 0.0165m^2$ , $\rho = 998kg/m^3$ and the initial condition is: $V_m(0) = 0m/s$ . The response is presented for different values of $F_{legs}$ varying from 0.5 to 3N. Notice that by applying larger friction forces through the legs, the module travels with smaller speeds and can even "anchor" itself ( $V_m = 0$ ). . . . .	95
7-7	The mesh used for the CFD analysis on the mobility module. The mesh on the inlet, outlet sections as well as the floating body is presented. .	97
7-8	Mesh of the fluidic section. . . . .	97
7-9	CFD results for velocity vectors around the floating body. Simulation was done under $V_{rel} = 2 m/s$ (direction from right to left (see Fig. 7-5) and $P = 200kPa$ . No flow separation on the trailing edge. . . . .	100
7-10	CFD results for static pressure distribution around the floating body. Simulation was done under $V_{rel} = 2 m/s$ (direction from right to left (see Fig. 7-5) and $P = 200kPa$ . Placing the sensor nose at the trailing edge seems to be the optimal solution. . . . .	101
7-11	CFD results for static pressure distribution around the floating body. Simulation was done under $V_{rel} = 0.01 m/s$ (direction from right to left (see Fig. 7-5) and $P = 200kPa$ . Almost no pressure variation around the body. . . . .	101
8-1	The mobility module prototype inside a 100mm pipe section. The module is stable, due to the support provided by the legs. . . . .	104
8-2	The mobility module floating through section A of the experimental setup. The six photos ([a]-[f]) show the motion of the mobility module from left to right. . . . .	106
8-3	The mobility module floating through section B of the experimental setup. The six photos ([a]-[f]) show the motion of the mobility module from left to right. . . . .	107

8-4	The mobility module floating through the right branch of section C of the experimental setup. The six photos ([a]-[f]) show the motion of the mobility module from right to left. . . . .	108
8-5	The mobility module floating through the left branch of section C of the experimental setup. The three photos ([f]-[h]) show the motion of the mobility module from right to left. . . . .	109
A-1	The front panel of the LabVIEW vi on the host PC. User can select “AC/DC/IEPE” in the “Input Configuration” box. One can also specify the sampling rate along with the number of scans per survey. A “Stop” button is available in order to be able to stop the procedure at any time. Various indicators including a “Waveform Graph” are also available for the user. . . . .	116
A-2	The front panel of the LabVIEW vi on the FPGA. User can select “AC/DC/IEPE” in the “Input Configuration” box. One can also specify the sampling rate. A “Start” and “Stop” button are available in this vi. Indicators including “Buffer Underflow” and “Buffer Overflow” are also shown in this interface. . . . .	116
A-3	The first part of the block diagram of the LabVIEW vi on the host PC. Notice that this part is connected to the second part shown in Fig. A-4.	117
A-4	The second part of the block diagram of the LabVIEW vi on the host PC. Notice that this part is connected to the first part shown in Fig. A-3. . . . .	118
A-5	The third part of the block diagram of the LabVIEW vi on the host PC. Notice that this part is not connected to neither of the first or second parts shown in Fig. A-3 and Fig. A-4. . . . .	119
A-6	The first part of the block diagram of the LabVIEW vi on the FPGA. Notice that this part is connected to the second part shown in Fig. A-7.	120
A-7	The second part of the block diagram of the LabVIEW vi on the FPGA. Notice that this part is connected to the first part shown in Fig. A-6.	121

# List of Tables

5.1	Summary of measured leak flow rate and line pressure for different leak sizes. . . . .	64
5.2	Signal Power calculation for each leak case. The ratio of each power relative to the no-leak case is also presented. Standard deviation is also presented to show repeatability of signal power. . . . .	66
5.3	Signal Power calculation for each leak case. The ratio of each power relative to the no-leak case is also presented. . . . .	69
5.4	Power calculations for various positions upstream, downstream and at leak position . . . . .	75
7.1	Mesh characteristics . . . . .	98
7.2	CFD Results for different values of relative velocity $V_{rel}$ . . . . .	99



# Chapter 1

## Introduction

### 1.1 Problem Definition

*“What is a leak and where does it come from?”* The unintentional release of fluid from a pipeline can be defined as **“leak”**. Pipeline leaks may result, for example, from bad workmanship or from any destructive cause, due to sudden changes of pressure, cracks, defects in pipes or lack of maintenance. Water transmission and distribution networks may deteriorate with time due to corrosion, soil movement, poor construction standards and sometimes also due to excessive traffic loads or even induced vibration.

### 1.2 Motivation

In most cases, the deleterious effects associated with the occurrence of leaks may present serious problems and, therefore, leaks must be quickly detected, located and repaired. The problem of leak even becomes more serious when it is concerned with the vital supply of fresh water to the community. In addition to waste of resources, contaminants may infiltrate into the water supply. The possibility of environmental health disasters due to delay in detection of water pipeline leaks have spurred research into the development of methods for pipeline leak and contamination detection.

Leaking in water networks has been a very significant problem worldwide, es-

pecially in countries where water is scarce. This issue has stimulated our interest towards *the design and development of a mobile floating sensor* for accurate leak detection in water distribution networks.

Leaks in water pipes create acoustic emissions, which can be sensed to identify and localize leaks. Leak noise correlators and listening devices have been reported in the literature as successful approaches to leak detection but they have practical limitations in terms of cost, sensitivity, reliability and scalability. A possible efficient solution is the development of an in-pipe traveling leak detection system. In-pipe sensing is more accurate and efficient, since the sensing element can get very close to the sound source. Currently in-pipe approaches have been limited to large leaks and larger diameter pipes.

The development of such a system requires clear understanding of acoustic signals generated from leaks and the study of the variation of the signal with different pipe loading conditions, leak sizes and surrounding media. It also requires a “careful” design of the system that will be traveling along the water pipes while at the same time carrying the corresponding sensors for leak detection.

### 1.3 Thesis Objectives

The objective of this thesis is the analysis and design of an appropriate floating mobile sensor for the in-pipe sensing of leaks within a water distribution network. In this thesis, this includes the study of two different things, namely the “*Sensing Module*” as well as the “*Mobility Module*”. A brief description of each one of them is presented in the following paragraphs. A schematic of the mobile floating sensor is presented in Fig. 1-1.

The autonomous in-pipe leak detection system consists of four different modules (Fig. 1-2); each of which has its own significance and role. A brief summary of each module is presented here. Note that this thesis focuses only on the first two modules.

- *Sensing Module*: The sensing module is the module in the system that is responsible for the sensing and identifying of leaks along a pipeline. The design



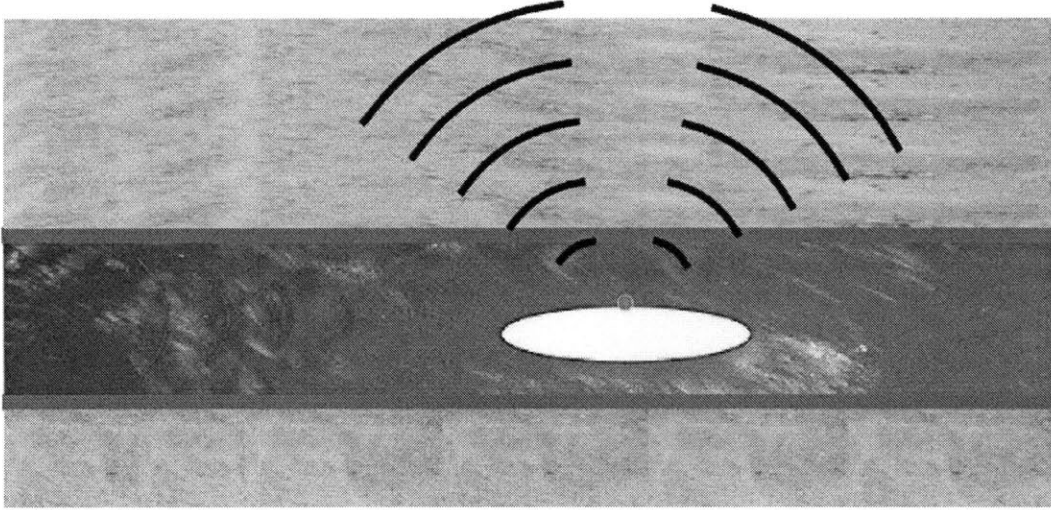


Figure 1-1: Schematic of the mobile floating sensor concept. The pipeline is buried underground and the “yellow” mobile sensor is floating, while at the same time communicating with the “outer world” and sensing for leaks.

of the sensing module requires the development of an appropriate technique for in-pipe leak detection. In addition the sensing module’s design part includes first of all understanding of the physical phenomenon of a leaking pipe and in addition to that the experimentation and selection of the appropriate sensors and instrumentation for accurate leak detection.

The sensing module may also carry other sensors as well, e.g. sensors for localization. This thesis is focused on the leak detection sensing element only.

- *Mobility Module:* The mobility module is the module in the system on which the sensor and all other instrumentation will be mounted. Moreover, the design of the “floating body” needs to be carefully studied because the deployment of a mobile sensor in a pipe network can be considered as an invasive detection technique. Thus, the body itself needs to be as less “invasive” to the flow field as possible to avoid signal corruption.
- *Communications Module:* This module is responsible for the communication between the in-pipe floating system and an above ground receiver. Experimental investigation of the signal propagation through different media (sand, clay, water, etc.) is needed to improve the design of this module. Discussion of this

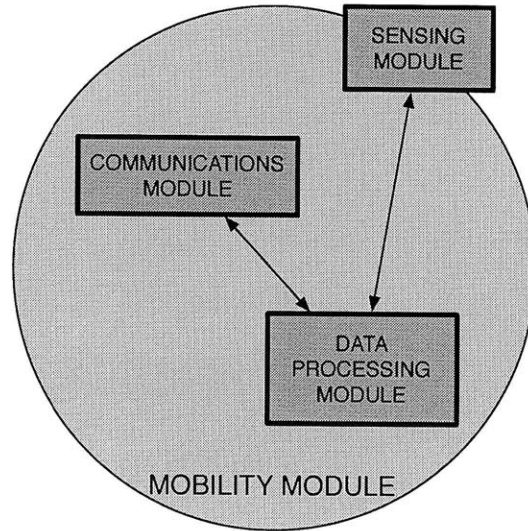


Figure 1-2: The four different subsystems of the floating mobile sensor.

module is outside the scope of this thesis.

- *Data Processing Module:* This module is responsible for post-processing the data stemming from the sensing module as well as the communications module. The miniaturized memory storage technology is currently available but the power requirements to process large amount of data are still challenging for the present design. Discussion of this module is outside the scope of this thesis.

## 1.4 Structure of the Thesis

Chapter 2 discusses the background and literature review of concurrent leak detection techniques. The sensing module is discussed in chapter 3, while the experimental setup that was designed and built is presented in chapter 4. Finally the experimental results and corresponding analyses for leak detection are discussed in chapter 5.

Next, chapter 6 presents the design of the mobility module and chapter 7 the corresponding analysis. Finally chapter 8 discusses the experiments conducted on the mobility module using the experimental setup described in chapter 4. Our conclusions and recommendations for future works are stated in chapter 9.

# Chapter 2

## Background

### 2.1 Introduction

This chapter discusses the state-of-the-art leak detection methods and robotic devices. Those different techniques are listed and evaluated as per efficiency and limitations. The most critical functional requirements of a “floating mobile sensor” are also listed in this chapter.

### 2.2 Water Losses

Potable water is a critical resource to human society. Failure and inefficiencies in transporting drinking water to its final destination wastes resource and energy. With limited access to fresh water reserves and increasing demand of potable water, water shortage is becoming a critical challenge. So, addressing water losses during distribution presents significant opportunity for conservation.

Leaks are the major factor for unaccounted water losses in almost every water distribution network; old or modern. Vickers [1] reports water losses in USA municipalities to range from 15 to 25 percent. The Canadian Water Research Institute [2] reports that on average, 20 percent of treated water is wasted due to losses during distribution and other unaccounted means. A study on leakage assessment in Riyadh, Saudi Arabia shows the average leak percentage of the ten studied areas to be 30

percent [3]. Losses through leaks represent a significant portion of the water supply, hence identification and elimination of leaks is imperative to efficient water resource management.

Unaccounted water losses include metering errors, accounting errors and sometimes theft; however, typically the greatest contributor to lost water is caused by leaks in the distribution pipes [4],[5]. Failure at joint connections is the usual cause for leaks in pipes. Corrosion, ground movement, loading and vibration from road traffic all contribute to pipe deterioration over time and eventual failure [5]. Old or poorly constructed pipelines, material defects, inadequate corrosion protection, poorly maintained valves and mechanical damage are some other factors contributing to leaks [6].

## **2.3 Leak Detection Techniques**

### **2.3.1 Overview**

In this section some of the most significant concurrent methods for leak detection in pipelines will be discussed.

#### **Water Audits - Metering**

Mays [4] and Hunaidi [5] report various techniques for leak detection. Water losses can be estimated from water audits. The difference between the amounts of water produced by the water utility and the total amount of water recorded by water usage meters indicates the amount of unaccounted water. District metering offers a slightly higher level of insight into water losses than bulk accounting by isolating sections of the distribution network (into districts), measuring the amount of water entering the district and comparing the amount of water recorded by meters within the district. While the amount of unaccounted water gives a good indication of the severity of water leakage in a distribution network, metering gives no information about the locations of these losses.

## **Listening Devices**

Acoustic equipment and more specifically “listening devices” have been widely used by water authorities worldwide for locating leaks in water distribution networks [5]. These include various systems, among them:

- Listening Rods
- Aquaphones
- Geophones (Ground Microphones)

All listening devices are based on the same “sensing” technique, since all of them are using sensitive materials such as piezoelectric elements to sense leak-induced sounds and/or vibrations. Those sensing elements are usually accompanied by some signal amplifiers and filters to make the leak signal stand out. The operation of those listening devices is straight-forward, but the efficiency depends on the user’s experience [7].

To operate a listening device an experienced user is required. The user carries the equipment above ground, tries to follow the pipe map and at the same time is focused on pinpointing a “high-amplitude” acoustic signal with his headset or his monitor (Fig. 2-1).

## **Leak Noise Correlators**

The state of the art in leak detection techniques lies on the “Leak Noise Correlators”. Those devices are more efficient, get more accurate results and depend less on user experience than the listening devices [8].

Leak Noise Correlators are portable microprocessor-based devices that use the cross-correlation method to pinpoint leaks automatically. In most cases either vibration sensors (e.g. accelerometers) or acoustic sensors (e.g. hydrophones) are used at two distinct pipe locations (usually in openings within a water distribution network, such as fire hydrants) that of course need to bracket the location of the suspected leak. If the leak is located somewhere between the two measurement points but not

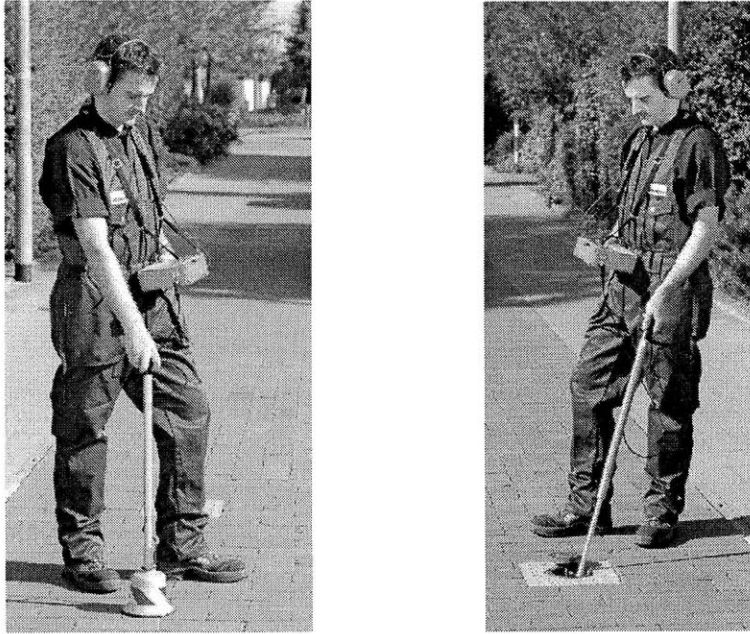


Figure 2-1: Leak detection in water pipelines using the *Sewerin Aquaphone A100*. [Picture from [www.sewerin.com](http://www.sewerin.com)]

in the middle, then there is a time lag between the measured leak signals by the two distinct sensors. This time lag is pinpointed by the cross-correlation function of the leak signals. The location of the leak can be easily calculated using a simple algebraic relationship using the time lag, the distance between the sensors and the propagation velocity of the wave signal in the pipe [9].

This method is destined to fail if there are more than one leaks present between the correlators, which is a very common case in real networks. Another problem associated with this method is that there are cases when there is no access to the pipe close to the leak. In these cases a deployment of a mobile sensor is necessary. Moreover, they can be unreliable for quiet leaks in cast and ductile iron pipes and for most leaks in plastic and large-diameter pipes. Correlators are also expensive and remain beyond the means of many water utilities and leak detection service companies. A typical leak noise correlator is shown in Fig. 2-2.

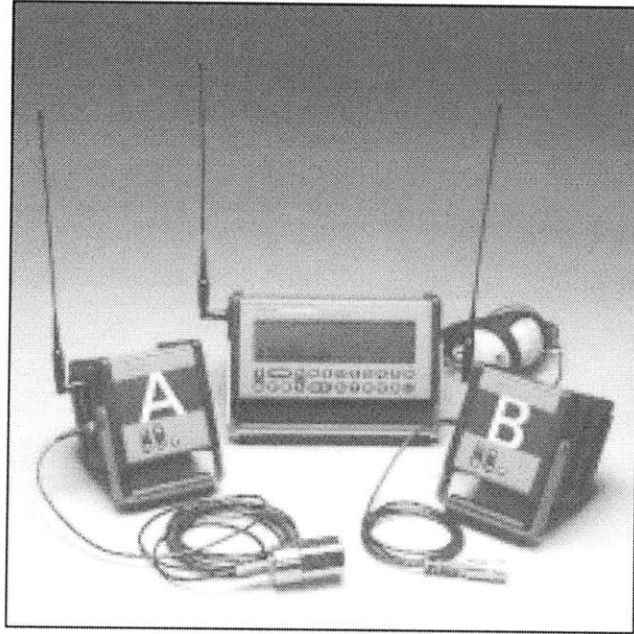


Figure 2-2: Typical Leak Noise Correlators. Sensor A, Sensor B and Correlator device. [Courtesy of Dantec Measurement Technology]

### Pressure Transients

Pressure transients have been used to formulate inverse transient algorithms for leak detection and localization of both single and multiple leaks. Inverse transient formulation involves collecting pressure data during the occurrence of transient events followed by minimization of the difference between observed and estimated parameters. The estimated parameters are calculated through hydraulic transient solvers [10], [11]. The method has shown success in detecting leaks in laboratory conditions under high leak flow rates. Karney studied the applicability and effectiveness of inverse transient analysis to the detection of leaks in real water distribution systems [12]. This method constitutes a low-cost and easy-to-implement alternative; however its feasibility has yet to be fully established in actual field conditions. In addition, there are risks of introducing controlled transients into the distribution system. The method relies on the availability of an accurate transient model of the network and system parameters that are often impractical or expensive to obtain.

## Tracer Gas Technique

Several non-acoustic methods like infrared thermography; tracer gas technique and ground-penetrating radar (GPR) have as well been explored as potential leak detection methods. Tracer Gas Technique involves the injection of a non-toxic, insoluble in water gas, into an isolated pipe section. The gas is then pressurized and able to exit the pipe through a leak opening and then, being lighter than air, permeates to the surface through the soil and pavement. The leak is located by scanning the ground surface directly above the pipe with a highly sensitive gas detector (Fig. 2-3).

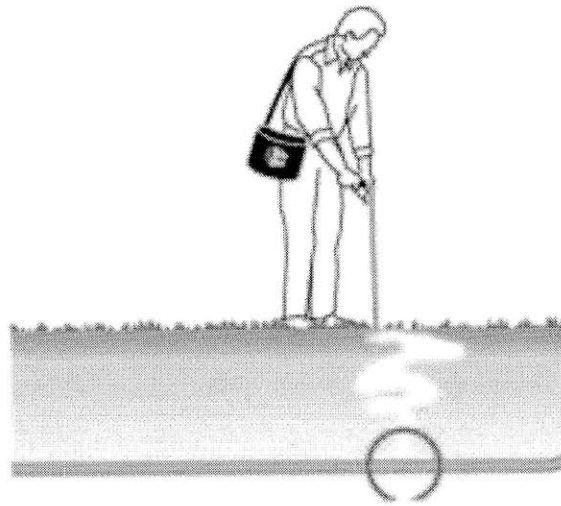


Figure 2-3: Tracer Gas technique sketch.

## Thermography

The principle behind the use of thermography for leak detection in water-filled pipes is that water leaking from an underground buried pipe is changing the thermal field of the adjacent soil. The resulting temperature gradients can be picked up by the corresponding equipment, e.g. infrared cameras. The method requires scanning of the pipe network above ground and the procedure is almost the same as in the GPR or the Tracer Gas Technique. An experienced user is required to walk, following the map of the network and searching for leaks in the pipe network.



## Ground-Penetrating Radar (GPR)

This technique uses a radar that can detect voids in the soil created by leaking water as it circulates near the pipe, or segments of the pipe which appear to be buried deeper than they are because of the increase of the dielectric constant of adjacent soil saturated by leaking water.

GPR waves are partially reflected back to the ground surface when they encounter an anomaly in dielectric properties, for example, a void or pipe [13]. An image of the size and shape of the object is formed by radar time-traces obtained by scanning the ground surface. The time lag between transmitted and reflected radar waves determines the depth of the reflecting object. A typical GPR device is presented in Fig. 2-4.



Figure 2-4: The *RADIODETECTION RD1000* Portable Ground Penetrating Radar System.

### 2.3.2 Summary and Evaluation

In this section the most efficient leak detection techniques will be summarized and evaluated as per advantages, limitations, cost and accuracy. Pros and cons of each

method will be presented in table form.

**Listening Devices** : Locating the loudest sound of leak by sound transducers placed on the ground surface above the pipe.

- + Most commonly used
- + Acceptable accuracy
- + Simple to carry and move
- Depends on the operator skills
- Not effective for small leaks
- Affected by background noise
- Depends on pipe size, material
- Depends on water table level, system pressure
- Loose soil muffles sound
- Exact pipe location must be known
- More suitable for hard surfaces
- Depth less than 2 m

**Acoustic with Correlation** : A correlation algorithm uses two vibration transducers' signals installed on the pipe at two locations bounding the leak with pipeline information.

- + Good accuracy
- + Acceptable price
- + Minimal operator training
- Leak should be between two listening points
- Fails in case of multiple leaks
- Accuracy relies on input of pipe features
- Not suitable for plastic pipes
- Good sensor contact is essential
- Accuracy depends on the distance of the leak to measuring points
- Sometimes there is no access to the pipe close to the leak
- External noise interferes with the signals

**Tracer Gas Technique** : A tracer in the pipe escapes through the leak and is

detected at ground surface.

- + Effective method in case of emergency that requires isolating the pipe with no flow
- Very expensive
- Time consuming
- Exact pipe location must be known
- Limited to depth less than 2 m

**Thermography** : Locating the temperature differences in soil caused by leaking water using infrared radiation.

- + Non-contact, nondestructive
- Very expensive
- + Able to inspect large areas from above ground with 100% coverage
- Significant operator experience
- Detection depends on the soil characteristics, leak size, and burial depth
- + Locates subsurface leaks as well as voids and erosion surrounding pipelines
- Application limited by ambient conditions

**Ground Penetrating Radar** : Uses electromagnetic radiation of the radio spectrum, and detects the reflected signals from subsurface structures. It detects voids created by the leaking water or anomalies in the depth of the pipe due to soil saturation with leaking water.

- + Variety of media
- Significant operator experience
- + Detects objects, voids, cracks
- Expensive (hardware & software)
- + Penetration up to 15m
- High energy consumption
- Depth of penetration depends on soil type

All methods discussed so far are searching for leaks above the ground with all the corresponding implications and limitations. Past experience has shown that in-pipe

inspection is much more accurate, less sensitive to random events and external noise and also more deterministic, due to the fact that it is less subjective to the user's experience. Moreover, pipe inspection from the inside brings the "sensing module" closer to the source and consequently the system itself is capable of pinpointing very small leaks. In general such systems face difficult challenges associated with communication, powering and are in general expensive to build.

## 2.4 Inspection Robots

In the area of in-pipe inspection systems, there are many examples of prior-art robotic systems for use in underground piping. Most of them are however focused on water- and sewer-lines, and meant for inspection, repair and rehabilitation. Some examples are shown in Fig. 2-5. As such, they are mostly tethered; utilizing cameras specialized tooling and usually are designed to operate in empty-pipe-conditions.

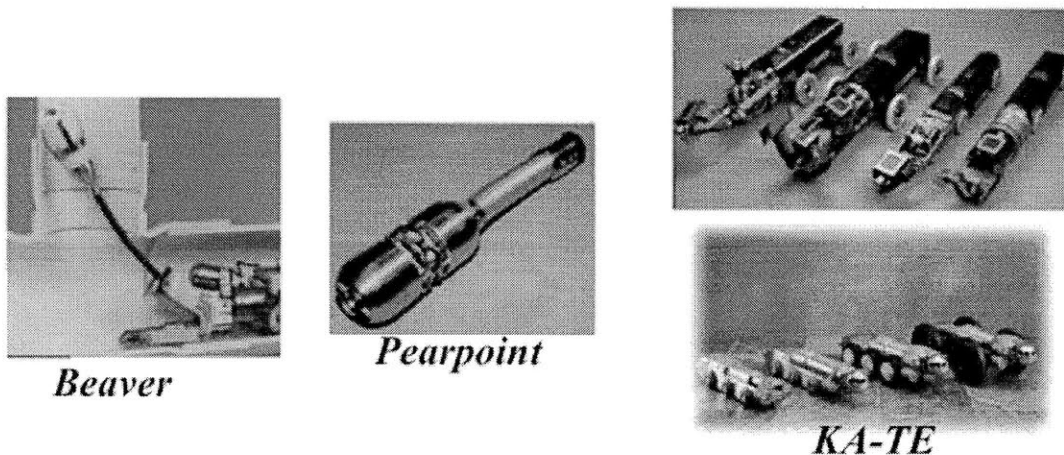


Figure 2-5: Some state-of-the-art leak inspection robots.

Three of the more notable exceptions are the autonomous *Kurt I* system from GMD used for sewer monitoring, the tethered gas main cast-iron pipe joint-sealing robot *CISBOT* and the *GRISLEE* robot, Fig. 2-6. The latter is a coiled-tubing tether deployed inspection, marking and in-situ spot-repair system.

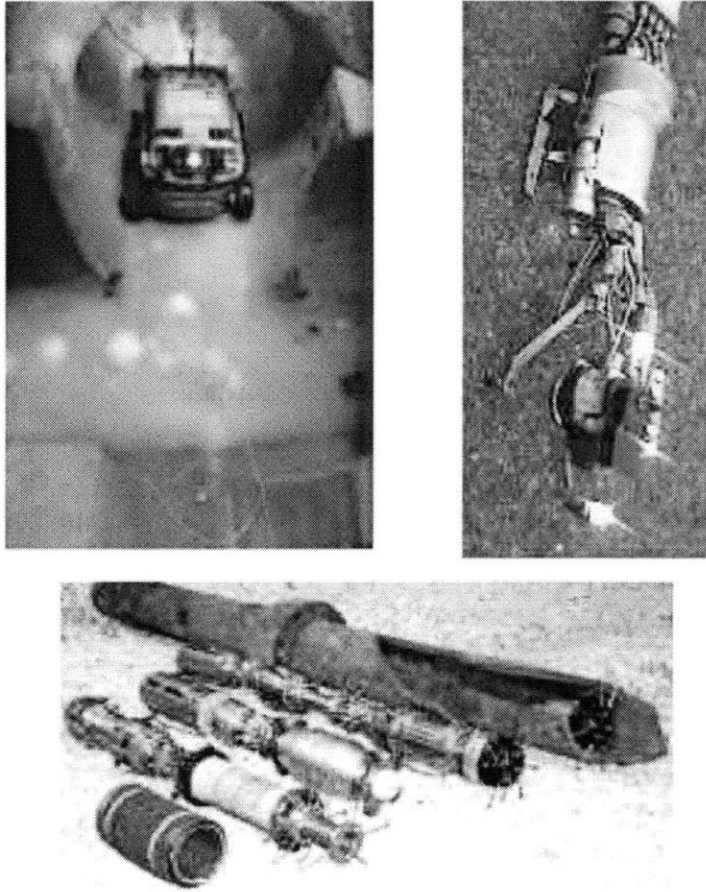


Figure 2-6: Top Left: Un-tethered Autonomous *Kurt I*, Top Right: *CISBOT*, Bottom: *GRISLEE*

There are also robots that have been developed for in-pipe inspection such as corrosion, cracks or normal wear and damage. State of the art robots are usually four-wheeled, camera carrying and umbilically controlled. Most of them are however focused on oil or sewer-mains. One of the most successful steps in building such a robot was developed by Schempf at CMU [14] with his untethered *Explorer robot*. The system is a long-range, leak-inspection robot, working in real-gas-pipeline conditions and is being controlled by an operator in real-time through wireless RF technology. The operator is constantly looking to a monitor and is searching for leaks visually via a camera.

Kwon built a reconfigurable pipeline inspection robot with a length of  $75mm$  and a modular exterior diameter changing from  $75mm$  up to  $105mm$  [15]. Controlling the speed of each one of the three caterpillar wheels independently provides a steering capability to the system.

Most of the state-of-the-art leak detection robots are able to travel along horizontal pipelines and only a small fraction of them can cope with complicated pipeline configurations, e.g. T-junctions, bended pipes etc. Even if some of them manage to cope with that they usually require a complete shut-down of the network and deployment of the system in an empty pipe such as the *MRINSPECT* [16].

The *Smartball* is a mobile device that can identify and locate small leaks in water pipelines larger than  $254\text{ mm}$  ( $10''$ ) in diameter constructed of any pipe material [17], as shown in Fig. 2-7. The free-swimming device consists of a porous foam ball that envelops a water-tight, aluminum sphere containing the sensitive acoustic instrumentation. This device is capable of inspecting very long pipes but cannot handle complicated pipeline configurations.

Bond presents a tethered system that pinpoints the location and estimates the magnitude of the leak in large diameter water transmission mains of different construction types [18]. Carried by the flow of water, the system can travel through the pipe and in case of a leak, the leak position is marked on the surface by an operator, who is following the device (Fig. 2-8). The system is tethered and thus all range limitations apply in this case.

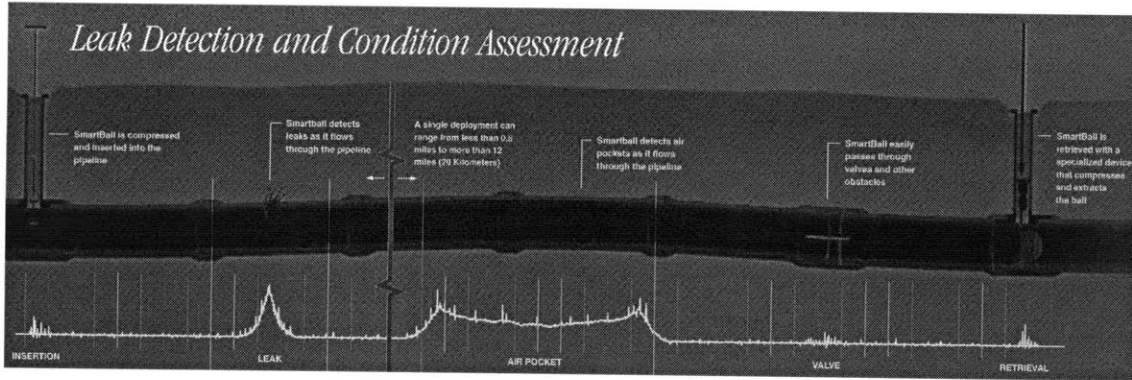


Figure 2-7: A typical leak detection survey with the *Smartball*.

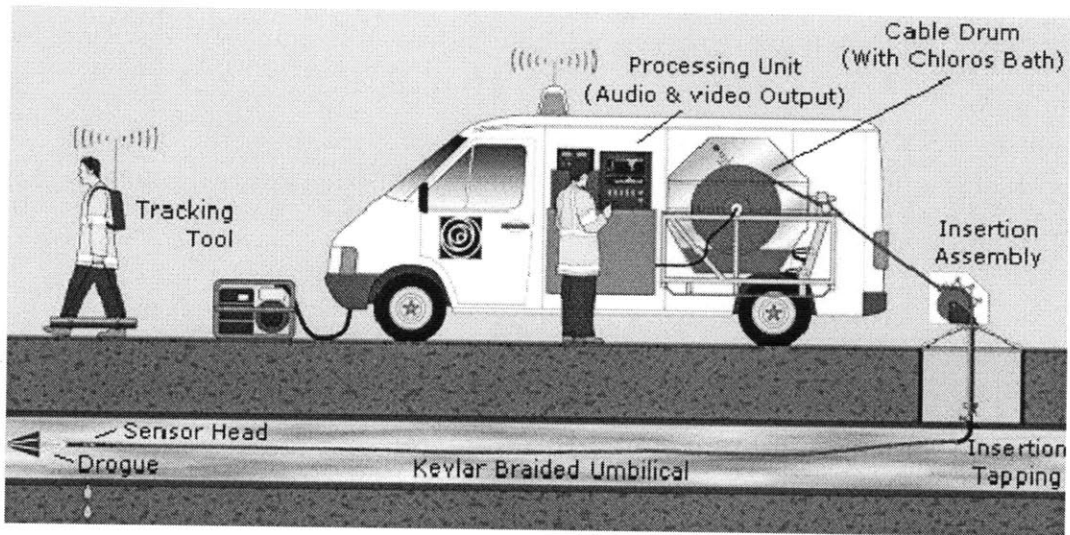


Figure 2-8: Sketch of the *Sahara* leak detection system.

## 2.5 System Functional Requirements

As presented in the previous sections many methods have been developed over the last few decades to detect leaks in water pipes. Leak detection using in-pipe sensing came to picture recently by different systems. Nevertheless, all of the state-of-the-art systems have limitations.

Our goal is to design a system that tackles the main problems and overcomes some of the limitations. The functional requirements of such a system may be listed as follows:

- *Autonomy*: The system should be completely autonomous (untethered). The system will be deployed in one point and will be retrieved from another point in the pipe network.
- *Leak Sensing Sensitivity*: The system is aimed at detecting “small” leaks in plastic (PVC) pipes (depending on the sensing element). Plastic pipes are the most difficult for leak detection [19], since sound and vibrations are greatly damped over small distances away from the leak. Thus, detecting leaks in plastic pipes requires deploying a mobile sensor that should be very close to the leak.
- *Working Conditions*: System will be deployed under the real pipe flow conditions, more specifically:
  - Line Pressure: 1 to 5 *bars*
  - Flow Speed: 0.5 to 2 *m/s* (in 100mm ID pipes which corresponds to a volumetric flow rate of up to 15.7 *lit/sec*).
- *Communication*: The system needs to be able to communicate with stations above ground and pinpoint potential leaks in the water network.
- *Localization*: The system needs to be able to localize itself within the water distribution network. This is essential for the accurate leak position estimation and the retrieval of the sensor from the network as well.



## 2.6 Chapter Summary

In this chapter various leak detection methods, systems and robotic devices have been listed and evaluated. Water audits, listening devices, leak noise correlators, pressure transients, tracer gas technique, infrared thermography and GPR are all promising techniques with advantages as well as limitations. The idea of an in-pipe moving sensor “swimming” along a pipeline and detecting leaks from the inside seems to be challenging but at the same time promising and more accurate, since the sensor will get very close to the source as it passes by the leak. Such a system has some functional requirements, that are also presented in this chapter.



# Chapter 3

## Sensing Module - Instrumentation

### 3.1 Introduction

This chapter will discuss the sensing module characteristics, i.e. the sensors' characteristics and the instrumentation used to acquire the signal in terms of both hardware and software. Specific details and specifications of the instrumentation that we used for experimentation will be given.

### 3.2 Sensor Overview and Characteristics

For the accurate leak detection two different sensors have been used. The first one is a hydrophone, presented in section 3.2.1, while the second one is a Dynamic Pressure Sensor (DPS). The latter one and its characteristics are discussed in section 3.2.2. Both of them are able to measure dynamic pressure fluctuations as we will see in the next sections.

#### 3.2.1 Hydrophone

The hydrophone that we used in our experiments is a *B & K* system with model number is 8103. This specific model is of a small size, high-sensitivity transducer for making absolute sound measurements over the frequency range  $0.1Hz$  to  $180kHz$

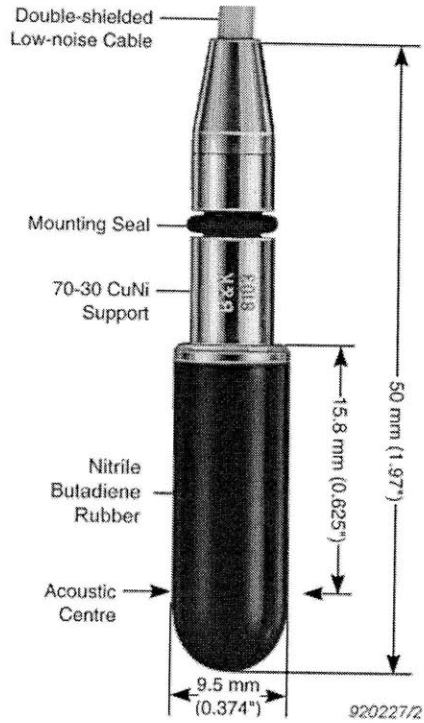


Figure 3-1: The hydrophone 8103 from B&K. Picture taken from <http://www.bksv.com>

with a receiving sensitivity of  $-211\text{ dB}$  with reference to  $1\text{V}/\mu\text{Pa}$ , which corresponds to  $25.9\ \mu\text{V}/\text{Pa}$  or approximately  $0.1786\ \text{V}/\text{psi}$ . It has a high sensitivity relative to its size and good all-round characteristics, which make it generally applicable to laboratory, industrial and educational use. Type 8103's high frequency response is especially valuable when making acoustic investigations of marine animals and in the measurement of the pressure-distribution patterns in ultrasonic-cleaning baths. It is also useful for cavitation measurements. Fig. 3-1 shows the sensor and its main dimensions. Fig. 3-2 shows the frequency response of the hydrophone as measured by the company after calibration. The flat frequency response over a large frequency range even at very low frequencies was the main reason why this product was selected for our experiments. The weight of the sensor plus the cable is 170 grams.

To power up this sensor we used the *WB-1372 DeltaTron Power Supply* from B&K (Fig. 3-3). A *Charge to DeltaTron* converter was also necessary, so we selected the type 2647 from B&K (Fig. 3-4).

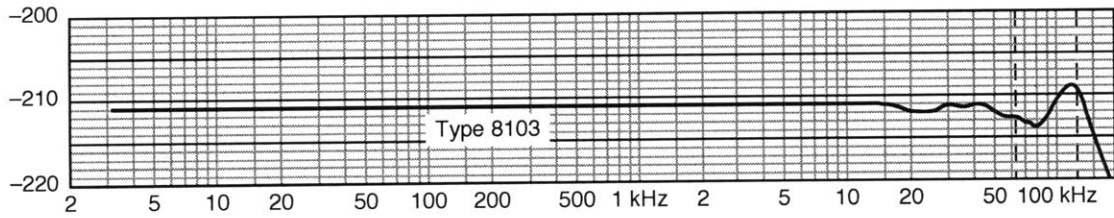


Figure 3-2: The receiving frequency response of the hydrophone sensor 8103 from B&K. Graph taken from <http://www.bksv.com>

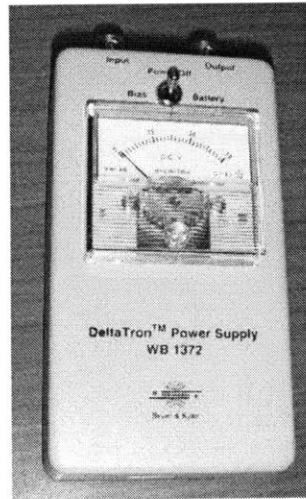


Figure 3-3: The WB-1372 DeltaTron Power Supply from B&K. Picture taken from <http://www.bksv.com>



Figure 3-4: The Charge to DeltaTron converter type 2647 from B&K. Picture taken from <http://www.bksv.com>

### 3.2.2 Dynamic Pressure Sensor (DPS)

The DPS that we used is model 106B52 from *PCB Piezotronics*. This is a very sensitive model with a sensitivity of  $5V/psi$  and a resolution of  $2 \times 10^{-5}$ . This sensor has also a very flat frequency response starting from approximately  $2.5Hz$ . The resonant frequency takes place at very high frequencies of the order of  $\geq 40kHz$ . The weight of this sensor is 35 grams. Fig. 3-5 shows a picture of the sensor while Fig. 3-6 presents a small sketch of all different subsystems within the sensor. To power up this sensor we used the 482A21 *Sensor Signal Conditioner* from *PCB Piezotronics* (Fig. 3-7).

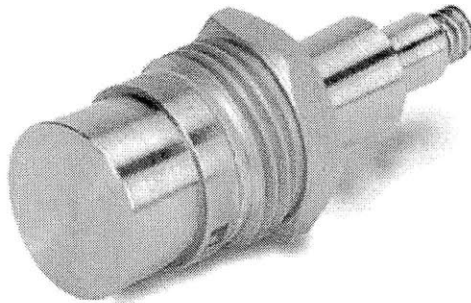


Figure 3-5: The Dynamic Pressure Sensor 106B52 from *PCB Piezotronics*. Picture taken from <http://www.pcb.com>

## 3.3 Instrumentation Characteristics

Except for the sensors and their accessories other instrumentation was used to acquire data and drive the signal to the host PC and store it before postprocessing. Those will be discussed in this section.

### 3.3.1 Amplifier

In all of our experiments with the hydrophone we used a low-noise voltage preamplifier. More specifically the model that we used was the SR560 from *Stanford Research Systems*.

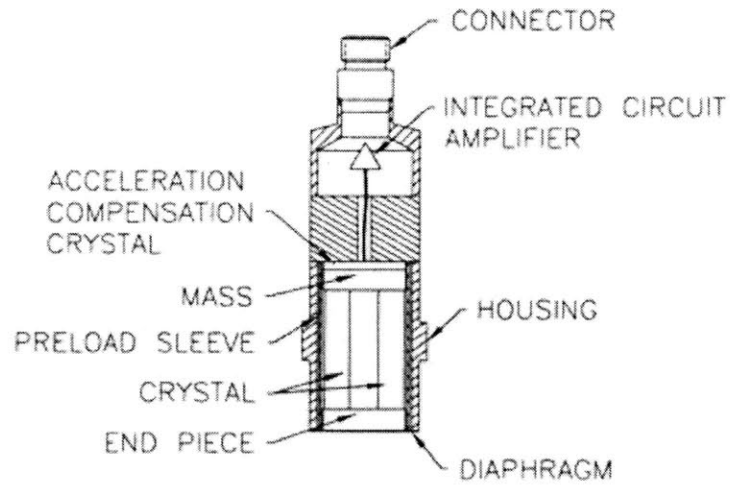


Figure 3-6: A sketch describing all the subsystems within the dynamic pressure sensor 106B52 from PCB Piezotronics. Picture taken from <http://www.pcb.com>

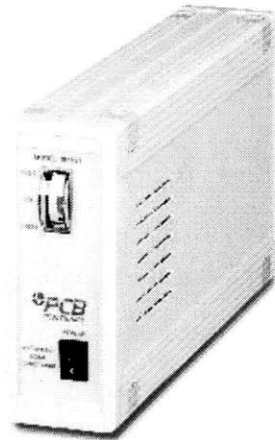


Figure 3-7: The 482A21 *Sensor Signal Conditioner* from PCB Piezotronics. Picture taken from <http://www.pcb.com>

The amplifier provides a variable gain from 1 to 50,000, either AC or DC coupled inputs and outputs as well as line or battery operation. It is also equipped with two configurable signal filters that the user can adjust according to will and apply low-, high- or even band-pass filter to the input signal. Filter cutoff frequencies can be set in a 1 – 3 – 10 sequence from 0.03  $Hz$  to 1  $MHz$ . A picture of the amplifier is shown in Fig. 3-8.

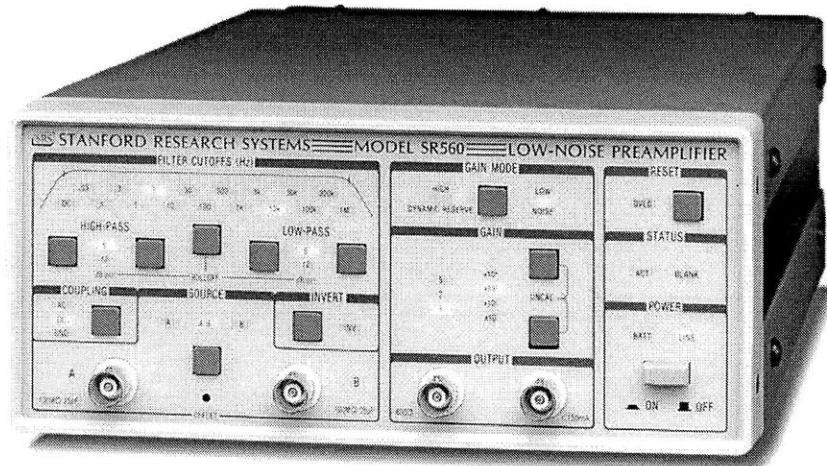


Figure 3-8: The SR560 amplifier from *Stanford Research Systems*.

### 3.3.2 Data Acquisition (DAQ) Hardware

The data acquisition system that was used consists of four different parts that are described in this section. For DAQ the signal is driven to a *National Instruments* 9234 4-channel, 51.2 $kHz$  maximum sampling rate, 24bit analog input module (Fig.3-9). This one sits on a *National Instruments* cRIO-9113 Reconfigurable Chassis (Fig.3-10). The system is driven by a *National Instruments* cRIO-9022 real-time controller with 256MB DDR2 RAM and a 533 $MHz$  processor (Fig.3-11). The controller is supplied with ethernet ports and by using one of them we connect it to the Host PC, where we record and post-process the signals.





Figure 3-9: The *National Instruments 9234* 24bit analog input module. Picture taken from <http://www.ni.com>

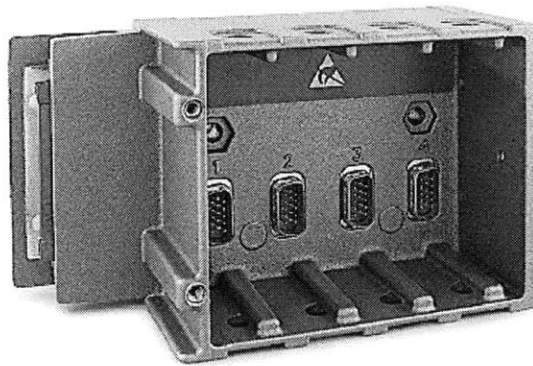


Figure 3-10: The *National Instruments 9113* chassis. Picture taken from <http://www.ni.com>

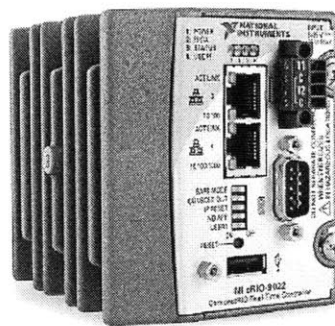


Figure 3-11: The *National Instruments 9022* real-time controller. Picture taken from <http://www.ni.com>

### 3.3.3 Connection Overview

#### Hydrophone Connection Overview

A charge to voltage *DeltaTron* converter is connected in series with the hydrophone and the sensor is powered by the *DeltaTron WB 1372* module. The output of the later module is then connected to a power amplifier and signal conditioner from *Stanford Research Systems*. The output of the amplifier is directed to the *NI 9234* module on a *cRIO-9113* reconfigurable chassis. The sampling rate can be selected manually by the user and can go up to  $51.2\text{KHz}$ . Signal is finally driven from the DAQ FPGA to the host PC for postprocessing.

#### DPS Connection Overview

The DPS has a built-in amplifier and produces 5V for 1 psi pressure fluctuation, so there is no need to connect it to the amplifier. It is directly connected to a 1-channel, line- powered, *ICP sensor signal conditioner* model *482A21* which provides constant current excitation to the sensor. The output of this power supply is directed to the *NI 9234* module on a *cRIO-9113* reconfigurable chassis. The sampling rate can be selected manually by the user and can go up to  $51.2\text{KHz}$ . Signal is finally driven from the DAQ FPGA to the host PC for postprocessing.

### 3.3.4 Data Acquisition (DAQ) Software

The DAQ software that we used consists of a couple of LabVIEW virtual instruments (vi's). The user is able to select the sampling rate  $f_s$  for the DAQ. The various options for the sampling rate are  $f_s = 51,200/n \text{ Hz}$ , where  $n = 1, 2, \dots, 30, 31$ . This means that the sampling rate range starts at  $1652\text{Hz}$  and goes up to  $51200\text{Hz}$ . The user is also able to see a real-time graph of the time-series signal captured. The interface that the user is able to see on the host PC under LabVIEW is presented in Fig. 3-12. For more information on the DAQ software please refer to Appendix A.

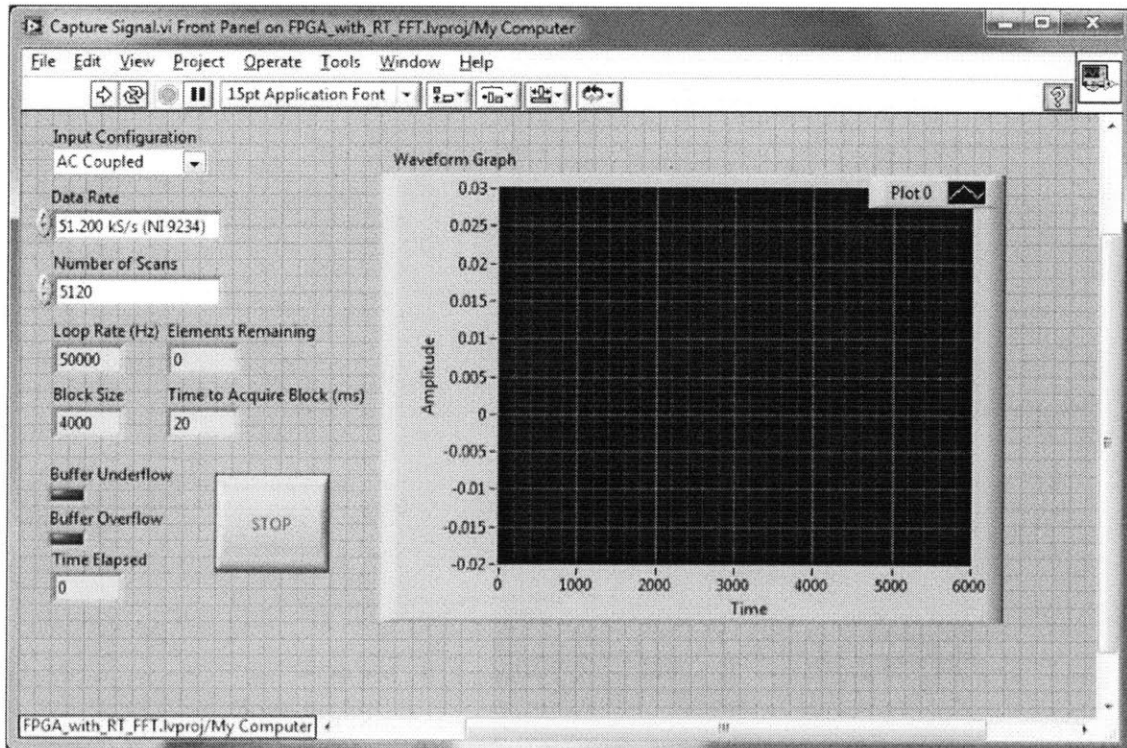


Figure 3-12: The user interface in LabVIEW for DAQ.

### 3.4 Chapter Summary

This section discusses the sensors, their accessories and the required hardware that were used to acquire the signals from the sensors and store them for postprocessing. A small description and detailed specifications of each module are described, as well as the connection of the different modules is presented.



# Chapter 4

## Sensing Module - Experimentation

### 4.1 Introduction

This chapter will discuss the experimental setup used to detect leaks in water pipes. An overview of the setup sections, as well as a description of the objectives of this experimental work will be given.

### 4.2 Experimental Setup Overview

The setup used for experimentation is shown in Fig. 4-1. It consists of 100mm ID plastic pipes (1.5m long), with the municipality water supply fed at one end, while the other end is fitted by a flow control valve. Fig. 4-2 shows the solid model of the test loop with some brief explanation on some features.

This setup allows pipe flow rates from 0 to 23 *lit/min*, which are considered very small, compared to actual network flows but they satisfy the current experimental objectives. A pressure gage is installed on the pipe for measuring the line pressure. The leak flow rate is measured using an *Omega* flow meter (Model *FDP301*) which can be used to measure flow rates as low as 0.3 *lit/min*.

A hydrophone is used to listen to leak noise and a dynamic pressure sensor (DPS) is used to pick up the water pressure disturbance due to the leak. Both the hydrophone and the pressure transducer can move relative to the leak location; upstream or

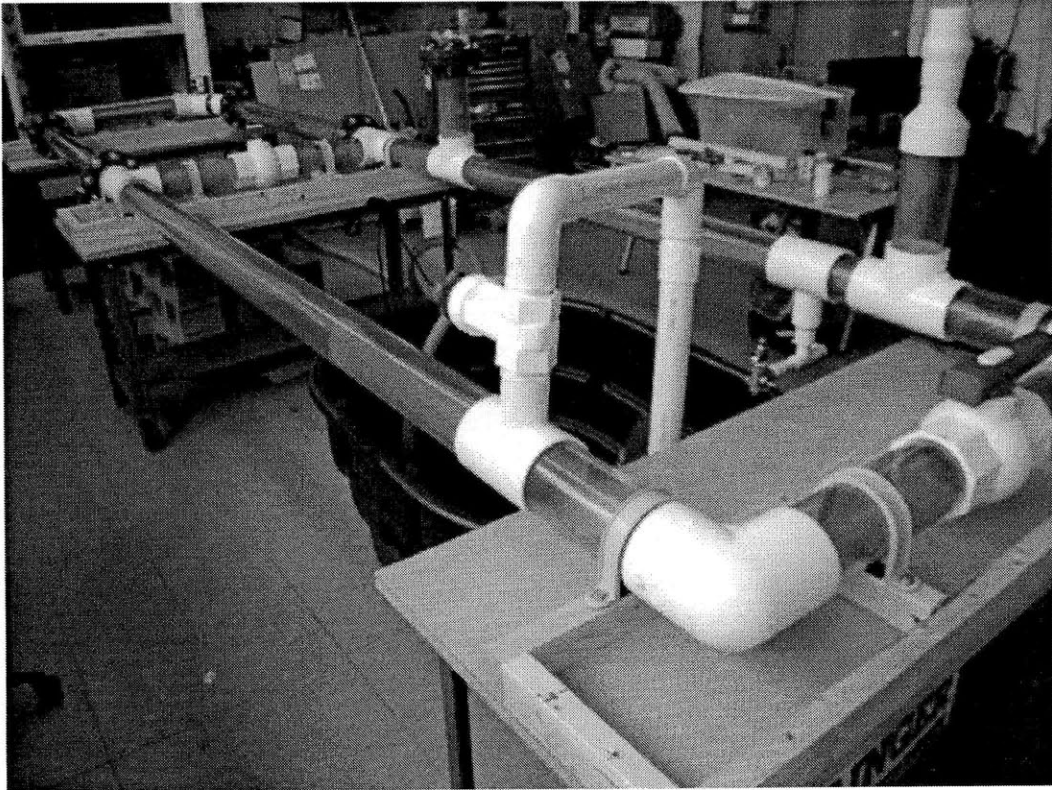


Figure 4-1: Test loop in the lab consisting mostly of 100mm ID pipe sections

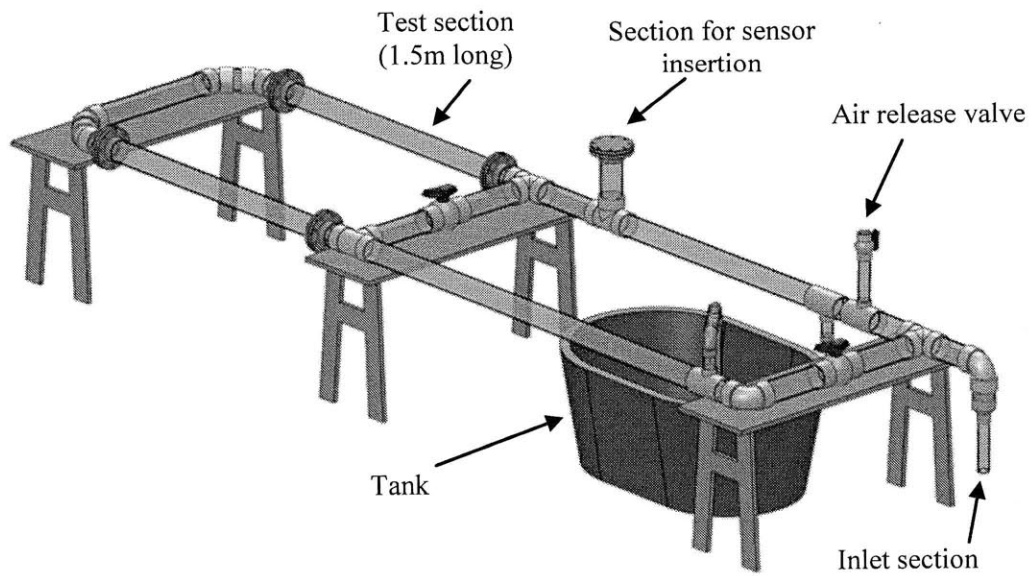


Figure 4-2: The solid model of the test loop.

downstream. The hydrophone was always centered at the centerline of the pipe being supported by a plastic 3D-printed part, see Fig. 4-3. The later one was moved along the pipe using magnets (Fig.4-4). The DPS is mounted flush on pipe wall using special adapter. The different installation of the hydrophone and the DPS is presented in Fig. 4-5.

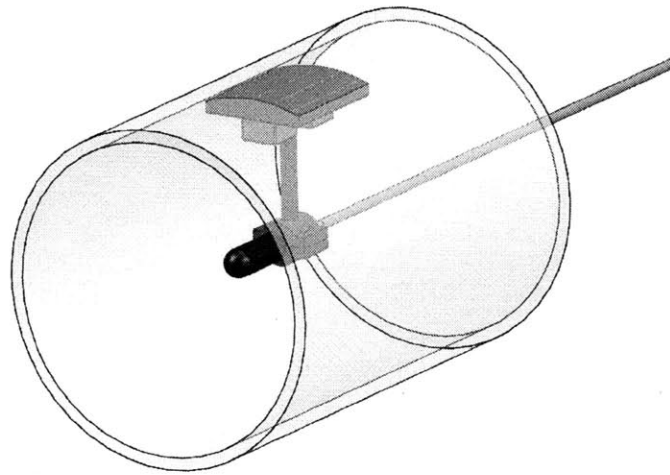


Figure 4-3: The solid model of the sensor-holder used to hold and move the hydrophone along the pipe. The sensor holder part is sketched in brown color.

### 4.3 Simulating Leaks

The simulated leaks are of two different types. Firstly, we simulated a leak by using a 1/8" (3.175mm) PVC valve and the valve opening is controlled based on the required leak flow rate (Fig. 4-6). A second type is simulated by drilling corresponding holes on the test section (Fig. 4-7). Each drill bit resulted in a different leak size with a different flow rate. Thus, leaks in this case are simulated by circular holes on the pipe body.

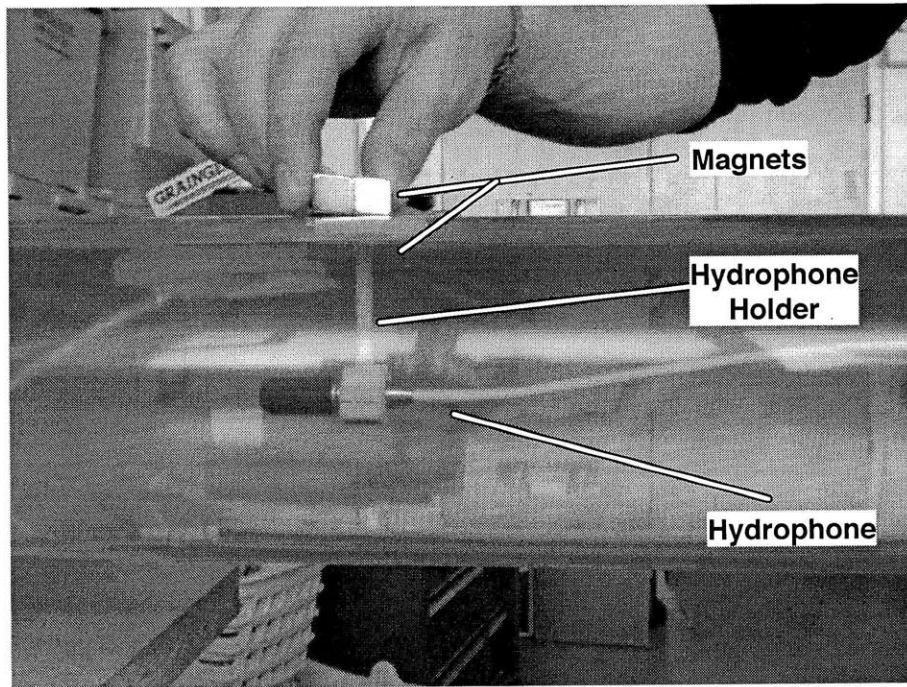


Figure 4-4: The actual sensor-holder while moving the hydrophone along the pipe. Magnets on both sides are used to move the sensor.

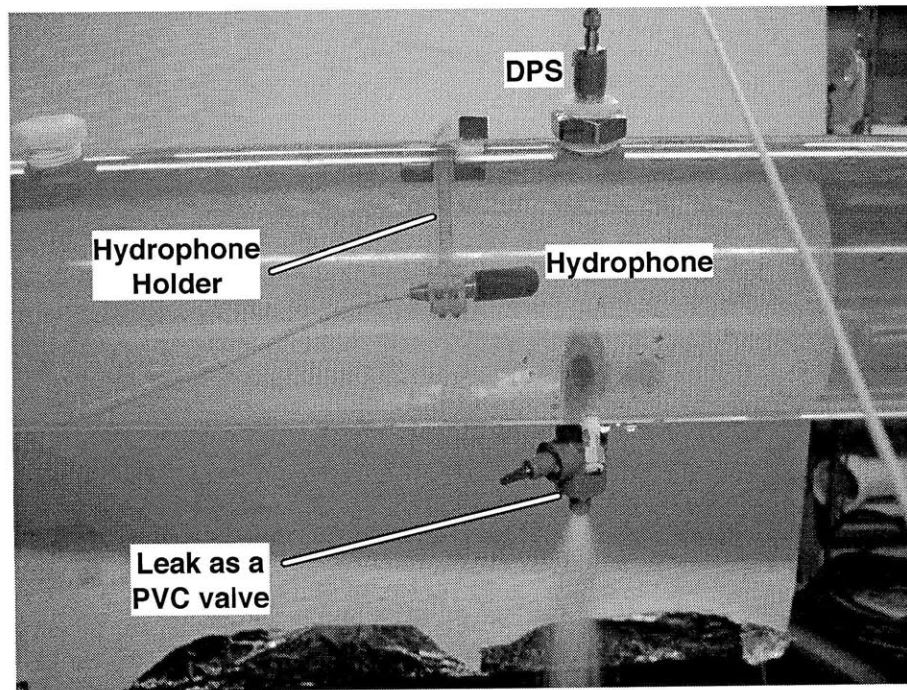


Figure 4-5: The DPS is mounted flush on the pipe body. The hydrophone is mounted on the sensor holder and is moving with the use of magnets from the outside. The 1/8" valve simulating a leak is also shown in the picture.



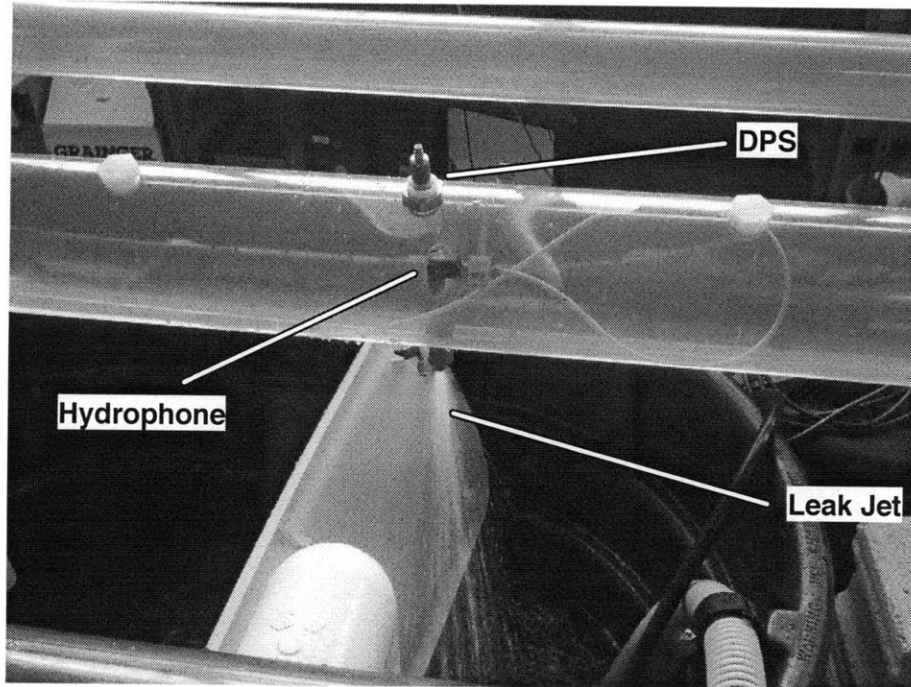


Figure 4-6: The 1/8" valve simulating a leak.

## 4.4 Experimentation Objectives

The objective of this experimentation is to characterize acoustic emissions stemming from a leak, simulated as a circular hole or a small valve, on a plastic water pipeline using a hydrophone or DPS. Experiments were done with 100mm ID PVC pipes, which is commonly used material and size in modern water distribution networks. Our goal was to come up with a “metric” or a way for leak detection.

The following parameters/conditions are to be studied during this experimentation for the sensing module:

- Leak size
- “Ambient” pipe flow
- Surrounding medium
- Location of sensor with respect to leak location

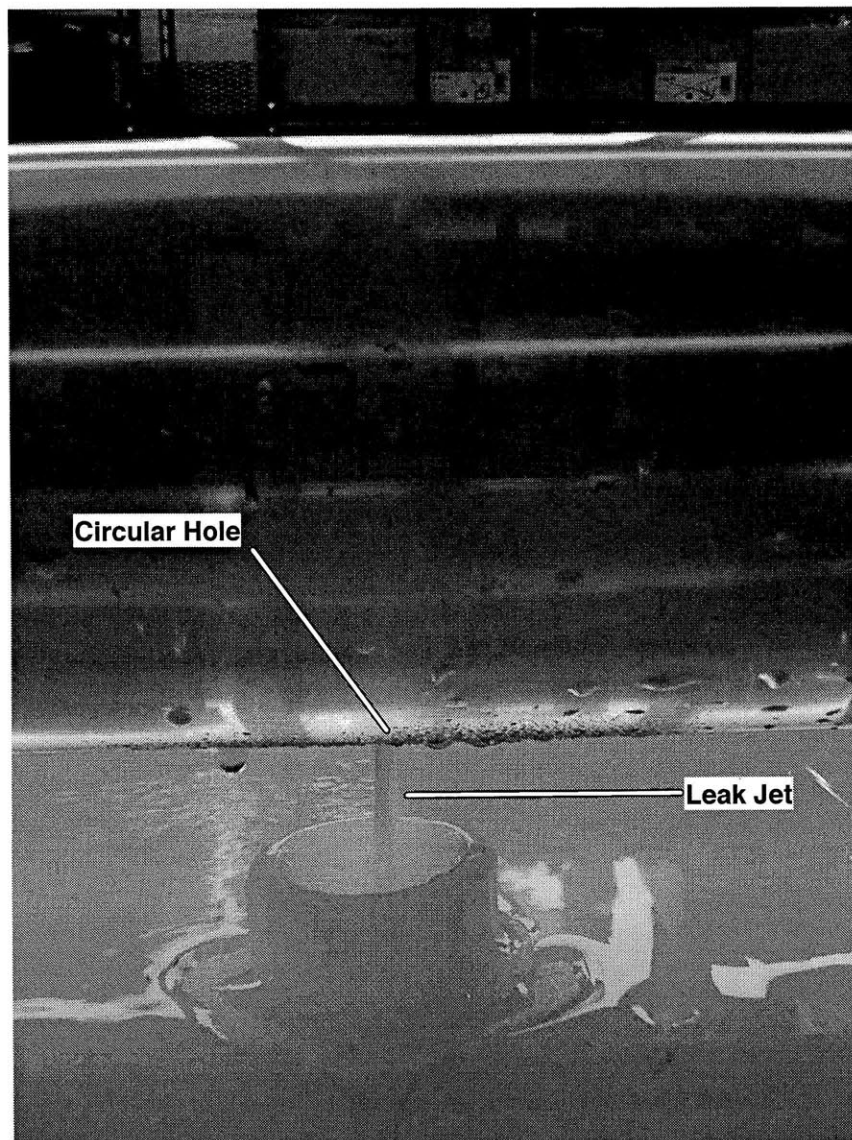


Figure 4-7: The circular hole simulating a leak.

## 4.5 Chapter Summary

In this section the experimental loop that was built for experimentation was discussed and its features were described. The different ways leaks were simulated are also presented. Finally, the objectives of the experimental work for the sensing module are listed.



# Chapter 5

## Sensing Module - Experimental Results

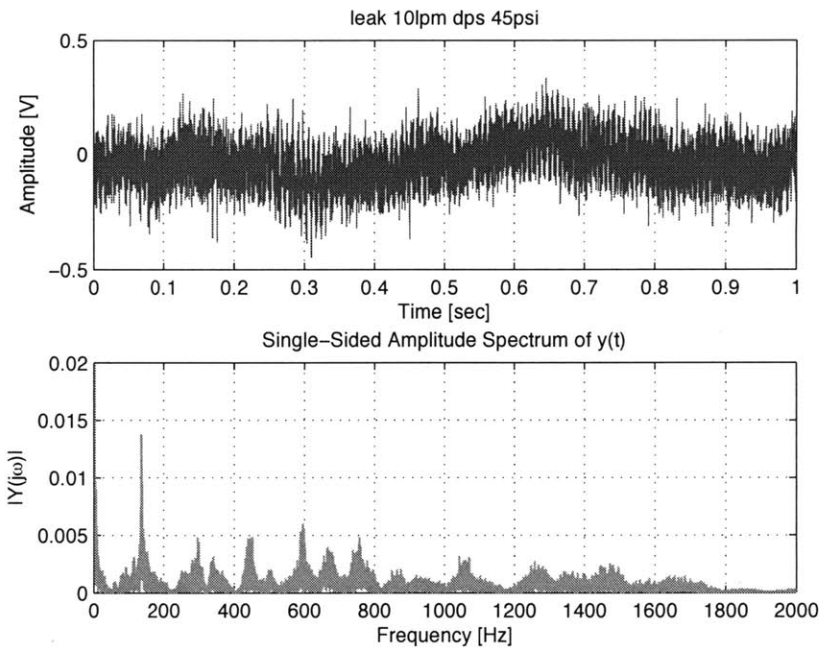
### 5.1 Introduction

This chapter will present the experimental results on leak detection using the hardware and software presented in chapter 3 as well as the experimental setup discussed in chapter 4.

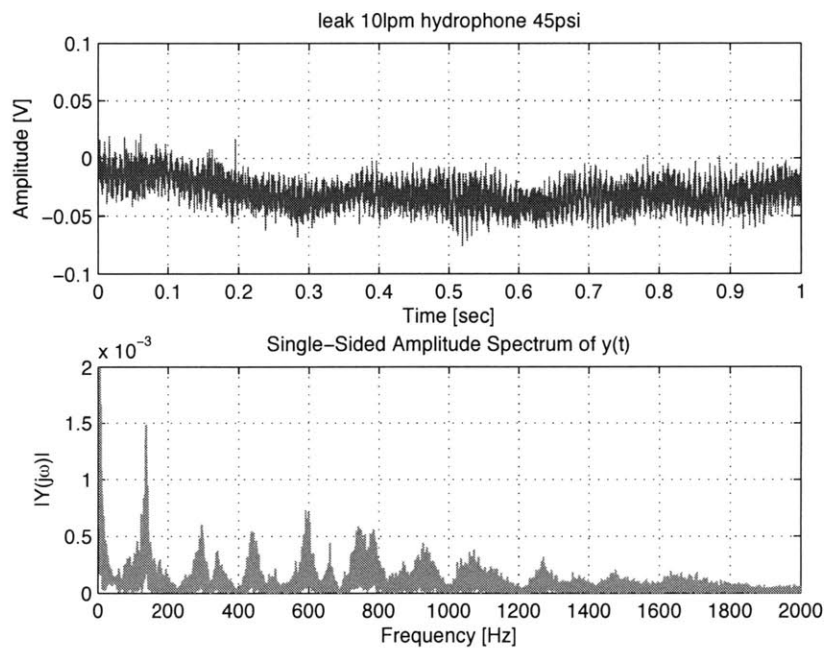
### 5.2 Hydrophone vs DPS

The first objective is to test the two sensors and understand their characteristics. To do so, we test the sensors under similar experimental conditions and study the captured signals. Signals for the same flow rates under the same conditions will be compared. To satisfy this experimental matrix, both the DPS and the hydrophone are used for signal capturing with a controlled leak to provide the basic knowledge on the previously mentioned objectives. Leak is simulated using a 1/8" PVC valve and the valve opening is controlled based on the required leak flow rate. Experiments were carried out with no pipe flow (pipeline end is closed). The pipe flow can be varied between 0 to 23 *lit/min*. Leak is always open to air for this set of experiments.

Fig. 5-1 attests the fact that both sensors capture the same signal; for the case



[a] Signal captured by DPS



[b] Signal captured by hydrophone

Figure 5-1: Signals captured by [a] DPS and [b] hydrophone for the case of a  $10\text{lit}/\text{min}$  leak. Pressure in the pipe is  $45\text{psi}$ . The time signal as well as the frequency spectrum of each case are shown.

of no pipe flow and a leak of 10 *lit/min*. Note that the scales on the time signals of Fig. 5-1 [a] and [b] are not the same due to the different output of each sensor; the hydrophone output is not pre-amplified and the sensors have different sensitivities. To postprocess signals a MATLAB code was built (see Appendix B).

Despite the different characteristics of each sensor and the different way they were placed inside the pipe, both sensors captured the same peak frequencies fairly well for all tests. They effectively sense the same pressure wave propagating in the pipe water and this reveals the fact that both sensors are mainly equivalent and can be used for leak detection. A wide range of frequencies appeared in the frequency spectrum as a result of induced turbulence due to partially opened leak.

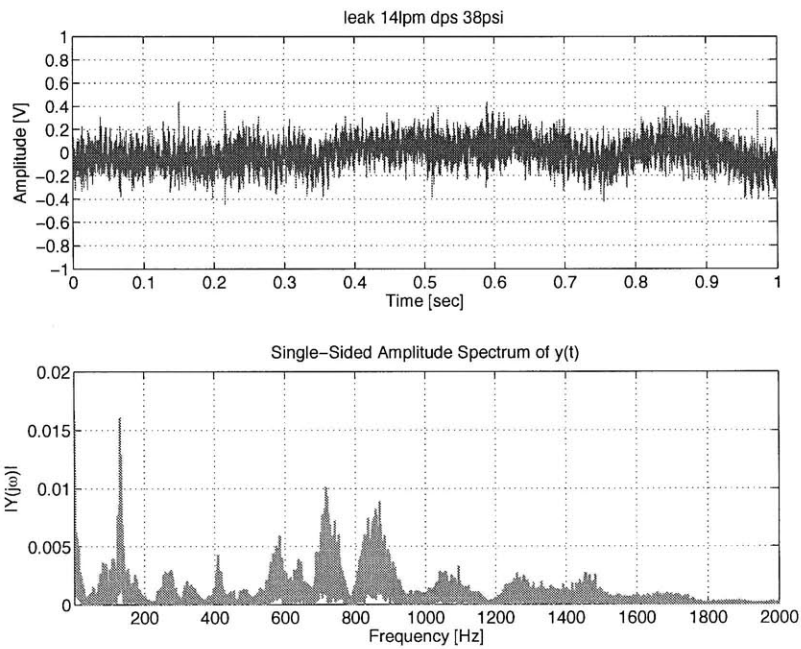
This experiment was repeated for different leak sizes by controlling the opening of the valve over different days. In all of the cases the signals captured by the two sensors were identical (see and compare the frequency spectra on Fig. 5-2, 5-3 for other leak flow rates). This can be justified by the fact that the two sensors are based on the same fundamental principle for sensing, namely capturing dynamic pressure fluctuations.

During the experiments the in-line pressure of 45*psi* was not constant but was oscillating about the mean value with a very slow frequency. This phenomenon appears on the frequency spectrum of all signals, since there are concentrated peaks in the very low frequency zone. This signatures have nothing to do with the leak and will be either filtered out or ignored for the rest of this work.

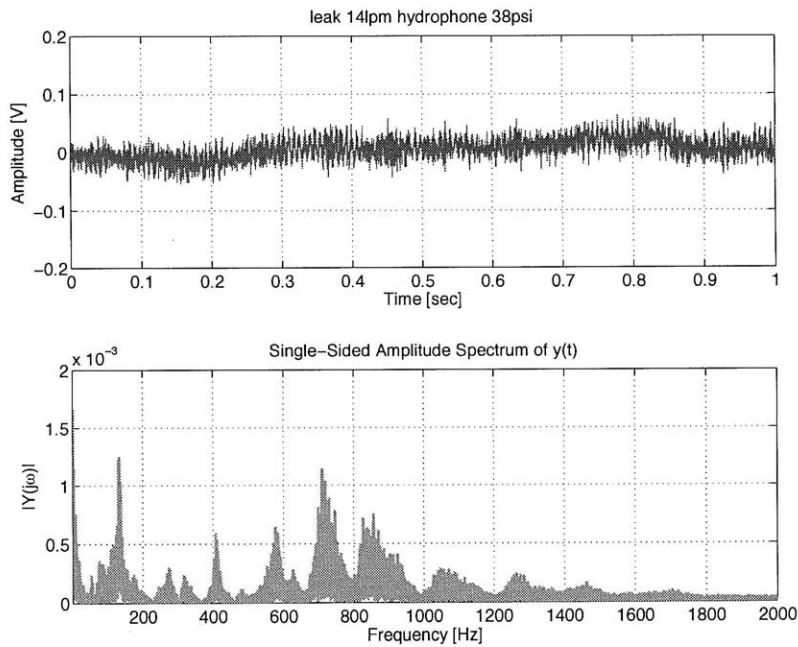
To summarize, we can use any of the two sensors for leak detection without any loss of information, i.e. *the two sensors are identical and can be used interchangeably*.

### 5.3 Effect of Leak Flow Rate

In this section the effect of the leak flow rate on leak signal is studied. The experiments conducted with leaks being simulated by a PVC valve are discussed in section 5.3.1 and with leaks as circular holes in section 5.3.2.



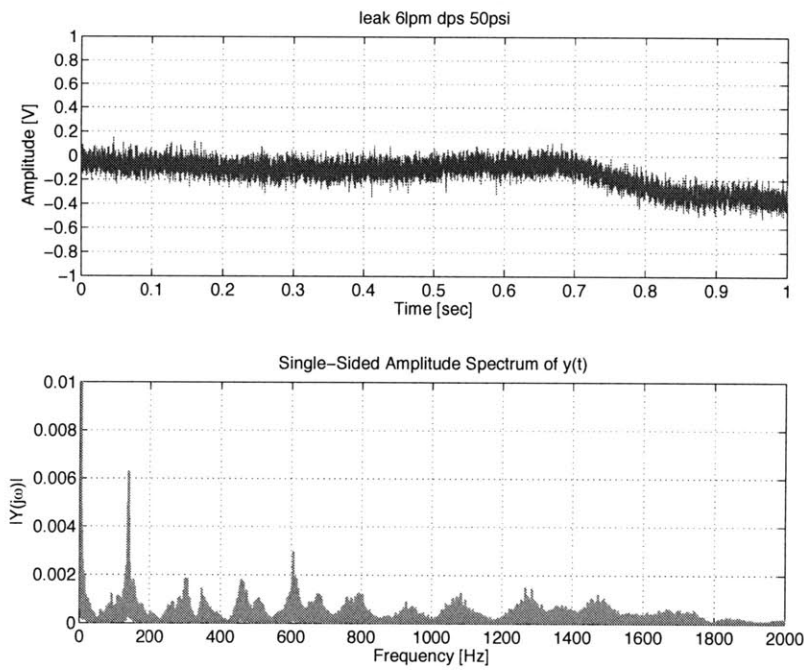
[a] Signal captured by DPS



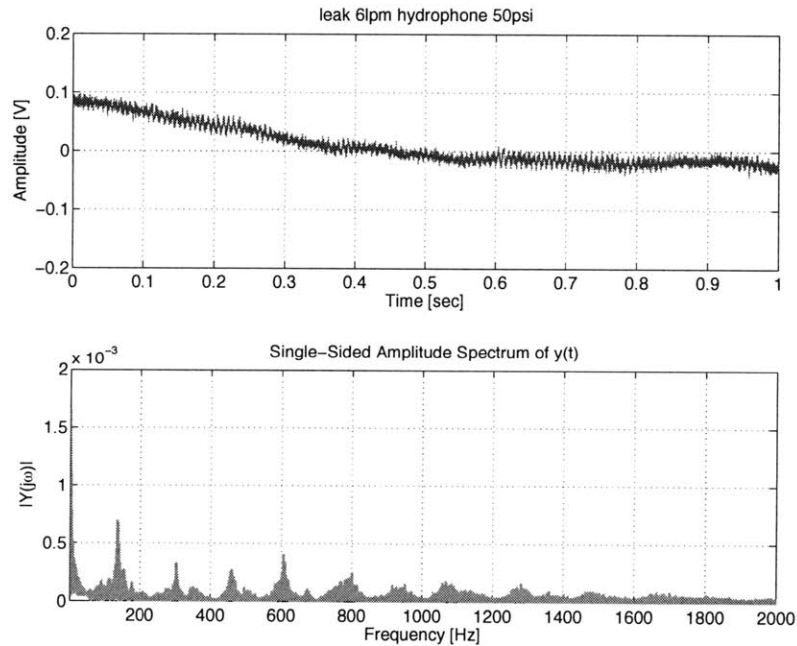
[b] Signal captured by hydrophone

Figure 5-2: Signals captured by [a] DPS and [b] hydrophone for the case of a 14lit/min leak. Pressure in the pipe is 38psi. The time signal as well as the frequency spectrum of each case are shown.





[a] Signal captured by DPS



[b] Signal captured by hydrophone

Figure 5-3: Signals captured by [a] DPS and [b] hydrophone for the case of a  $6\text{lit}/\text{min}$  leak. Pressure in the pipe is  $50\text{psi}$ . The time signal as well as the frequency spectrum of each case are shown.

### 5.3.1 Leak as a PVC Valve

The effect of leak flow rate on the frequency spectrum of the captured signal is given in Fig. 5-4 for leaks of 0, 2, 6, 10, 14, 18.5 *lit/min*, in the case of no pipe flow, using the DPS. Unwanted DC and low frequency ( $< 20Hz$ ) components were filtered out in this figure for the sake of clarity. *The figure alleviates the fact that increasing the leak flow rate increases the magnitudes of peak frequencies and hence the signal power.* Zero leak flow is almost flat with no peaks and is clearly distinguished from case of 2 *lit/min* leak. Some frequencies are more affected by the leak flow rate than others and small shift in the frequency for some peaks is noticed.

The signal diminished sharply for fully opened leak valve at 18.5 *lit/min*. This behavior is directly connected to the leak shape/type and the effect of having a partially or fully opened valve on the induced leak disturbances; which is out of the scope of this thesis. Moreover this phenomenon is also influenced by the fact that the line pressure is very low (10*psi*) for this case (pressure in the pipe drops significantly by fully opening the valve). As we will see thoroughly in the coming sections, a very low in-line pressure results in a very “silent” leak signal. Fig. 5-5 presents the same signal captured by the hydrophone. Same trends are observed even in this case as expected, since the two sensors are able to capture the same signals.

### 5.3.2 Leak as a Circular Hole

By simulating the leak as a circular hole, experiments were conducted with different leak sizes. As mentioned before, holes were drilled on the test section to simulate leaks. Size of the drilled holes ranged from 1*mm* to 6*mm* in diameter.

Each leak size resulted in a different leak flow rate as well as different pipe pressure. This happens because by increasing the leak size, the impedance decreases resulting in a lower pressure in the pipe. This phenomenon is mandated by the conservation of momentum and mass. The maximum static pressure was measured to be 56*psi* in the no-leak-scenario, as shown in Table 5.1. The pressure source, which was the building’s main water supply, had fluctuations in pressure resulting in different flow

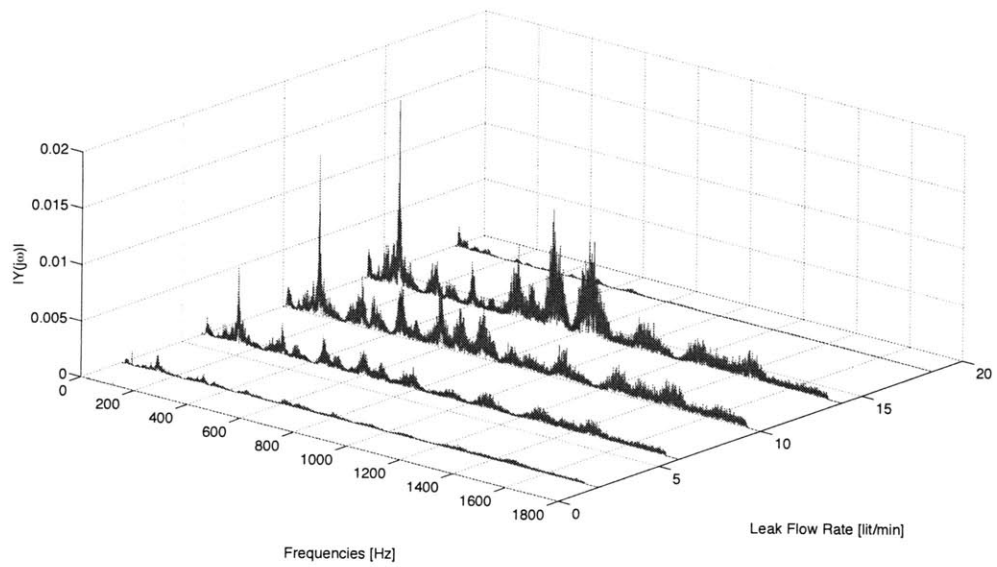


Figure 5-4: The frequency spectra for the signals captured by the DPS for different leak flow rates. The sensor is placed at the leak position.

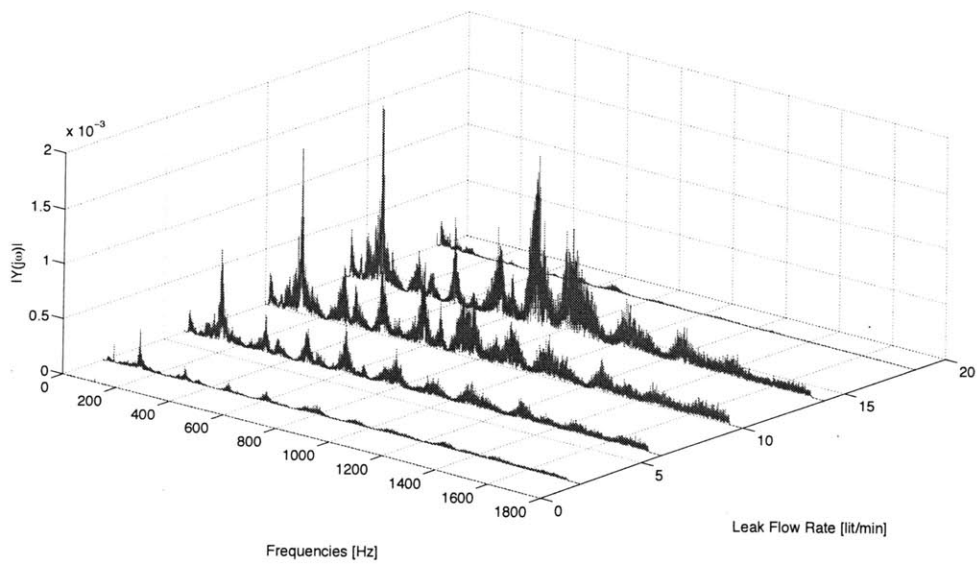


Figure 5-5: The frequency spectra for the signals captured by the hydrophone for different leak flow rates. The sensor is placed at the leak position.

rates even for the same leak size. The averages of those values are summarized in Table 5.1 in terms of both leak flow rates and line pressures.

Table 5.1: Summary of measured leak flow rate and line pressure for different leak sizes.

Leak Size	Leak Flow Rate [ <i>lit/min</i> ]	Line Pressure [ <i>psi</i> ]
no leak	-	56
1mm	0.8	54
2mm	11	44
3mm	12	43
4mm	17	24
5mm	21	21
6mm	23	14

Fig. 5-6 presents the frequency spectrum for the signals captured by the hydrophone for all leak cases. In each case the hydrophone was placed at the centerline of the pipe at the leak section (almost half a pipe diameter away from the leak). The figures show that the signal for the 2, 3, 4 and the 5mm leak size include rich power content in a wide frequency range. On the other hand for the 6mm case, frequency content is limited to 200Hz and power of the signal seems to be limited.

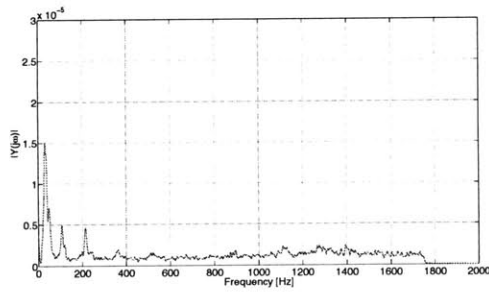
Thus, one can claim that different leak sizes/flow rates and pipe pressures result in a different leak signals with different frequency distributions. 1mm is a very small leak size and thus results in a very “silent” leak signal. This variation in the signal “power” motivated us in trying to quantify this phenomenon and to do so we calculated the power of the time signal.

Power of the discrete-time signal was calculated using:

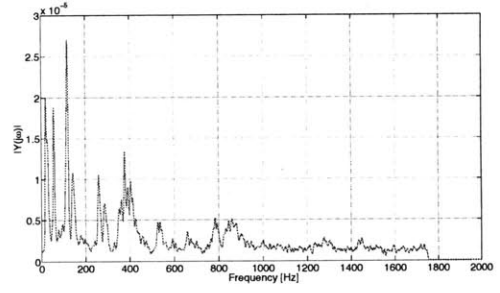
$$Power = \frac{Energy}{\Delta t} = \frac{\sum_{n=1}^N |x[n]|^2}{\Delta t} = \frac{\sum_{n=1}^N |x[n]|^2}{N} f_s \quad (5.1)$$

where  $x[n]$  is the discrete time signal vector in Volts,  $\Delta t$  is the total time of signal acquisition in sec,  $N$  is the total number of elements in  $x[n]$  and  $f_s$  is the sampling frequency in kHz, which in this work is set to be 51.2kHz.

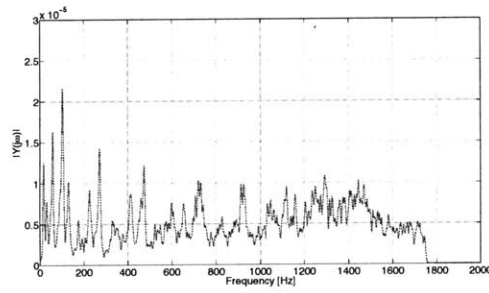
Power of the observed signals is presented in Table 5.2 for all cases. The table



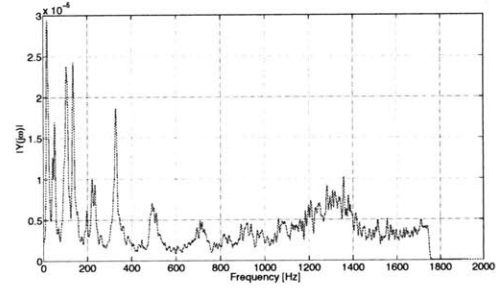
1mm



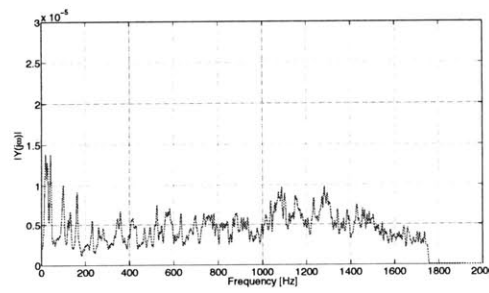
2mm



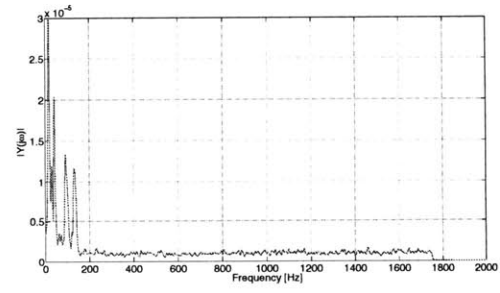
3mm



4mm



5mm



6mm

Figure 5-6: Leak signals for 1mm up to 6mm leak sizes. The frequency spectrum for each case is presented. Leak is open to air.

presents the average values for the calculated signal powers after repeating the experiments 3 times in the same day. Standard deviation is less than 10% of the mean calculated value in each case showing high consistency and repeatability. Frequency spectra of the signals are also similar over different days, which again shows high consistency.

Table 5.2: Signal Power calculation for each leak case. The ratio of each power relative to the no-leak case is also presented. Standard deviation is also presented to show repeatability of signal power.

Leak Size	Signal Power [ $V^2/sec$ ]	STD	Power Ratio
no leak	$1.14 \times 10^{-4}$	5.12%	1.00
1mm	$5.55 \times 10^{-4}$	5.65%	4.85
2mm	$7.33 \times 10^{-4}$	2.50%	6.41
3mm	$2.83 \times 10^{-3}$	8.34%	24.76
4mm	$2.54 \times 10^{-3}$	3.24%	22.22
5mm	$2.36 \times 10^{-3}$	8.72%	20.65
6mm	$9.57 \times 10^{-4}$	8.10%	8.37

By observing the powers of the 1 and 2mm cases one can see that they are of the same order of magnitude as the no-leak case, but still several times higher than that (power ratio is smaller than 10). For 3, 4 and 5mm we get powers significantly higher than the no-leak power, and thus one can trigger an alarm for the presence of a leak. Nevertheless, for the 6mm leak size the signal power decreases again and the ratio is again smaller than 10, because of very low (almost 14psi) line pressure. ***Very low line pressures result in very “silent” leak sounds.***

To calculate the signal power, the time signal was filtered using a digital FIR band-pass filter with cutoff frequencies set at 20Hz and 1800Hz. The lower cutoff frequency was selected to reject low-frequency sensor and network noise, while the latter one to eliminate high-frequency noise. Moreover, there is almost no “energy” in frequencies above this upper limit, since the frequency spectra in these regions look almost flat with no significant peaks. The code in MATLAB that was used for the creation of those filters is given in Appendix C.

To summarize, a *“power metric” of the captured signal is proposed to calibrate the leak detection system by using a reference signal that corresponds to the no-leak scenario.* A leak alarm is signaled by comparing power of the captured signal to that of the reference signal, which is the no-leak signal. In case of in-pipe measurements, signaling an alarm, while avoiding false alarms would be a very challenging task. Thus, careful calibration of the sensor is needed. In this context, one needs to recognize that acoustic signals due to existing leaks (at steady-state) are very likely to be of low power, and may be overshadowed by acoustic energy associated with small turbulence at pipe bends and surface irregularities at different positions.

## 5.4 Effect of Medium Surrounding Pipe

In real underground water distribution network the pipelines are buried in the ground and are surrounded by soil or can also be under a water streamline like a river. Thus, whenever a leak occurs the leak jet will be hitting the wet soil and the water surrounding the pipe rather than be free to air. In this section the results of experiments conducted with different pipe-surrounding media and the effect of these different “boundary conditions” on the leak signal are studied. For the sake of simplicity only the results with the hydrophone sensor are presented. The DPS showed same trends.

Fig. 5-7 [a] presents the test section used for the sand experiments. The figure shows the hydrophone mounted on the sensor-holder and the magnets used to move the sensor along the pipe. The black rubber rings are used to seal existing holes-leaks. Each of these rings was removed to simulate a leak of different size. The tank container that was filled with sand is shown in Fig. 5-7 [b]. Water jet coming out of the pipe was hitting the sand. The same experimental setup was used for the water experiments too; the container was filled with water instead of soil.

Experiments were conducted for the  $4mm$  leak with different surrounding media being air, sand and water and the captured signals are presented in Fig. 5-8. As before, the average line pressure in the system was  $24psi$  for all cases.

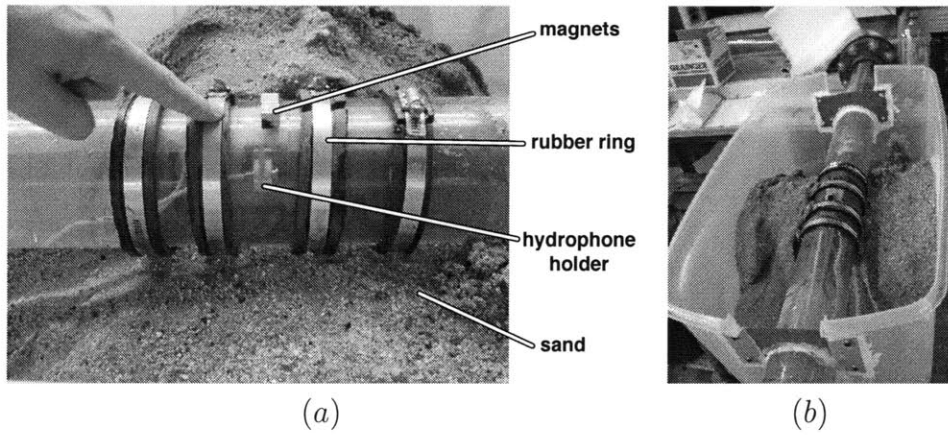


Figure 5-7: The test section for the “sand” experiments. A tank filled with sand was used. Leak jet was hitting the sand at the bottom.

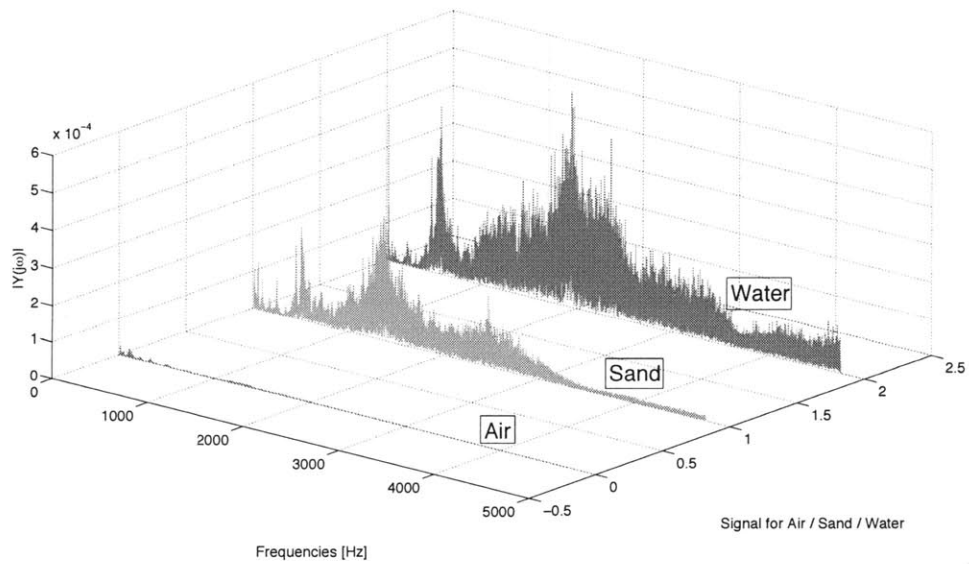


Figure 5-8: The frequency spectra of the leak signals captured in air/sand/water. Green/Air, Orange/Sand and Red/Water. Power of the signal in sand and water is more than the same power for the signal in air. Moreover the frequency spectra is “wider” for those two cases in comparison to the “air experiments”.



It is observed that the signal power is higher for leaks in sand and water than the leak in air. Moreover, the frequency spectrum for sand and water is wider than the corresponding signal for air, where almost all the peaks in the frequency spectrum are confined in the region  $0 - 1800Hz$ . This means that the sound generated by leaks surrounded by sand and water include wider range of frequencies than the signal of the same leak opened to air. Moreover, as it will be presented next the power of the signal for different surrounding media is much higher.

Table 5.3 presents the signal power calculation for the no-leak, leak in air, sand and water cases. The ratio of each case with respect to the no-leak scenario is given for comparison. ***It is observed that the power of the leak signal is the highest in water followed by the signal in sand.*** Again the results are repetitive in 5 runs within a day showing high repeatability (standard deviation is less than 10% of the average value for each case).

Table 5.3: Signal Power calculation for each leak case. The ratio of each power relative to the no-leak case is also presented.

Case	Signal Power [ $V^2/sec$ ]	Power Ratio
no leak	$1.14 \times 10^{-4}$	1.00
Air	$2.54 \times 10^{-3}$	22.22
Sand	1.35	11810
Water	4.78	41816

The time signal was filtered using a digital FIR band-pass filter with cutoff frequencies set at  $20Hz$  and  $1800Hz$  for the air-case and with cutoff frequencies set at  $20Hz$  and  $4800Hz$  for the sand and water cases.  $4800Hz$  was used as the upper cut-off frequency since it was observed that the leak signal for water and air has broader spectra and that there is almost no content in the region above almost  $5000Hz$ .

***It can be claimed that the “power-metric” discussed so far can be used as a reliable technique to identify leaks in sand or water compared to the leaks in air.*** Leaks in water or sand are closer to the “real-world” scenario, since pipes are buried underground and are surrounded by wet sand in the presence of leaks. As seen from Table 5.3 the ratio of powers “explodes” for the sand and water

cases when comparing it to the reference signal, namely the no-leak case.

To sum up, we found out that even though a 4mm hole was easily being detected by leaking into air just by comparing it to the no-leak case, the same hole creates a more “noisy” signal that can be captured by the hydrophone when leaking into either water or sand. ***This results in a signal with significantly more power and thus a leak that can be detected even easier by a moving sensor from the inside of a pipe.*** Calculating signal power and comparing it to the reference signal can be a very promising technique for accurate leak detection in underground buried pipes.

## 5.5 Effect of Pipe Flow

The case of no pipe flow represents a good test on sensors sensitivity and the effect of leak flow rate. However, a leak detection system inside a real pipe network will be exposed to the actual conditions of line pressure and flow. One may guess that it will make a big difference on the acquired leak signal.

Fig. 5-9 shows the effect of having pipe flow (10lit/min was selected for demonstration) on the frequency spectrum, using the hydrophone. This flow velocity is very low for a 100mm pipe; however, it has a great effect on the signal captured by the sensor. The wide frequency spectrum for the no pipe flow case has turned to only few peaks at low frequency range ( $< 400Hz$ ). A noticeable shift in peak frequencies between the two cases is also clear. A more general picture for the effect of pipe flow rate at a given leak flow rate is presented in Fig. 5-10. The leak flow rate is kept constant at 8lit/min while the main pipe flow rate is changed from 0 to 14lit/min. ***As the ratio of pipe flow to leak flow increases; particularly when  $Q_{pipe}/Q_{leak} > 1$ ; the leak signal is diminishing and only the low frequency components remain.*** Although the pressure was not kept constant for these cases due to setup limitations, this may be attributed to the tradeoff between acoustic power reflection and power transmission across the leak, as the amount of power transmission along the main pipe would be relatively larger at higher volume velocities. It should be

mentioned here that the no leak signal for the same pipe flow condition is negligible and almost flat in almost all frequency range.

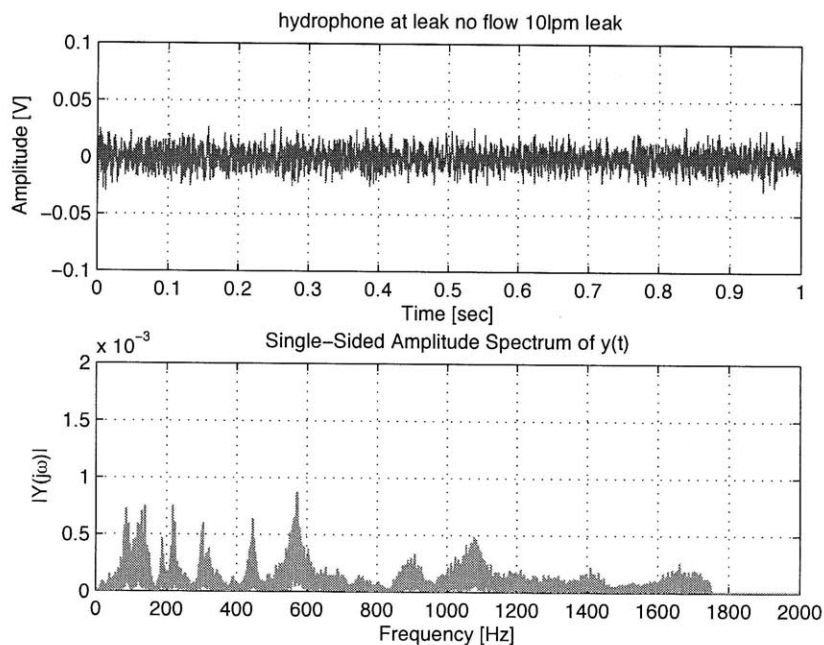
As complementary information, Fig. 5-11 presents the effect of leak flow rate on the frequency spectrum for the case of pipe flow of  $8\text{lit}/\text{min}$ . Again, unwanted DC and low frequency ( $< 20\text{Hz}$ ) components were filtered out in this figure for the sake of simplicity. All tested leak flow rates had distinguished signatures on the frequency spectrum, compared to the no leak case, indicating the ability of the sensors to detect very small leaks under these conditions of pipe flow.

To signal a leak alarm, in general, one must have a reference signal profile of the healthy pipeline (no leak situation). In the case of in-pipe measurements, signaling an alarm, while avoiding false alarms is the most challenging task. Thus, the development of proper detection algorithms as well as proper signal processing methods is necessary at this point. For instance, the difference between a side branch and a leak port may become indistinguishable. Acoustic signals due to existing leaks (at steady-state) are very likely to be of low power transmission. Again, the need for careful calibration of the sensor is pointed out.

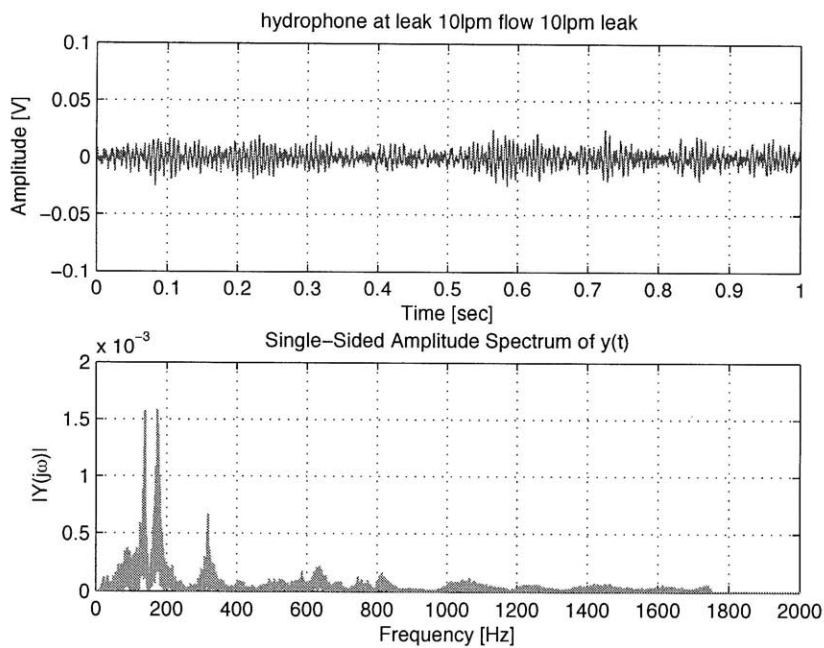
Fig. 5-12 shows the calculated power of the time signal for both cases with and without pipe flow, at different leak flow rates. The power of the signal is increasing for increasing leak flow rate (exception is the fully open valve case, which is not included in this figure). Similar trends using hydrophone and DPS were found. *Flow rates above  $2\text{lit}/\text{min}$  can be detected easily by calculating the signal power and comparing it to the reference signal of no leak.*

## 5.6 Effect of Sensor Position

In this section the effect of sensor position with respect to the leak position on the leak signal will be presented. The final goal is to design a mobile sensor that will be able to detect leaks in water distribution networks. Hence it is important to understand the effectiveness of our sensors in sensing for leaks with the variation of distance from the leak.



[a] No pipe flow; Leak Flow rate = 10lit/min



[b] Pipe Flow 10lit/min; Leak Flow rate = 10lit/min

Figure 5-9: Effect of having pipe flow on frequency spectrum - sensor used: hydrophone

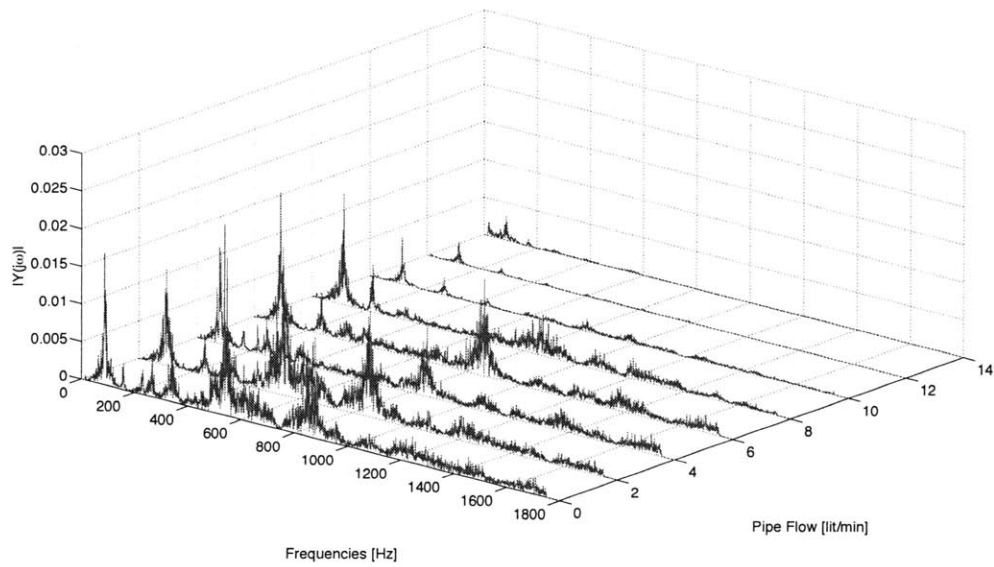


Figure 5-10: Effect of pipe flow rate on leak signal for constant leak flow rate of  $8\text{lit}/\text{min}$  - sensor used: DPS

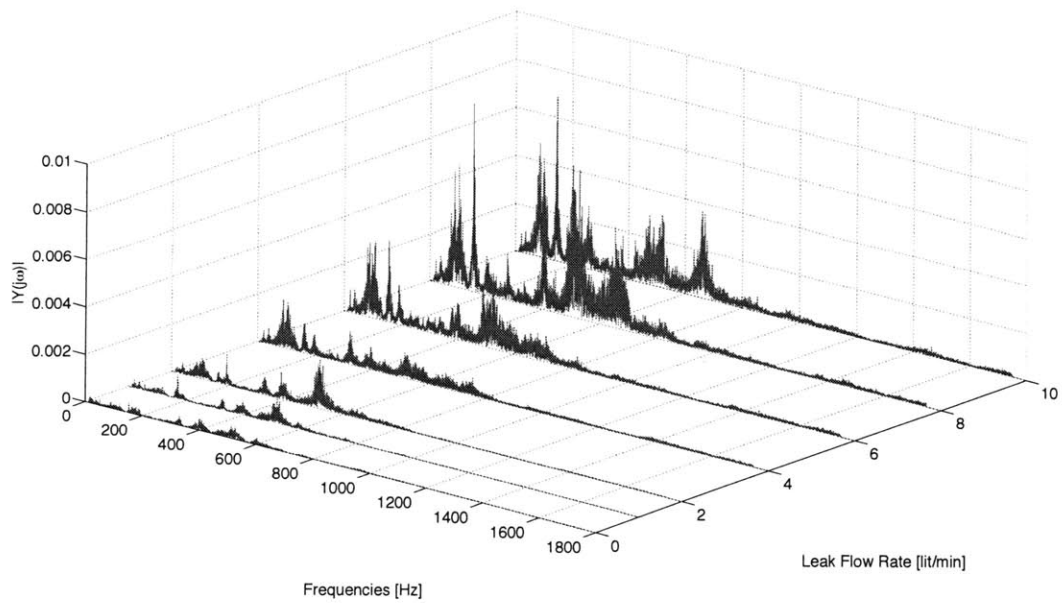


Figure 5-11: Effect of pipe flow rate on captured signal; pipe flow  $8\text{lit}/\text{min}$  - sensor used: DPS

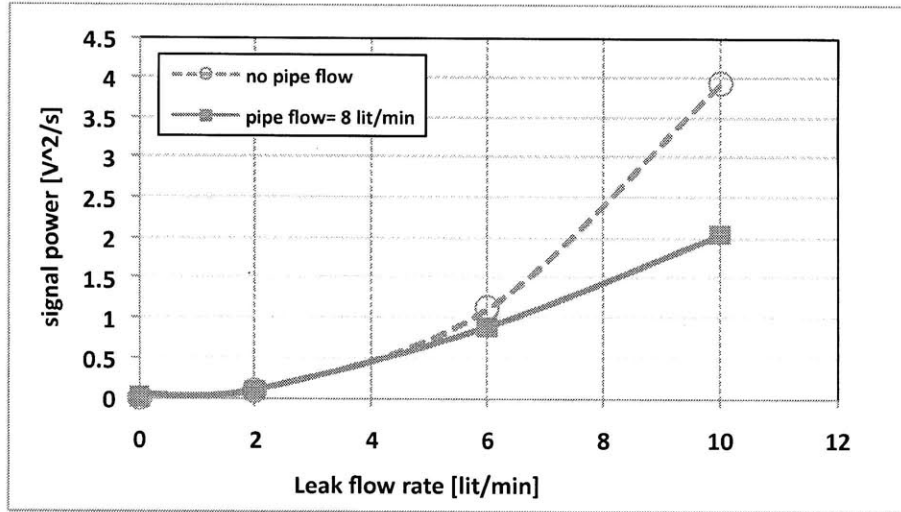


Figure 5-12: Calculated power of leak signal with and without pipe flow - sensor used: hydrophone

For this study the location of the hydrophone was changed to 7 different locations along the pipe upstream and downstream of the leak. The origin was set at the leak position (0), the 3 different upstream positions were (-5", -10" and -15") and the 3 downstream positions were (+5", +10" and +15"). The results for experiments in water for a 4mm leak are presented; the experiments in air and sand show similar variations.

Fig. 5-13 presents the frequency spectra for the signals captured at all 7 positions along the pipe. It is observed that the signal captured when the hydrophone was at the leak position has the highest power. Signal seems to be more clear and "strong" upstream, rather than downstream. Moreover, measurements taken upstream had rich frequency content in the range 900 – 1550Hz, while signals at the leak position had a wide spread of frequencies ranging between 400 – 3500Hz. The case is completely different for measurements taken at downstream locations. The power of the signal is less and peaks are in completely different locations. It is believed that these differences in the signal characteristics can be explained by the directional "anisotropic" characteristics of the sensor.

In order to quantify this variation in the signal the power was calculated again and is presented in Table 5.4 .

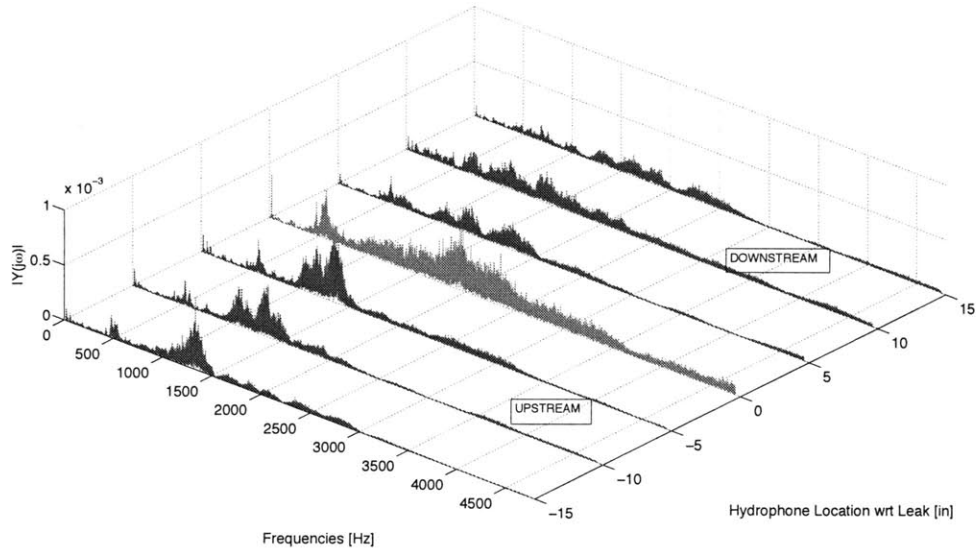


Figure 5-13: Frequency spectra for signals captured for 4mm leak; Pipe is surrounded by water and the hydrophone was placed at different positions upstream and downstream of the leak location.

Table 5.4: Power calculations for various positions upstream, downstream and at leak position

Position	Signal Power [ $V^2/sec$ ]
15" upstream	0.99
10" upstream	1.34
5" upstream	2.40
at leak	4.78
5" downstream	1.33
10" downstream	0.93
15" downstream	0.52

From the measurements we can conclude that the sensor position affects the leak signal significantly. *However the “power metric” of the signal can be used to identify a potential leak easier upstream than downstream since power of signal is higher in this region and seems to decay slower with distance. But the effectiveness of the sensor is maximum at the leak and in the proximity of the leak as expected.*

## 5.7 Chapter Summary

In this chapter the experimentation with different sensors under different conditions is described. A hydrophone and a DPS were used for leak detection, while leaks were simulated either by a plastic valve in the system or by circular holes on the pipe walls.

After experimentation we concluded that both the hydrophone and the DPS produce the same signal, even though they are mounted differently in the system. Another significant result is that the leak size and flow rate affect the captured signal's signature and power.

We proposed the use of a metric, namely the signal power, for leak detection. By calculating the power of the time signal and comparing it to a reference signal of a "healthy" pipe we can detect and identify the presence of a leak in the pipeline. This is supported by the fact that a leak on a pipe buried underground creates acoustic signals of high power. This happens because the leak jet is directly hitting water or soil.

Results on pipe flow are also presented, showing that as the ratio of pipe flow to leak flow increase the leak signal is diminishing and only the low frequency components remain. Finally, leak signal seems to be stronger upstream rather than downstream. Nevertheless the signal power is maximum at the leak and in the proximity of the leak, where the sensor has better chances to pick it up.

The work presented in this chapter is also published in [20] and [21].



# Chapter 6

## Mobility Module - Design

### Characteristics

#### 6.1 Introduction

This chapter discusses the second subsystem of our mobile floating sensor, namely the “Mobility Module” and shows the design of the latest prototype as well as the evolution of the design process by presenting some earlier prototypes.

#### 6.2 Functional Requirements

We may start this discussion by listing some of the most important functional requirements for the mobility module:

- *Size*: The mobility module has to be able to detect leaks in concurrent water networks. Distribution water pipes of the size of  $100mm$  are of our interest in the present work since this is a very common size in most water networks.
- *Complicated Pipeline Configurations*: The system will be able to travel not only in straight pipes but also in more complicated parts such as pipe bends. To cope with even more complicated parts like pipe branching, the body design may need some modification, e.g. add more modules together via flexible joints.

- *Free Floating:* The module is going to passively float inside the pipe with a speed  $V_m$ , smaller or equal to the speed  $V_w$  of flowing water.
- *Shape:* The module’s external hull needs to be carefully designed to be “non-invasive” to the flow. This means that the effect of the existence of the module in the pipe on the leak signal is negligible or minimum.
- *Stability:* The module needs to be able to stabilize itself within the pipe to avoid induced turbulence and noise and avoid hitting the walls while floating.
- *Speed Control:* The module has to be able to control the floating speed  $V_m$  in a smart and efficient way. Reducing the module speed may be needed for fine or accurate leak detection at “suspicious” locations. This requirement was not considered in the current design.

## 6.3 Mobility Module Design

### 6.3.1 Design Overview

The 2D front and side views of the external hull of the mobility module is shown in Fig. 6-1. The 100mm ID pipe has also been drawn for referencing. One should be able to notice the main body as well as the “stabilizing” legs that stick to the pipe wall. The three legs on each side of the module are placed in equal distances between one another at angles of  $120^\circ$ . The black “nose” at the front part of the main body represents the sensing element (dps or hydrophone). The 3D solid model is presented in Fig. 6-2 with some explanation about the different parts. A 3D model of the module inside a pipe is shown in Fig. 6-3.

In this design the module is “sliding” passively along the pipeline. It is important to notice the attached sliders (ball slides) at the upper end of each leg. Those ball slides impose a point contact between each leg and the inner pipe wall. Thus, the module is supported by a total of six contact points.

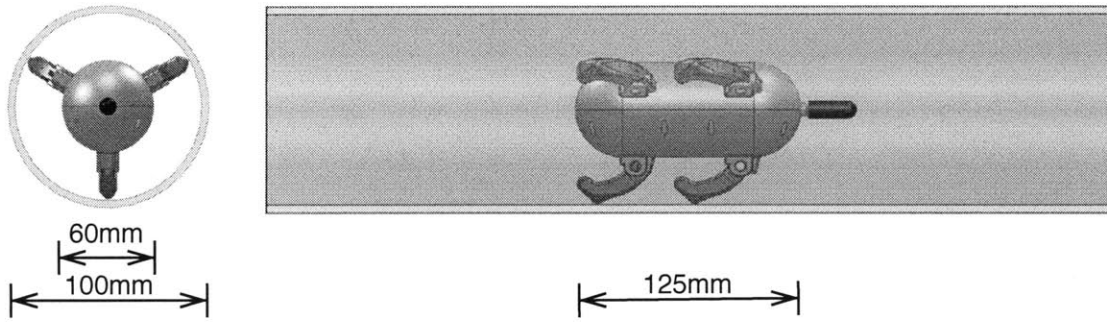


Figure 6-1: The design of the mobility module. [Left] Front View. [Right] Side view.

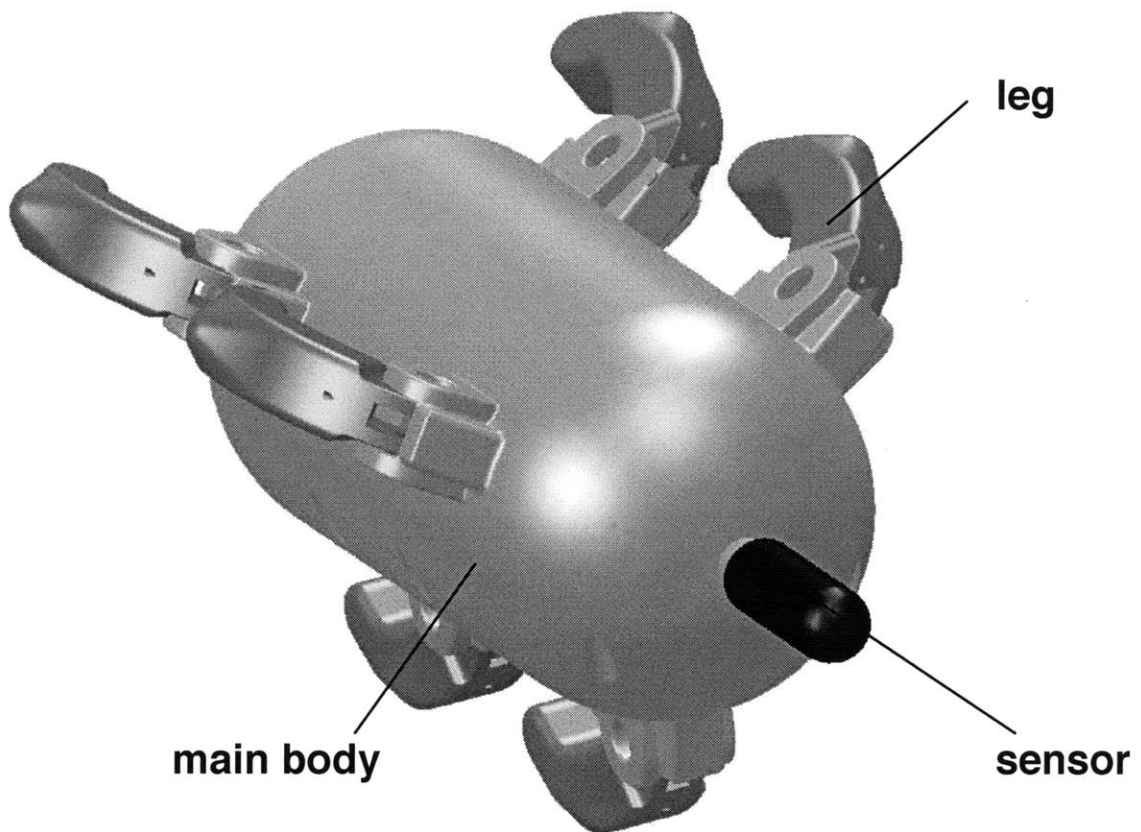


Figure 6-2: A zoom in the mobility module's solid model. Explanation on different parts is sketched.



Figure 6-3: The 3D solid model of the mobility module. Model is shown inside a 100mm pipe section.

The six legs are used for the module’s stability and speed control. First, they provide the required support and stability to the module. Instability of the module would cause it to hit the walls and corrupt the signal captured by the sensor. Secondly, they provide some friction force, somehow controllable, and as discussed in section 7.2.3, this force can be used to “control” the speed of the module.

For this work the legs are completely passive. They are supported by torsional springs and thus add some compliance to the support of the mobility module. The legs are able to pivot about the rotate point and thus compensate for smaller or larger diameters inside the nominal 100mm pipe diameter. For future designs the legs will be actuated actively to add controllability to the system.

Each leg is carefully designed to compensate for “sharp edges” inside the pipelines. By “sharp edges” we mean rapid changes in the diameter size. In connections, unions and in general in the interface between different parts of the pipe network sharp edges may be present. To be able to travel along those the module needs to be able to compensate for those rapid changes smoothly without interrupting its movement.

The main body was designed taking into account the sizing considerations that are presented later in section 7.2.1 and the choice of the streamlined body shape is justified in section 7.3. The position of the sensor as well as the legs are also justified in the same section.

The different parts for this module were 3D printed using ABS plastic on a *Dimension SST 2300* printer. The 3D printed leg prototype is presented in Fig. 6-4, while the rest of the parts is shown in Fig. 6-5, 6-6. All different parts are presented together in Fig. 6-7. The assembled prototype is presented in Fig. 6-8.

### **6.3.2 Earlier Versions Overview**

Previous designs included disadvantages and flaws and could not compensate all the requirements set in section 6.2. To reach the point of designing and prototyping the module shown in section 6.3.1 many other prototypes were designed, manufactured and tested, some of which will be presented in this section.

One of the early prototypes is shown in Fig. 6-9. This was our third prototype

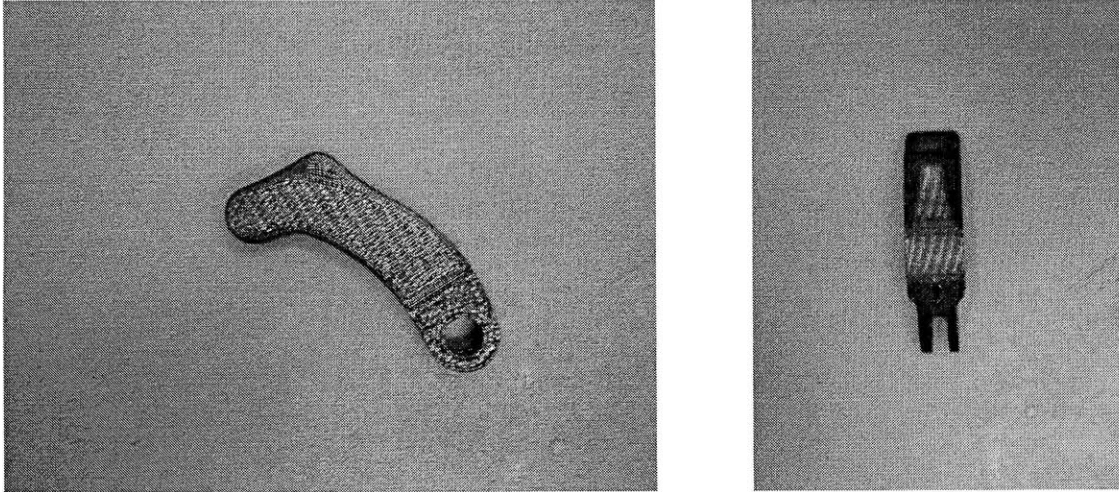


Figure 6-4: The 3D printed prototype of the leg. Material is ABS plastic.

and includes almost the same main body and only 3 legs. Each leg was equipped with two wheels to allow moving along the pipe walls. The module is totally unstable and in case the force acting on the module to push it forward is slightly eccentric the module becomes unstable and the legs lose contact with the walls.

To improve the design we tried to increase the length of contact. To do that we put the two wheels of each leg further apart. The legs remained three and we developed our next prototype, shown in Fig. 6-10. Still, the module was unstable.

We concluded that three legs are not enough to support the module inside the pipe. Thus, our next prototype had six legs as shown in Fig. 6-11. Six legs provide the required stability inside the pipe as expected.

Various changes took place after prototype #6 to reach the form of the final one. Those included changes in the design of the legs to compensate for “sharp edges” along the pipeline, in the orientation of the legs, using sliders instead of wheels and impose point contact among each slider, etc.

## 6.4 Chapter Summary

In this chapter the functional requirements of the mobility module are presented. The design and manufacturing of the latest prototype is shown. This last prototype meets

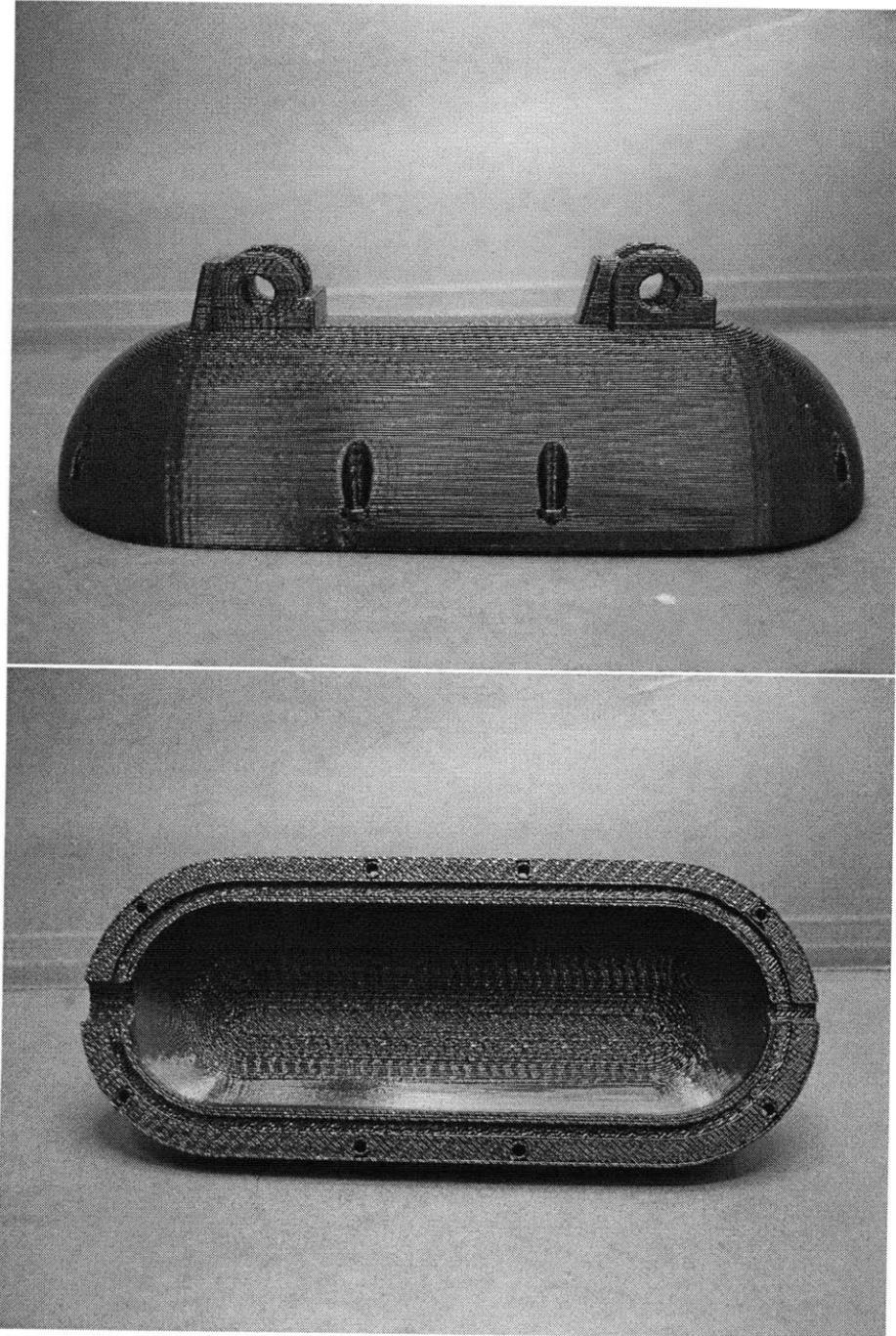


Figure 6-5: The 3D printed prototype of the upper part of the external hull. Material is ABS plastic.



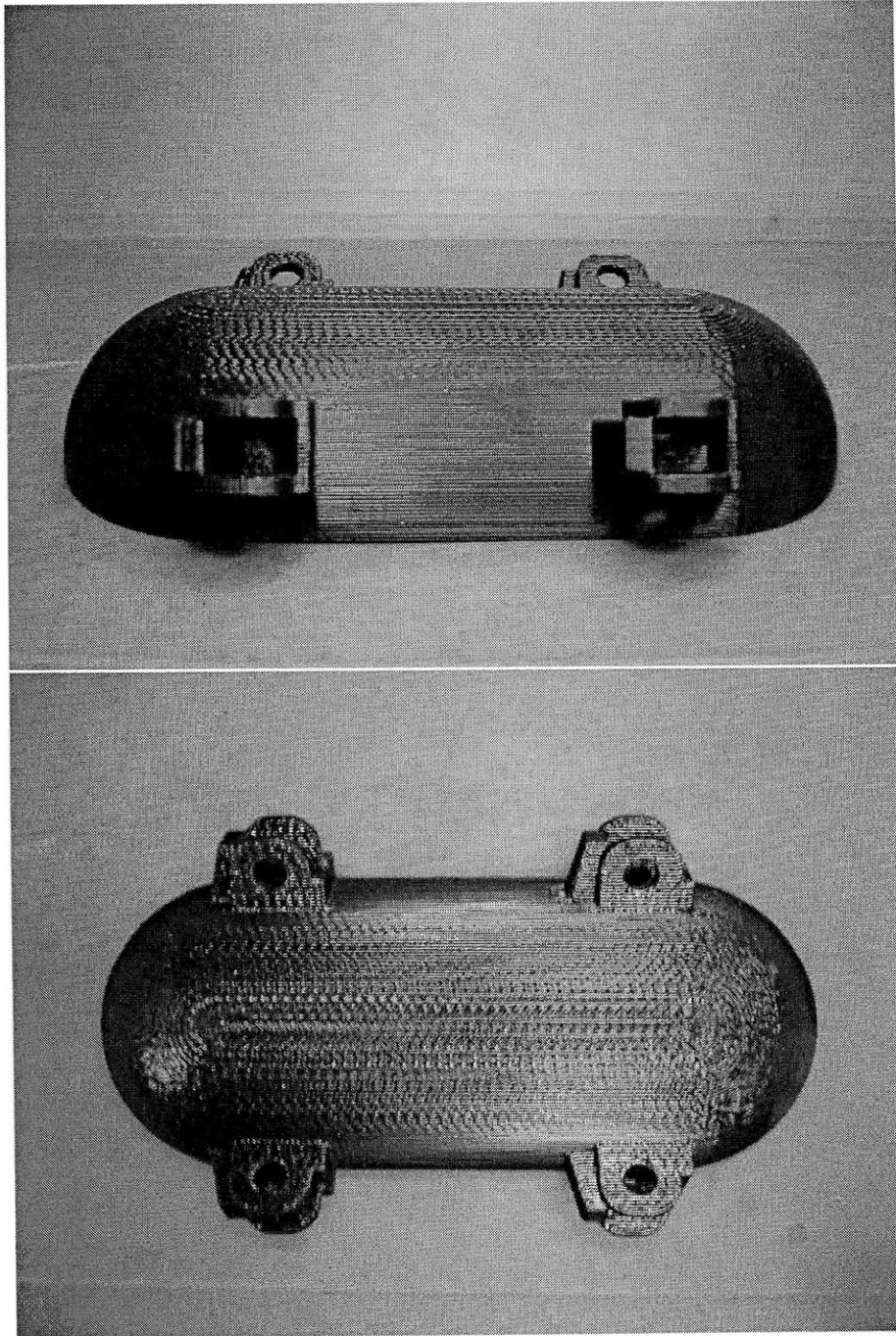


Figure 6-6: The 3D printed prototype of the lower part of the external hull. Material is ABS plastic.



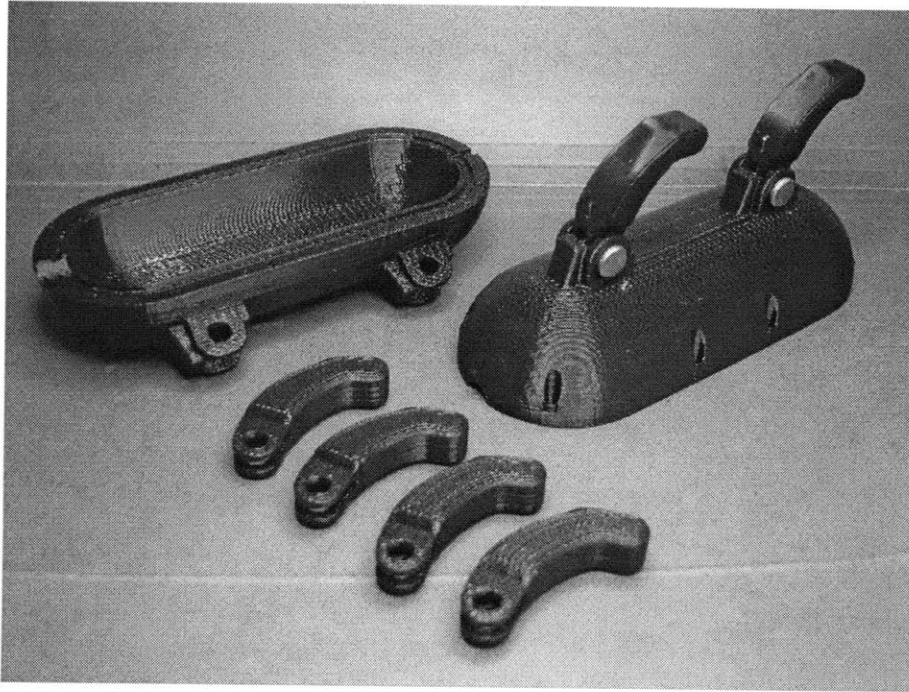


Figure 6-7: The 3D printed parts of the mobility module. Material is ABS plastic.



Figure 6-8: The assembled mobility module.

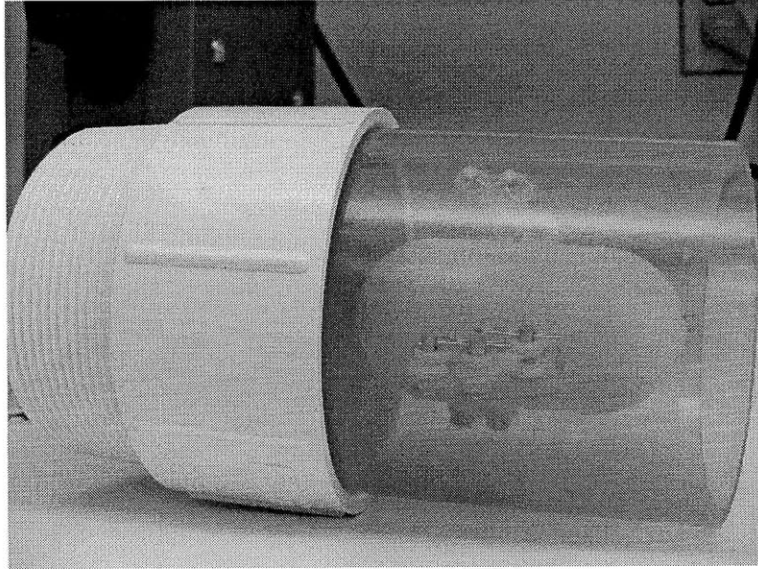


Figure 6-9: The prototype # 3.

all functional requirements set earlier. On the contrary this was not the case with some older prototypes that are presented in the last part of the chapter to show the evolution of the design process.

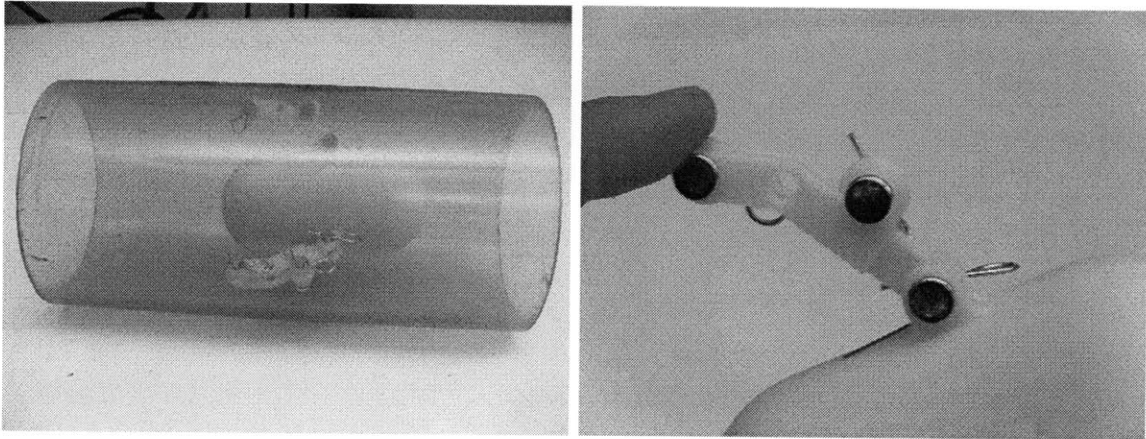


Figure 6-10: The prototype # 4. The module inside the pipe is shown in the left figure. The details of the leg are presented in the right figure.

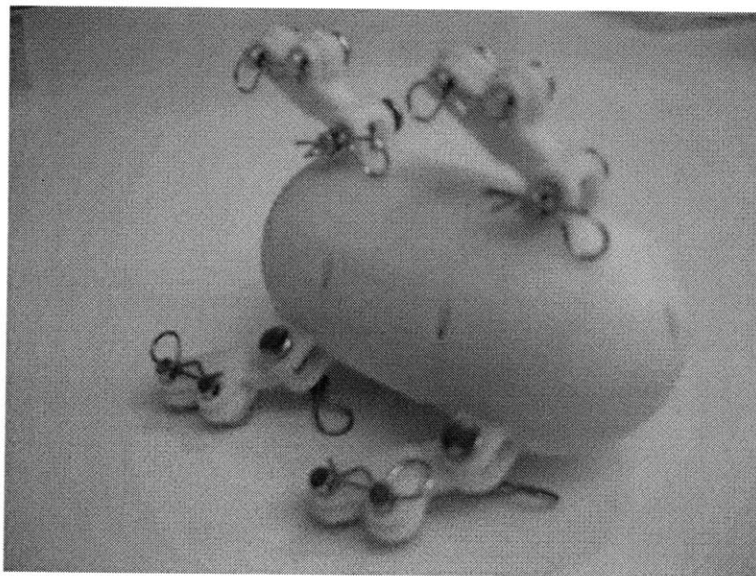


Figure 6-11: The prototype # 6.



# Chapter 7

## Mobility Module - Analysis

### 7.1 Introduction

In this chapter the analysis of the mobility module will be presented. Size considerations, DoF inside the pipe, motion as well as CFD analysis for the mobility module are presented in this section to support the design we selected and presented in the previous chapter.

### 7.2 Analysis

#### 7.2.1 Size Limitations

The main challenge in the design of the mobility module is the fact that this module will host all other instrumentation and equipment, while at the same time it needs to be as small as possible in order to satisfy all space limitations within a very strict pipe environment. The simplest limitation that one could think of is that the system's diameter or width should be no more than the pipe's ID, which in this case is  $100\text{mm}$ . However the sizing of the module depends not only on the pipe ID but also on the pipe geometry.

Let's now consider that the mobility module has a cylindrical shape with diameter  $H$  and length  $L$ . Consider the case when the module tries to pass a  $90^\circ$  bend of an

angle  $2\theta$  as the case shown in Fig. 7-1. The projection of the body in the plane will look like a rectangle with dimensions  $H$  and  $L$ .

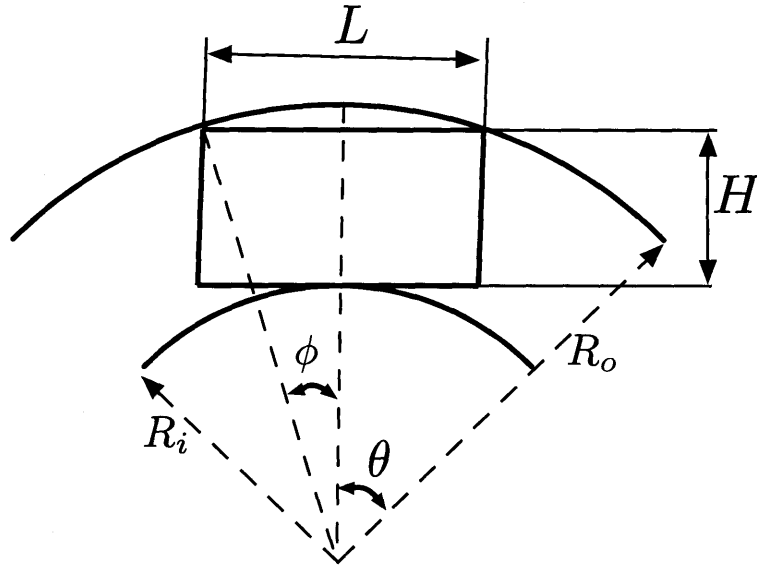


Figure 7-1: A 2D sketch of a cylindrical mobility module inside a bended pipe.

If  $R_i$  and  $R_o$  represent the inner and outer diameters of the bend then by trigonometry we can get:

$$L = 2R_o \sin \phi$$

or simply calculate the enclosed angle  $\phi$  as a function of  $L$ :

$$\phi(L) = \arcsin(L/2R_o) \quad (7.1)$$

The following equation also holds:

$$H_{max}(L) = R_o \cos[\phi(L)] - R_i \quad (7.2)$$

Note that the angle  $\phi$  is a function of the length  $L$ .

Eq. (7.1),(7.2) can be used to calculate the angle  $\phi$  and the maximum height  $H$  given the length  $L$  as well as the pipe dimensions, namely  $R_i$  and  $R_o$ . Most water pipes use  $R_i < 0.5D$ , while at the same time we can write:  $R_o = R_i + D$ . As

an example we present here the case where:  $R_i = 25mm$  and  $R_o = 125mm$  (So  $D = 100mm$ ). Fig. 7-2 shows the curve of the maximum allowable  $H_{max}(L)$  over  $L$  for the given pipe dimensions.

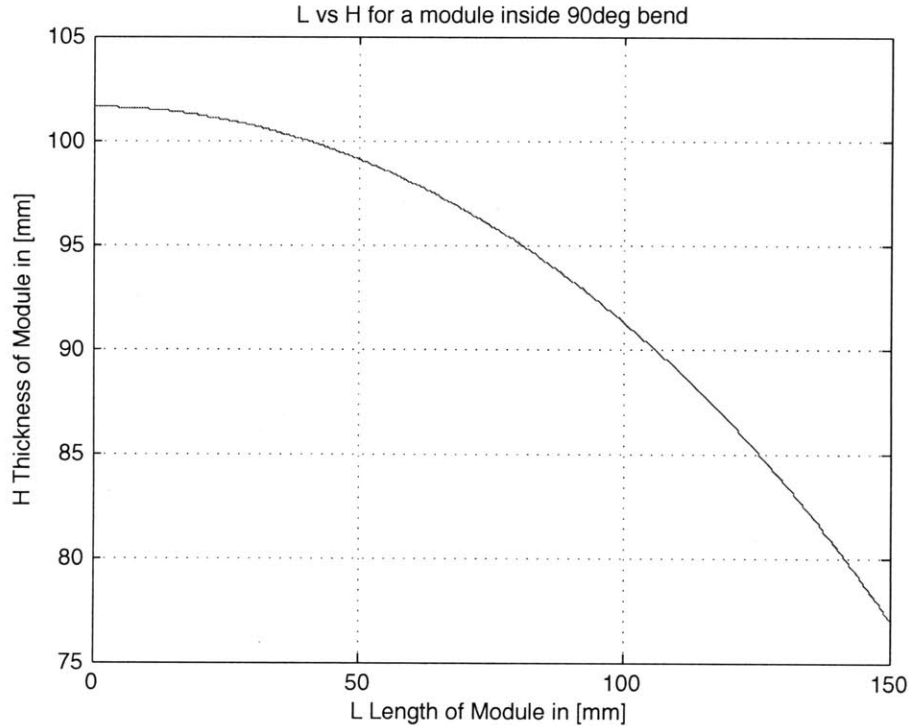


Figure 7-2: Maximum allowed thickness  $H_{max}$  of the mobility module for a given length  $L$ .

As indicated in Fig. 6-1 the module's length is  $125mm$ . Eq. (7.1,7.2) imply that the height should be less than  $85mm$  in order for the system to be able to "fit" in bends and also T-junctions. In our design we took this fact into consideration when sizing the different parts. Moreover, our module is not of an exact cylindrical shape since we avoided to include sharp edges in our design.

### 7.2.2 Degrees of Freedom

The position and orientation of a body in 3D space can be described by six parameters. Thus, the autonomous in-pipe leak detection system traveling within a pipe can also be totally characterized by six parameters as well. We will call them Degrees of Freedom (DoF) for the rest of this chapter.

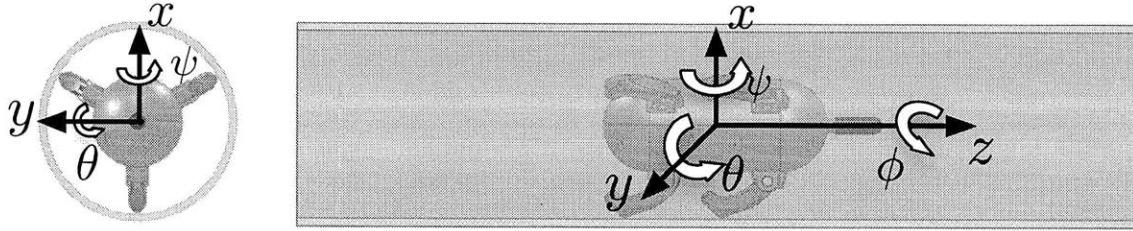


Figure 7-3: The design of the mobility module. [Left] Front view. [Right] Side view.

We chose the following coordinates to fully describe the orientation and position of the system inside a pipeline:

$$\begin{bmatrix} x \\ y \\ z \\ \phi \text{ (roll)} \\ \theta \text{ (pitch)} \\ \psi \text{ (yaw)} \end{bmatrix}$$

Fig. 7-3 shows the DoF of the system within a pipe. In order for the system to be able to travel along the  $z$ -axis smoothly, some DoF need to be constrained. Those are  $x, y, \theta$  and  $\psi$ . The constraint of the  $\phi$  coordinate is not considered crucial at this point. Of course there is no constraint set on the  $z$  coordinate.

To summarize one can see that the current design and placement of the stabilizing legs offer the required constraints to the  $x, y, \theta$  and  $\psi$  coordinates. Thus, the system is always placed in the middle of the pipe section and travels smoothly along the  $z$  direction collinearly to the longitudinal axis of the pipe.

### 7.2.3 Motion

The legs attached to the module can be used for controlling its speed but also for “anchoring” the module in place, i.e. forcing the module’s speed to go to zero ( $V_m \rightarrow 0$ ). This is extremely important when the system needs to have some more time to “sense” (or listen) to a leak or even if the system needs to transmit a large package of data to the receiver above ground. In this case “anchoring” may be the best option.



If the body is floating passively with speed  $V_m$  in a pipe where water is flowing in the same direction with speed  $V_w$ , then the relationship  $V_m \leq V_w$  holds, as implied in Fig. 7-4. By controlling the position of the legs, e.g. via step motors, it is possible to control  $V_m$  and also force  $V_m \rightarrow 0$ .

By using a reference frame that is moving with the body, the mobility module seems to be stationary, water seems to flow with the relative speed  $V_{rel} = V_w - V_m$  and pipe seems to be moving to the left with a speed of  $V_m$ , see Fig. 7-5. This analysis is used for force calculations and later for flow (CFD) simulation of the body motion inside the pipe.

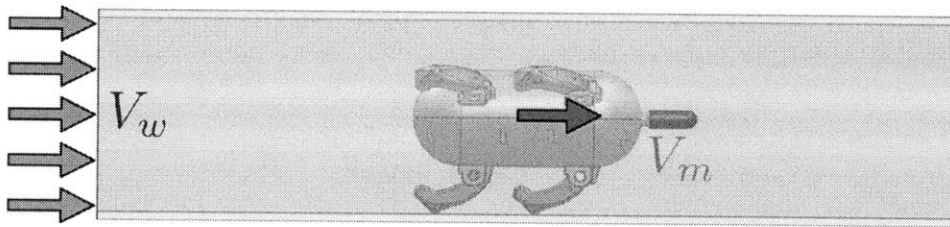


Figure 7-4: Body is floating within the pipe with speed  $V_m$ , while water speed is  $V_w$ .

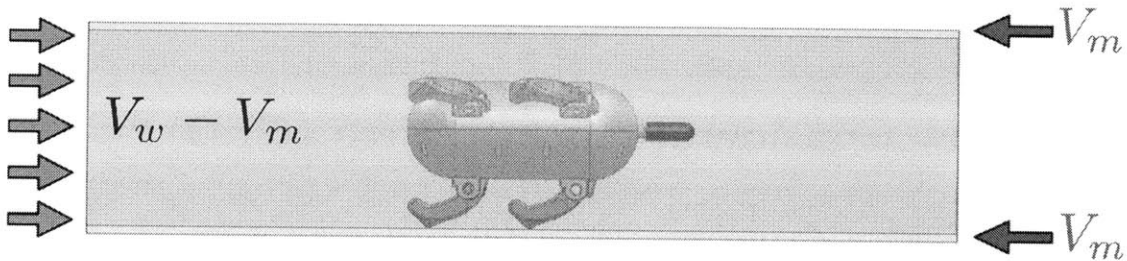


Figure 7-5: Body can be considered to be stationary in this case and water is flowing at a lower speed, namely  $V_{rel} = V_w - V_m$ . Notice that in this frame of reference the pipe wall is also moving with  $V_m$ .

The total drag force can be computed from:

$$F_D = 0.5C_D\rho AV_{rel}^2 \quad (7.3)$$

where  $V_{rel} = V_w - V_m$  is the relative velocity,  $C_D$  the drag coefficient of the module,  $A$  the reference area,  $\rho$  the density of water.

To withstand this force and control its speed, the module itself is applying another force, on the opposite direction, by using the 6 legs utilizing friction. Let this force be  $F_{legs}$ .

A force balance on the body will give:

$$m\dot{V}_m = 0.5C_D\rho AV_{rel}^2 - F_{legs}$$

which leads to the differential equation:

$$m\dot{V}_m = 0.5KV_m^2 - KV_wV_m + 0.5KV_w^2 - F_{legs} \quad (7.4)$$

where:  $K = C_D\rho A$  is a constant. Notice that  $m$  represents the mass of the mobility module.

Eq. (7.4) is a nonlinear differential equation of  $V_m$ . We can consider the force  $F_{legs}$  as the “input” to the differential equation, or else the “control variable”. Typical responses of the system are shown in Fig. 7-6 for different values for  $F_{legs}$ . One should notice from the response that by applying a different friction force with the legs the system is able to ”control” its steady state speed value.

### 7.3 Flow Considerations in Design (CFD)

As mentioned before, the mobility module is to be deployed in the pipe and will travel with the flow. A floating body inside the pipe network can be considered as an invasive method to leak detection. Nevertheless, the current design has been selected to minimize the effect on the flow pattern, pressure distribution and potential leak

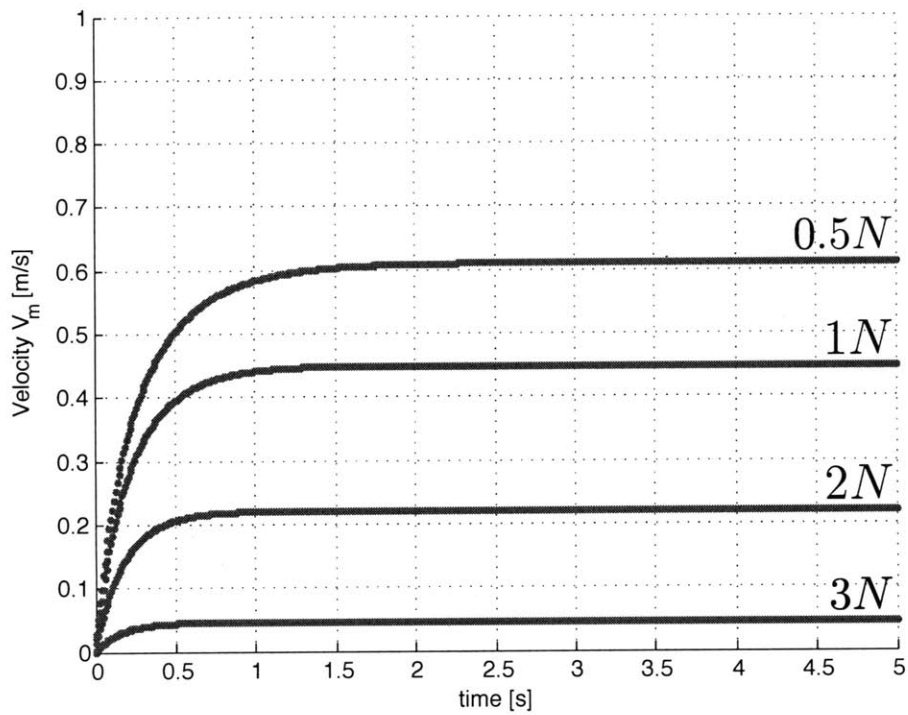


Figure 7-6: The response of the system's velocity for the following values:  $V_w = 1m/s$ ,  $m = 1kg$ ,  $C_D = 0.4$ ,  $A = 0.0165m^2$ ,  $\rho = 998kg/m^3$  and the initial condition is:  $V_m(0) = 0m/s$ . The response is presented for different values of  $F_{legs}$  varying from 0.5 to 3N. Notice that by applying larger friction forces through the legs, the module travels with smaller speeds and can even “anchor” itself ( $V_m = 0$ ).

signals by the presence of the mobility module.

To study the flow pattern around the body inside a  $100mm$  pipe, various computational fluid dynamic simulations have been performed with the *ANSYS CFD* package (*FLUENT*). Steady state 3D turbulent flow simulations have been used to study the flow field, the pressure distribution around the body, velocity vectors and the calculation of drag coefficient. The standard k-e model is used for turbulence and the inlet velocity and pressure outlet boundary conditions are applied. Only the flow around the external hull is simulated excluding the legs and sensor nose. This was done intentionally for simplicity since small effect of the legs and sensor nose is expected due to their small size and smooth design. Besides, the initial simulation results may lead to a good conclusion as where we should attach the sensor and the legs to the floating module and their optimum sizes and shapes.

This is of great significance, since the sensor needs to be able to capture the unaffected leak signal without disturbing the flow and superimposing any interference to the leak signal. This is because the sensing element is a very sensitive dynamic transducer searching for very low amplitude acoustic signals.

### 7.3.1 CFD Meshing

For the CFD study a simplified mobility module has been modeled. Nevertheless, the “model-body” and the original mobility module look almost the same and have the same dimensions.

The meshed model we used for the simulation is presented in Fig. 7-7. The inlet and outlet sections are presented. The mesh on the mobility module’s wall is also shown. A  $100mm$  ID pipe of length  $2m$  was modeled for the analysis. The mesh of the whole fluidic section is shown in Fig. 7-8.

Some characteristics of the mesh are presented in Table 7.1.

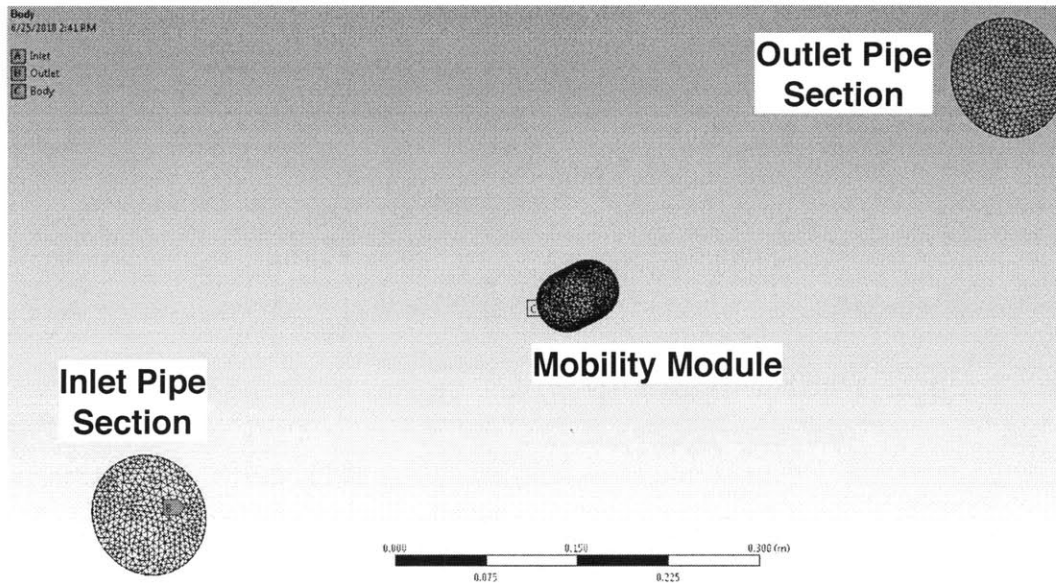


Figure 7-7: The mesh used for the CFD analysis on the mobility module. The mesh on the inlet, outlet sections as well as the floating body is presented.

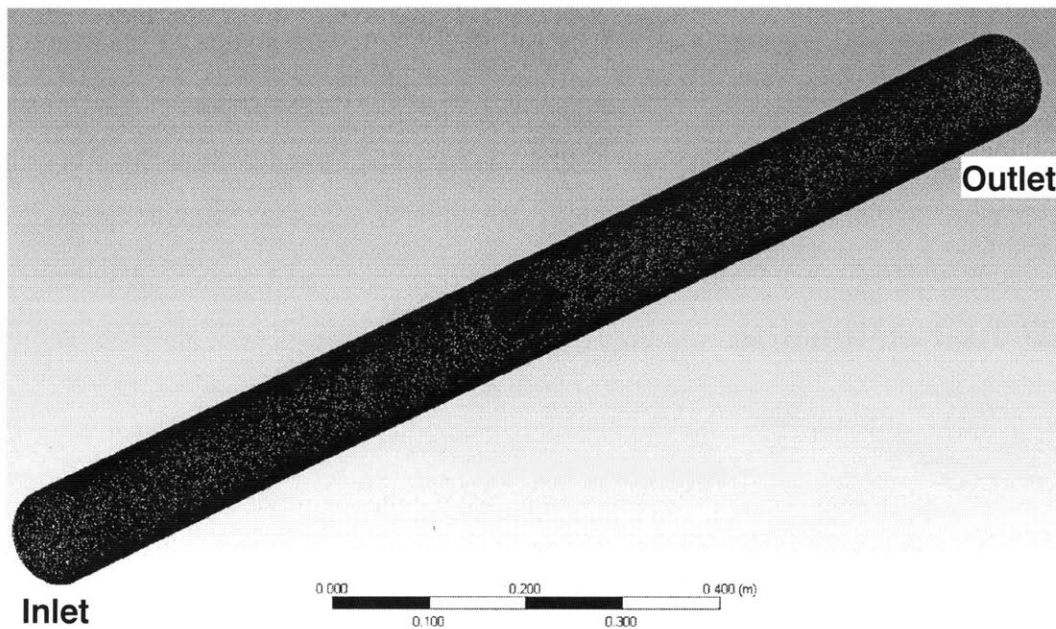


Figure 7-8: Mesh of the fluidic section.

Table 7.1: Mesh characteristics

Number of Elements	1.018.974
Number of Nodes	186.118
Maximum Skewness Factor	0.81
Average Skewness Factor	0.22
Length of Pipe	2m
Diameter of Pipe	100mm

### 7.3.2 CFD Problem Setup

It is considered that the maximum possible relative speed is  $2m/s$  which corresponds to a stationary body and flowing water at  $2m/s$ , as discussed in section 2.5. This will be the case if we force the body to stop ("anchor") inside the pipe with average water velocity of 2 m/s. In normal situations, the body should flow (swim) with a speed which is very close to the water speed and the relative velocity will be negligible in this case. Nevertheless, we will study this "worst case scenario" in depth in the following paragraphs.

The line pressure is set constant to 200 kPa for all simulations. The "pressure" boundary condition was applied to the outlet section of the model. The relative velocity  $V_{rel}$  was applied at the inlet section, while we modeled the pipe walls as moving walls with speed  $V_m$ , as implied by Fig. 7-5. The "no-slip" boundary condition was applied on the body's walls. The standard k-e model was used for the analysis.

### 7.3.3 CFD Results

Some of the results of the CFD simulations are summarized in Table 7.2 for a wide range of relative velocities between the floating body and water in pipe. As expected, the case for  $V_w = V_{rel} = 2 m/s$  while the body is not moving ( $V_m = 0$ ) can be considered as the worst scenario due to high viscous and pressure drag on the body.

The velocity vectors around the body are shown in Fig. 7-9 for a relative velocity  $V_{rel} = 2 m/s$ . The current streamlined design of the body results in no flow separation at the body surface indicating that no induced turbulence from the body itself is

Table 7.2: CFD Results for different values of relative velocity  $V_{rel}$ .

$V_{rel}$ [m/s]	2	1	.1	.01
$C_D$	0.198604	0.085836	.0017186	0.006766
$max V_{rel}^{flow}$	3.0713	1.4001	0.2462	0.4181

expected. As expected, the maximum velocity occurs in the clearance between the body and the pipe material.

The static pressure distribution around the body is shown in Fig.7-10 for a relative velocity  $V_{rel} = 2$  m/s ("worst" case scenario). There is a significant amount of pressure variations in this case. In Fig. 7-11 the same thing is shown but this time for a relative velocity of  $V_{rel} = 0.01$  m/s (body is floating with a speed of  $V_m = 1.99$  m/s which is very close to the water speed  $V_w = 2$  m/s). It is clear that in the later simulation the static pressure is almost constant around the body and this is due to the very small magnitude of the relative velocity  $V_{rel}$ .

Comparing the two figures but mostly focusing on Fig.7-10 , it is clear that attaching the sensor to the body in the clearance between the body and the pipe is not correct due to the high gradient in pressure in this region. The only feasible location is the trailing edge of the body where the flow region is not disturbed ahead due to the existence of the body. The length of this undisturbed flow region ahead the body diminishes as the relative velocity goes to zero. This means that a sensor nose of 3 or 4cm (as shown in Fig. 6-3) will be suitable for detecting clear leak signal in the pipe ahead of the sensor.

Since the placement of the sensor has been now justified, placing well designed legs in the clearance between the body and the pipe is expected not to affect the flow in the trailing side of the body, where the sensor is located.

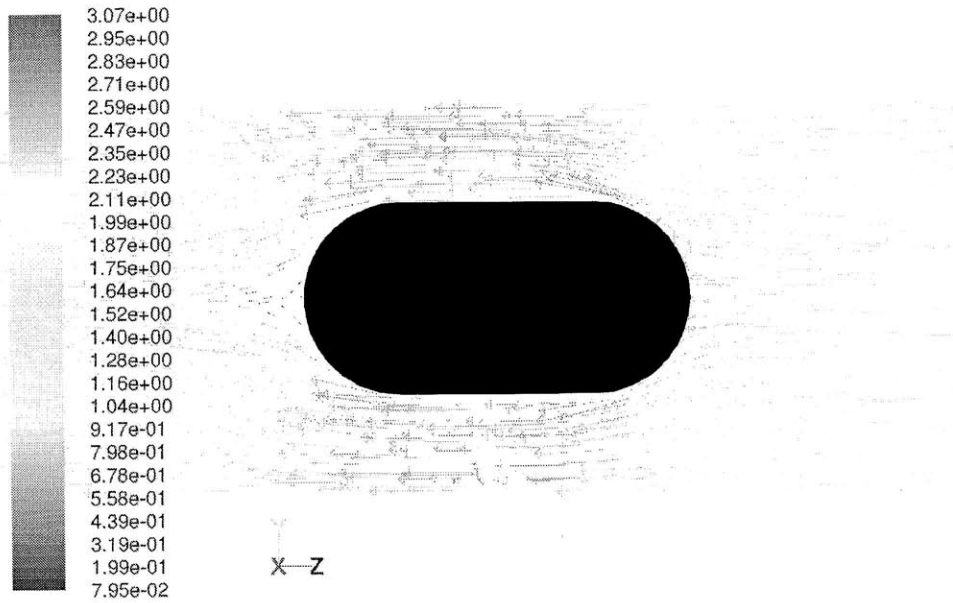


Figure 7-9: CFD results for velocity vectors around the floating body. Simulation was done under  $V_{rel} = 2 \text{ m/s}$  (direction from right to left (see Fig. 7-5) and  $P = 200 \text{ kPa}$ . No flow separation on the trailing edge.

## 7.4 Chapter Summary

In this chapter the mobility module's analysis took place. The main considerations regarding space limitations in design were presented and some equations for length and thickness were derived. Motion inside the pipe as well as DoF of the module were studied. Finally, the main shape of the module was justified by a CFD analysis.



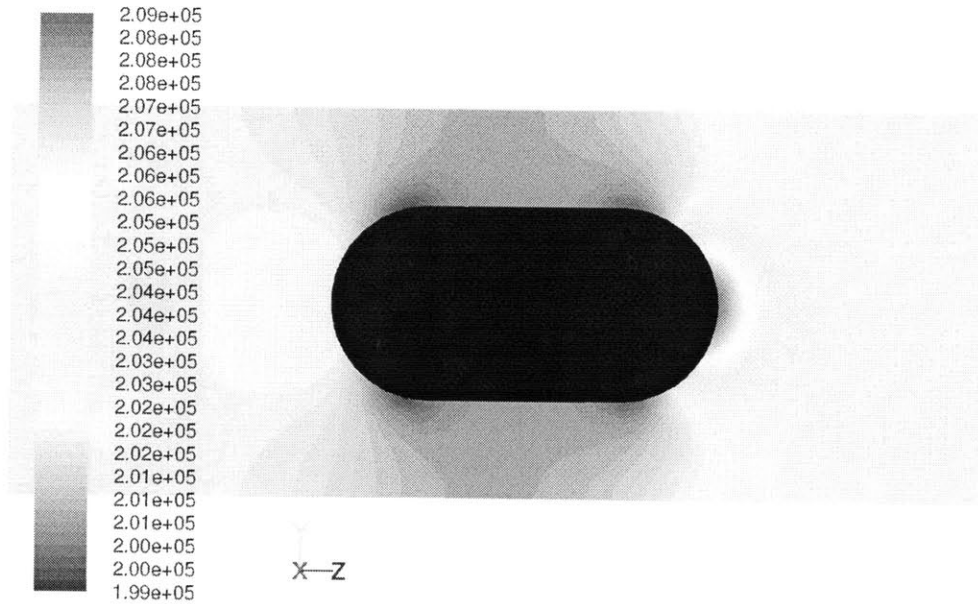


Figure 7-10: CFD results for static pressure distribution around the floating body. Simulation was done under  $V_{rel} = 2 \text{ m/s}$  (direction from right to left (see Fig. 7-5)) and  $P = 200 \text{ kPa}$ . Placing the sensor nose at the trailing edge seems to be the optimal solution.

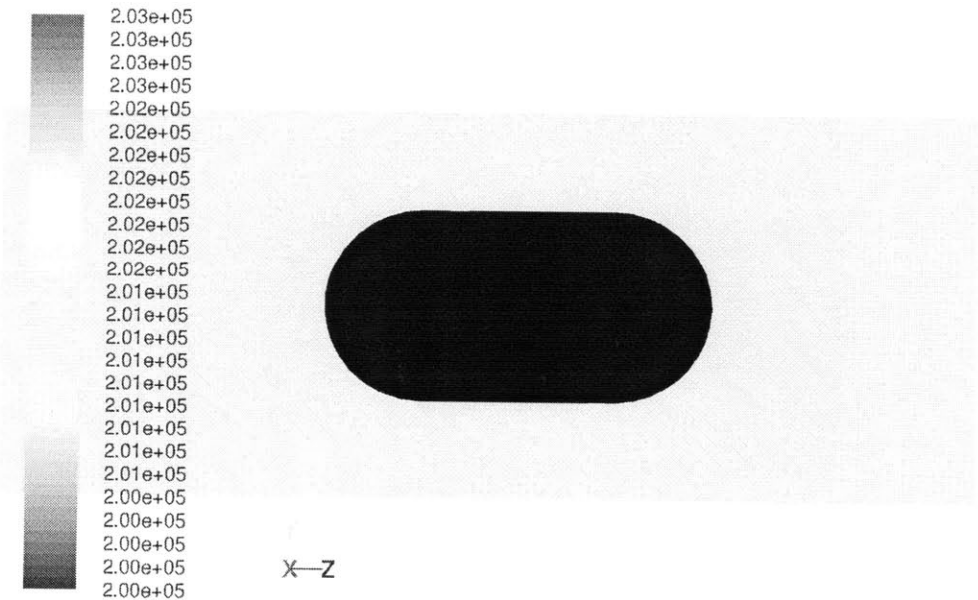


Figure 7-11: CFD results for static pressure distribution around the floating body. Simulation was done under  $V_{rel} = 0.01 \text{ m/s}$  (direction from right to left (see Fig. 7-5)) and  $P = 200 \text{ kPa}$ . Almost no pressure variation around the body.



# Chapter 8

## Mobility Module - Experimental Results

### 8.1 Introduction

This chapter presents the experimental results on the mobility module. For our experiments we used the experimental setup discussed in section 4-1. The pump provided the required high flow rates needed for the mobility module to be able to float inside the loop. The prototype that was used for experimentation is the one discussed in section 6.3.1. The module was tested to evaluate stability and floating inside complicated pipeline configurations, e.g. T-junctions and bends.

### 8.2 Stability

To evaluate stability we used a small pipe section with a size of  $100mm$ . The prototype was placed inside a straight pipe section and stability was tested (Fig. 8-1). As expected, the six contact points from the legs provide the required stability to the module and at the same time they constraint the necessary DoF that were discussed in section 7.2.2. In addition, the module is free to move along the  $z$ -axis of the pipe.

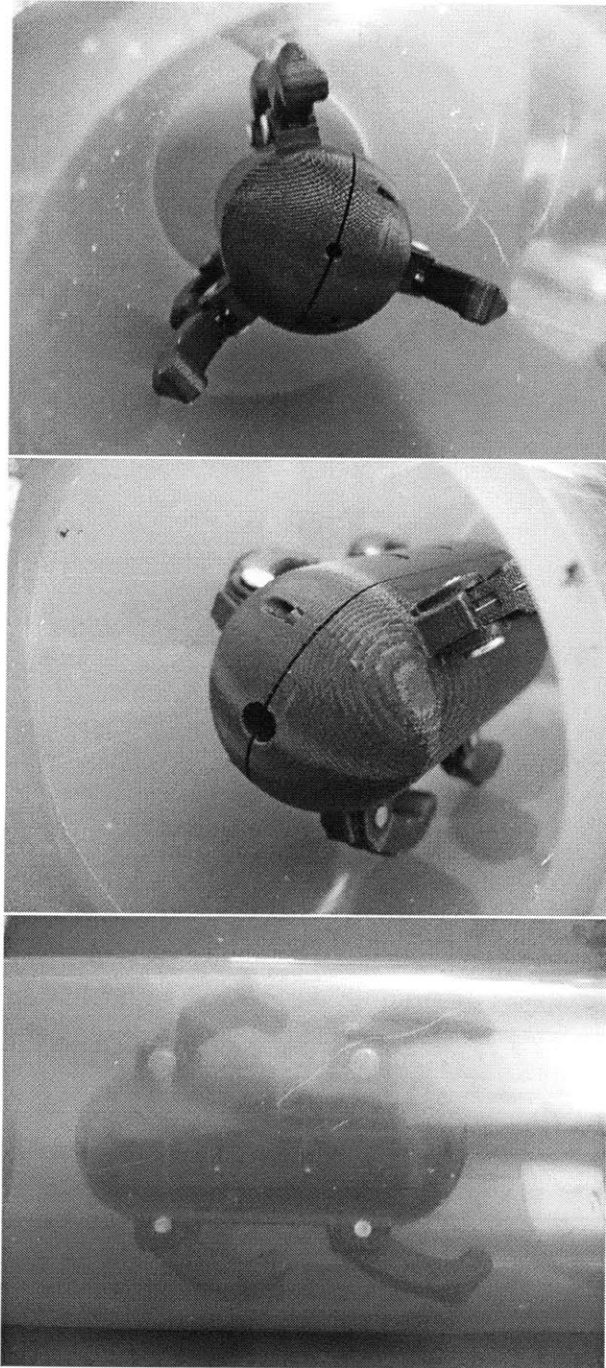


Figure 8-1: The mobility module prototype inside a 100mm pipe section. The module is stable, due to the support provided by the legs.

## 8.3 Floating

To evaluate how the module was able to float inside a “real” water distribution network we used the experimental setup in our lab. This setup mostly consists of 100mm pipe section connected with various connection elements, e.g. T-junctions, unions or bends.

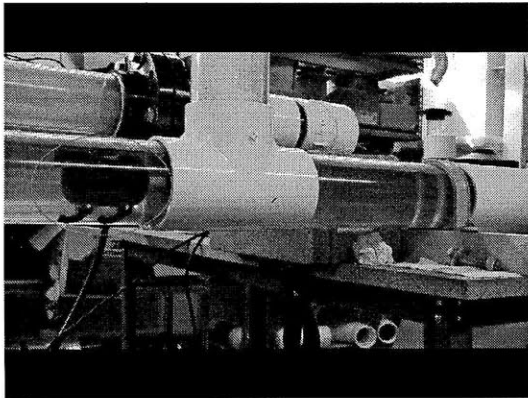
The floating of the mobility module was tested in 3 different sections. Section A consists of 2 straight pipes connected with a T-junction. Section B consists of flanged unions and some sensors mounted flush on the pipe walls, and finally section C consists of four 45° bends, flanged unions and a fully opened ball valve.

As it can be seen in Fig. 8-2 the module is able to float in the straight pipe sections and go through the T-junction in section A without any problems. In section B the module goes through the flanged unions and the straight pipe section with a steady and undisturbed floating motion (see Fig. 8-3). Finally, the module traverses the path in section C again by turning in the bends and overcoming any other obstacles without any problems. At the end of this section the module is being trapped by a net and removed from another T-junction. Fig. 8-4 and Fig. 8-5 show the floating of the module in section C.

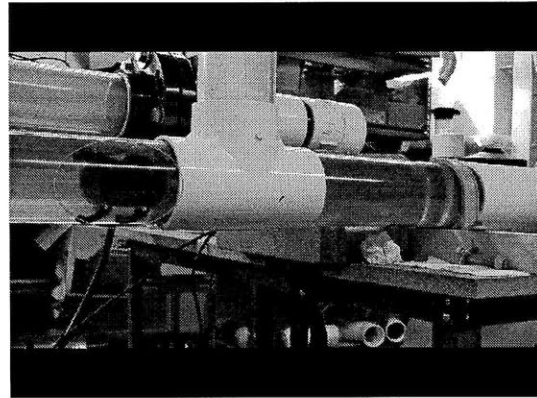
## 8.4 Chapter Summary

In this chapter the mobility module experimentation was discussed. The module was put inside the loop that was built for experimentation and stability and module’s floating was also tested. The module managed to travel along straight pipes, sections with bends, flanged unions as well as T-junctions with success.

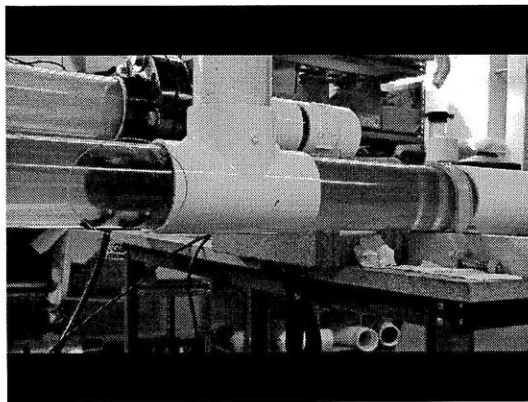
The work on the mobility module is also published in [22].



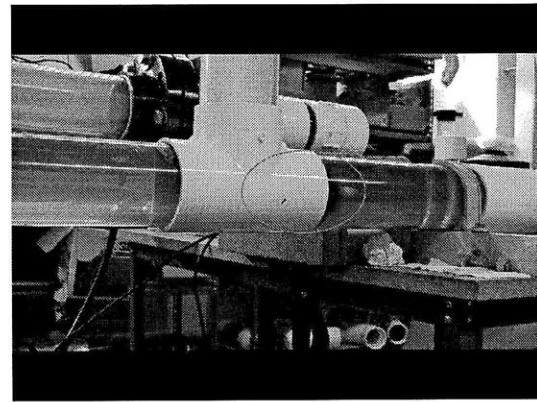
[a]



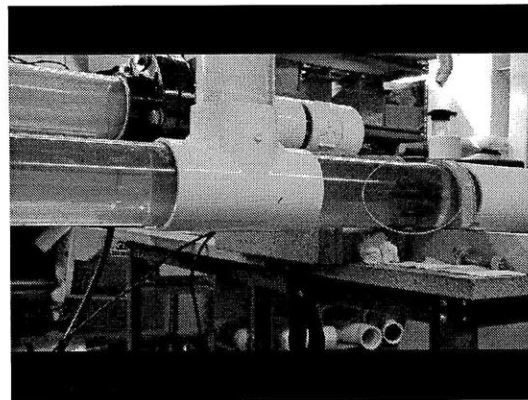
[b]



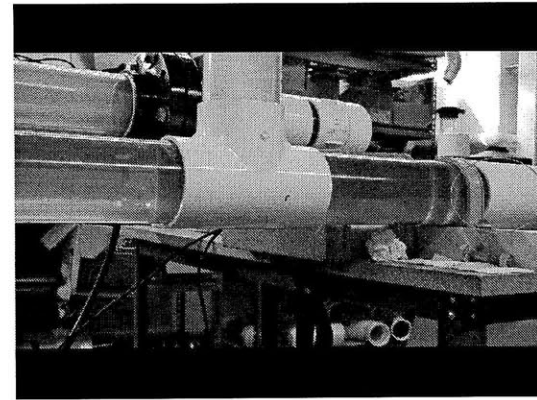
[c]



[d]

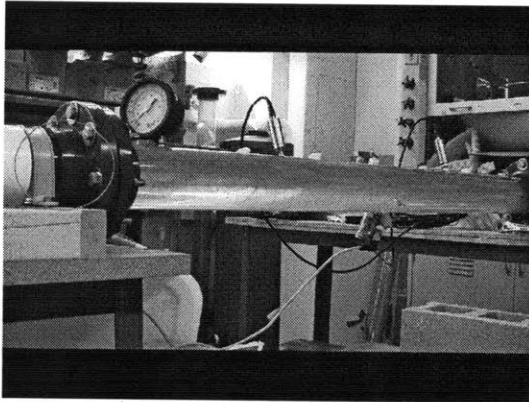


[e]

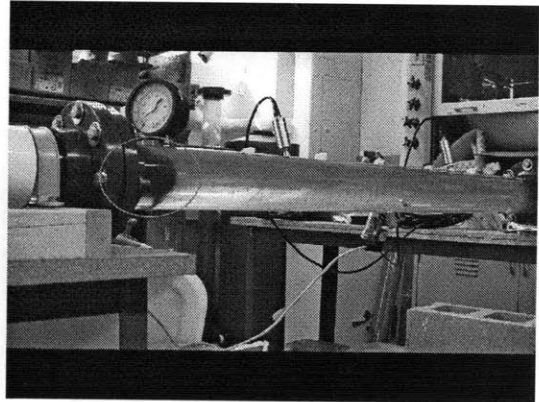


[f]

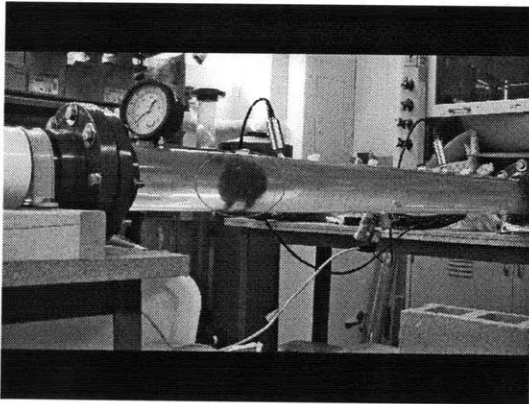
Figure 8-2: The mobility module floating through section A of the experimental setup. The six photos ([a]-[f]) show the motion of the mobility module from left to right.



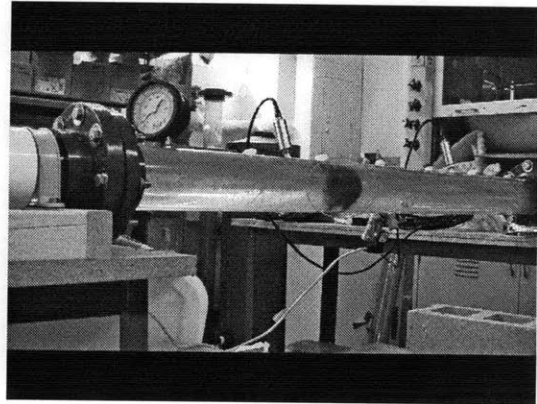
[a]



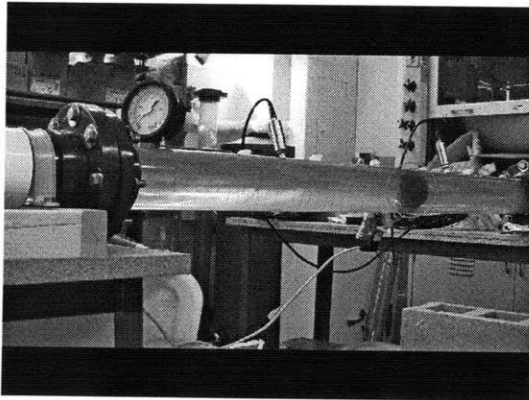
[b]



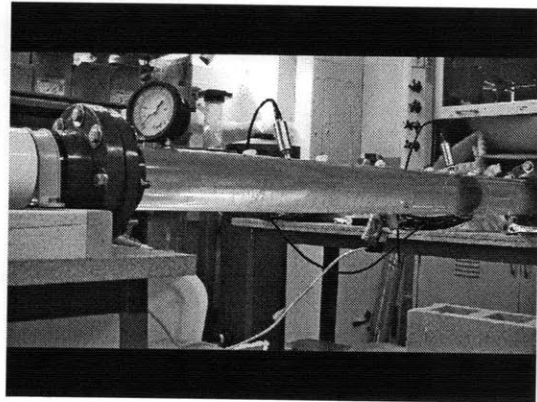
[c]



[d]



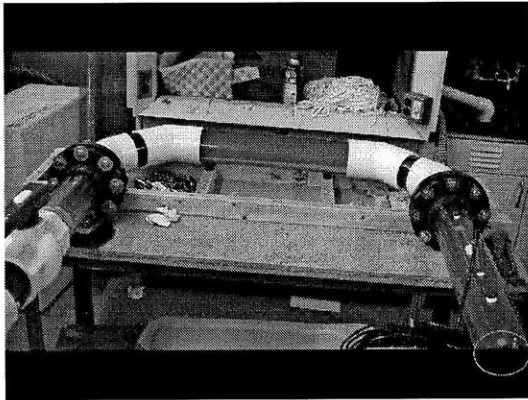
[e]



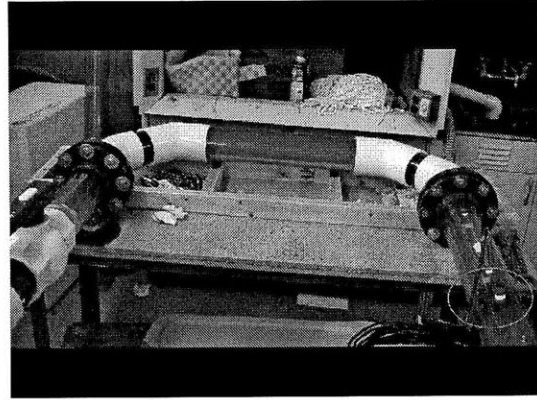
[f]

Figure 8-3: The mobility module floating through section B of the experimental setup. The six photos ([a]-[f]) show the motion of the mobility module from left to right.

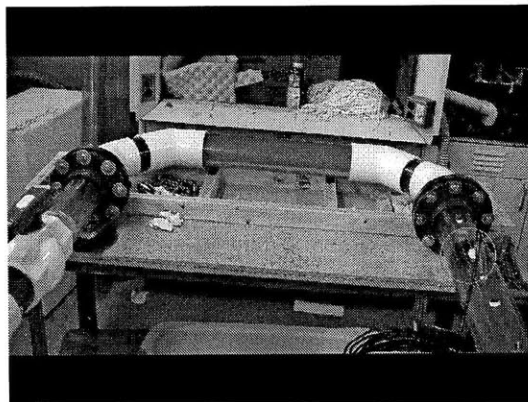




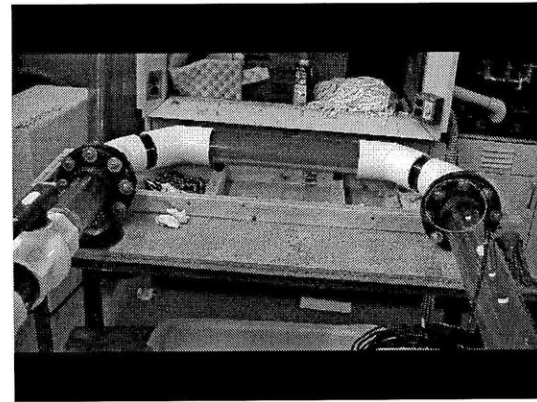
[a]



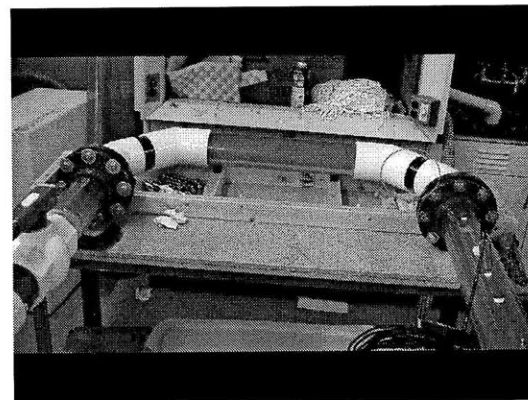
[b]



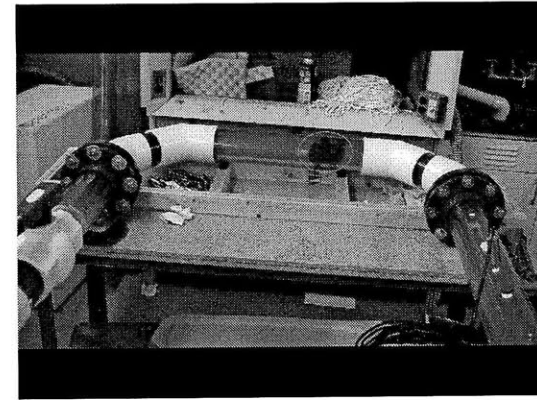
[c]



[d]



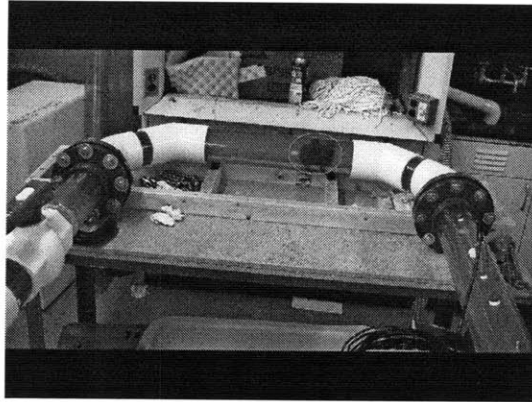
[e]



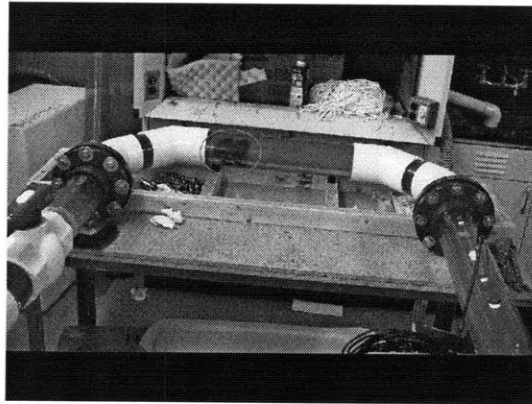
[f]

Figure 8-4: The mobility module floating through the right branch of section C of the experimental setup. The six photos ([a]-[f]) show the motion of the mobility module from right to left.

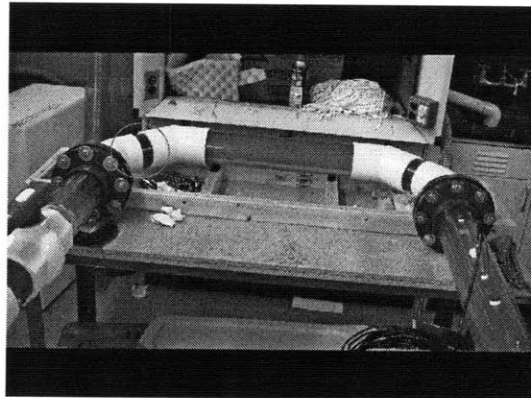




[f]



[g]



[h]

Figure 8-5: The mobility module floating through the left branch of section C of the experimental setup. The three photos ([f]-[h]) show the motion of the mobility module from right to left.



# Chapter 9

## Conclusions and Closing Remarks

### 9.1 Thesis Summary and Contribution

This thesis initially presented the major problem of leak and contamination in water filled pipes. Then, the motivation towards leak detection in modern water distribution networks was given. The thesis objectives along with the thesis structure were also laid out.

Water losses in concurrent water distribution networks were discussed. One of the most significant reasons for water losses is leaking pipes. To address this problem various leak detection techniques have been developed. An overview and evaluation of those techniques along with in-pipe inspection systems were provided. We concluded that most of the systems have limitations and disadvantages. Thus, in this thesis we propose an in-pipe sensor as a promising solution. Such a method has the following advantages and disadvantages:

**In-Pipe Sensor** : The system moves or “swims” inside the pipe to detect leaks internally

- + Capable of detecting **small leaks** in pipelines (of the order of *2lit/min*)
- + Can be inserted and retrieved from a pipeline *without disrupting its flow*
- + Can collect information about leaks *over many miles of pipelines* with a single deployment

- + *Independent of pipe materials*
  - Expensive relative to some existing techniques, e.g. listening devices
  - Communication with moving sensor is not easy
  - Powering the sensor is a challenging task
  - Needs insertion & retrieval openings
  - Self-generated noise can affect the measured signals

This thesis is mostly focused on two different modules, namely the Mobility and the Sensing Modules. The functional requirements for such a system were discussed. First, the sensing module was analyzed. Initially, the sensor specifications and details were given for both the hydrophone and the DPS; the two different sensors that were used for experimentation. Different accessories used with the sensors were also described in detail for completeness. Other instrumentation that was necessary for the sensing module and the experimentation were discussed in detail, including amplifiers, DAQ hardware and software.

For the experiments we designed and built an experimental setup <sup>1</sup> that is described in detail. This setup tries to “mimic” a real water distribution network. For our experiments we simulated leaks in different ways, including circular holes as well as small ball valves. Experimentation objectives for the sensing module were listed.

In order to understand the leak signal and signature, various experiments were carried out. Initially experiments with different sensors under the same conditions were conducted. Eventually, we concluded that the two sensors can capture the same signals and detect leaks in the same way. To study the effect of leak flow rate on captured signals, various experiments took place. The effect of media surrounding pipe (air, water and soil) was also investigated by conducting different experiments. The effect of pipe flow on captured leak signals as well as the sensor position influence on the signals were studied and discussed. We proposed a “power-metric” of the

---

<sup>1</sup>The author would like to thank Sumeet Kumar, Dr. Stephen Ho and Dr. Ajay Deshpande for their significant contribution in this task.

captured signal to calibrate the leak detection system by using a reference signal that corresponds to the no-leak scenario.

The mobility module was discussed next. First, the design of the mobility module was presented. In addition its functional requirements were listed. To present the evolution of the design ideas as well as the flaws of the previous designs some earlier prototypes were also discussed for completeness.

The analysis and design considerations of the mobility module were discussed in the later sections. Sizing limitations, degrees of freedom inside the pipe and motion analysis were essential studies that helped in the design process. A comprehensive CFD analysis was also done to study the flow around the mobility module and to evaluate the design of the main body of the system. To evaluate the design of our latest prototype in a “real” water distribution network we also conducted simple experiments in our test loop. Stability of the body as well as floating capabilities were evaluated and experiments showed that the final prototype meets all functional requirements set on the mobility module.

## 9.2 Recommendations for Future Work

Our next step is to test the mobility module prototype in our specially designed test loop in order to evaluate the CFD results with real data regarding the flow around the body as well as the interference of the body’s induced flow to the leak signal. *Our future endeavors include the implementation of the whole miniaturized system within a single body, being able to incorporate all modules in it, namely mobility, sensing, data processing and communication.*

Regarding the sensing module, our future goals include further experimentation with different leak shapes, line pressures and pipe materials. Further, experiments are being planned with “ambient” pipe flow in the pipe by utilizing a recently purchased 10HP pump. *Our ultimate goal is to design and build a smart, autonomous, pipe-traveling system for precise leak detection in a city level water distribution network.*



# Appendix A

## LabVIEW Code

This appendix presents the LabVIEW code developed for signal acquisition. The two different “vi’s” (Virtual Instruments) are shown in terms of both user interface and block diagrams. Detailed information is provided in the captions of the different figures.

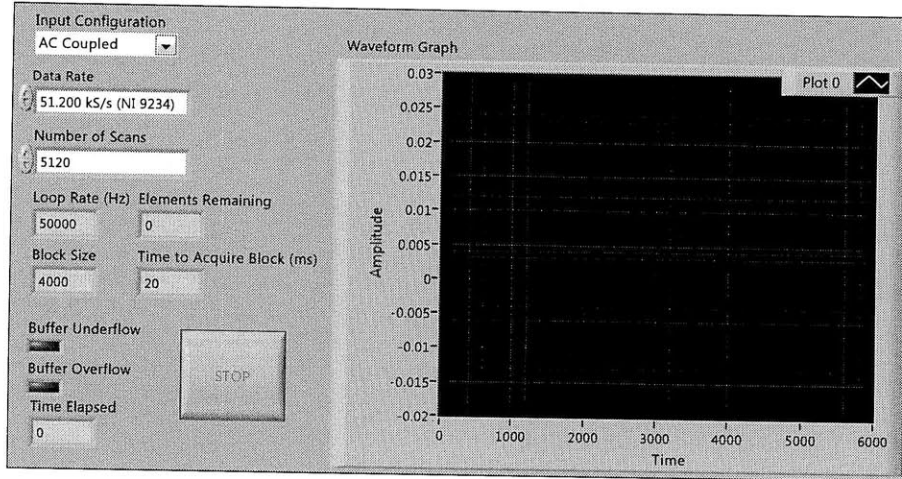


Figure A-1: The front panel of the LabVIEW vi on the host PC. User can select “AC/DC/IEPE” in the “Input Configuration” box. One can also specify the sampling rate along with the number of scans per survey. A “Stop” button is available in order to be able to stop the procedure at any time. Various indicators including a “Waveform Graph” are also available for the user.

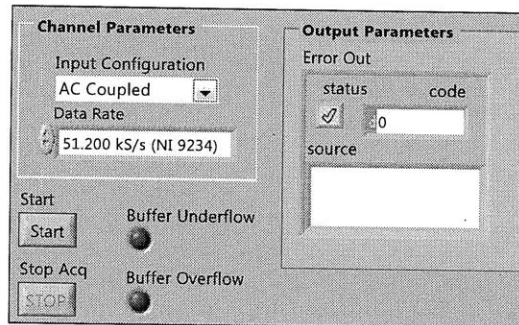


Figure A-2: The front panel of the LabVIEW vi on the FPGA. User can select “AC/DC/IEPE” in the “Input Configuration” box. One can also specify the sampling rate. A “Start” and “Stop” button are available in this vi. Indicators including “Buffer Underflow” and “Buffer Overflow” are also shown in this interface.



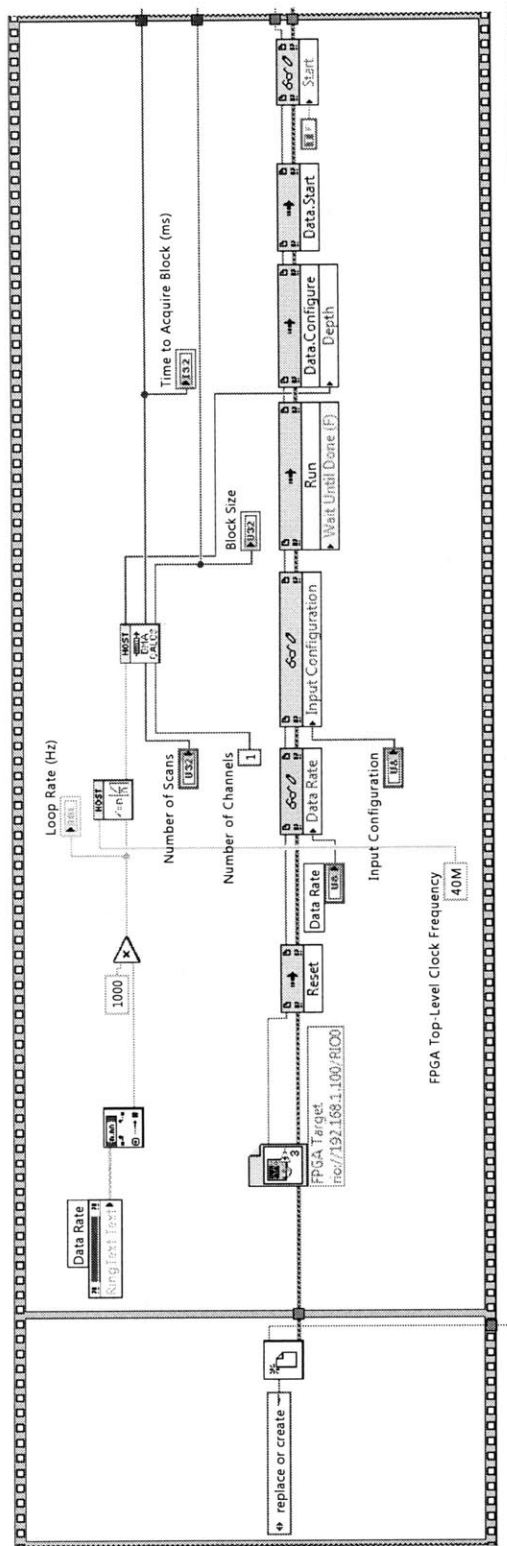


Figure A-3: The first part of the block diagram of the LabVIEW vi on the host PC. Notice that this part is connected to the second part shown in Fig. A-4.

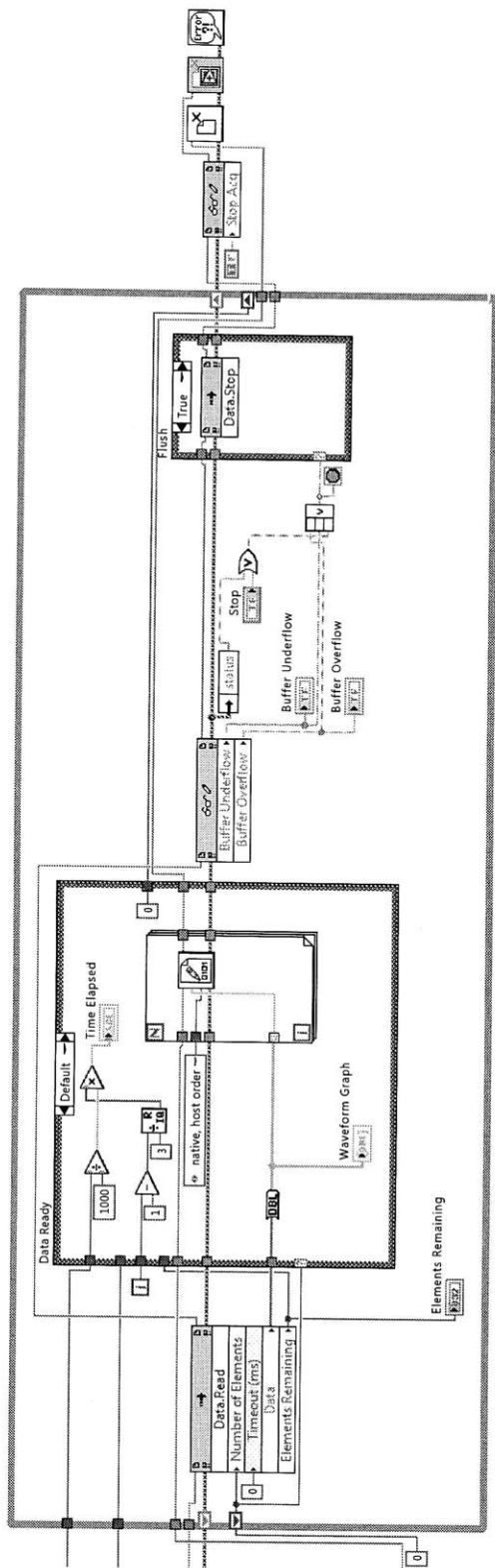


Figure A-4: The second part of the block diagram of the LabVIEW vi on the host PC. Notice that this part is connected to the first part shown in Fig. A-3.

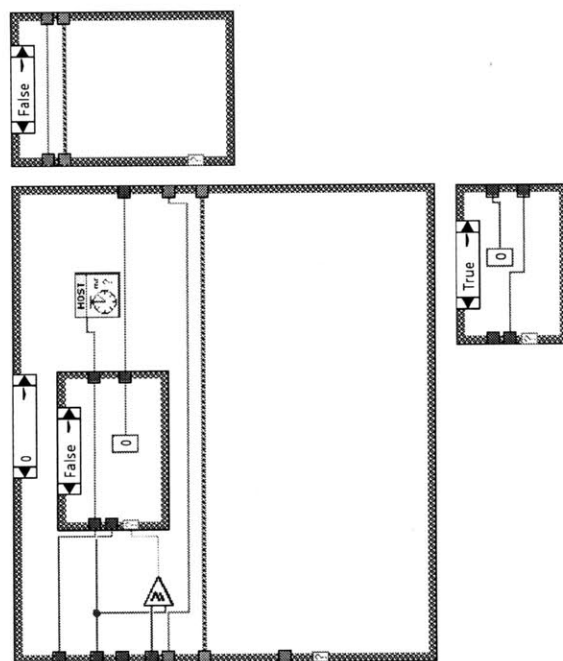


Figure A-5: The third part of the block diagram of the LabVIEW vi on the host PC. Notice that this part is not connected to neither of the first or second parts shown in Fig. A-3 and Fig. A-4.

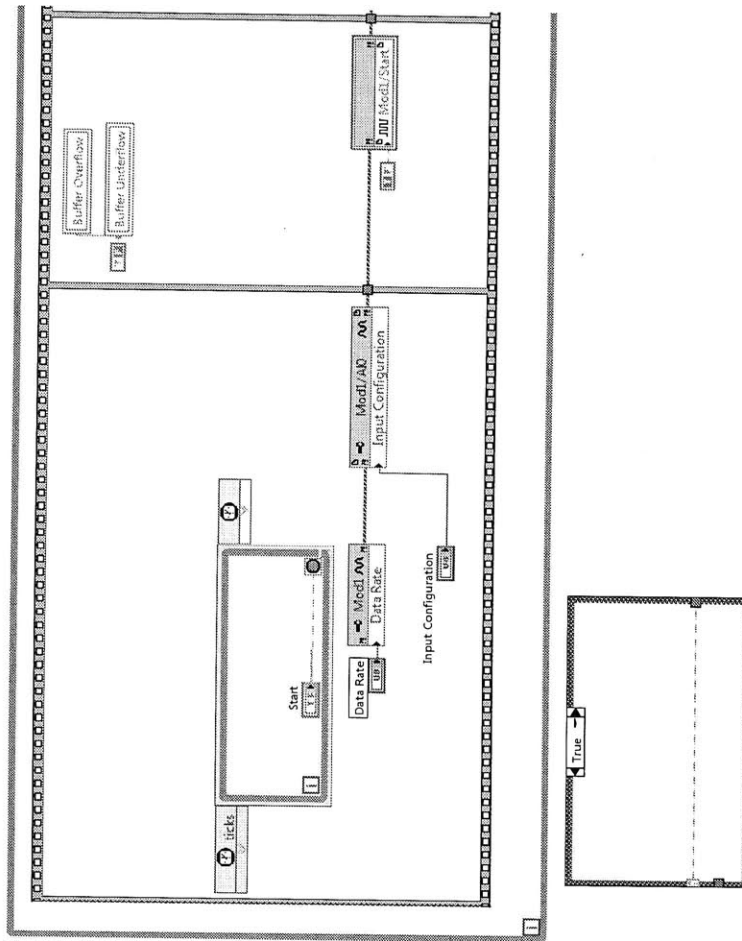


Figure A-6: The first part of the block diagram of the LabVIEW vi on the FPGA. Notice that this part is connected to the second part shown in Fig. A-7.

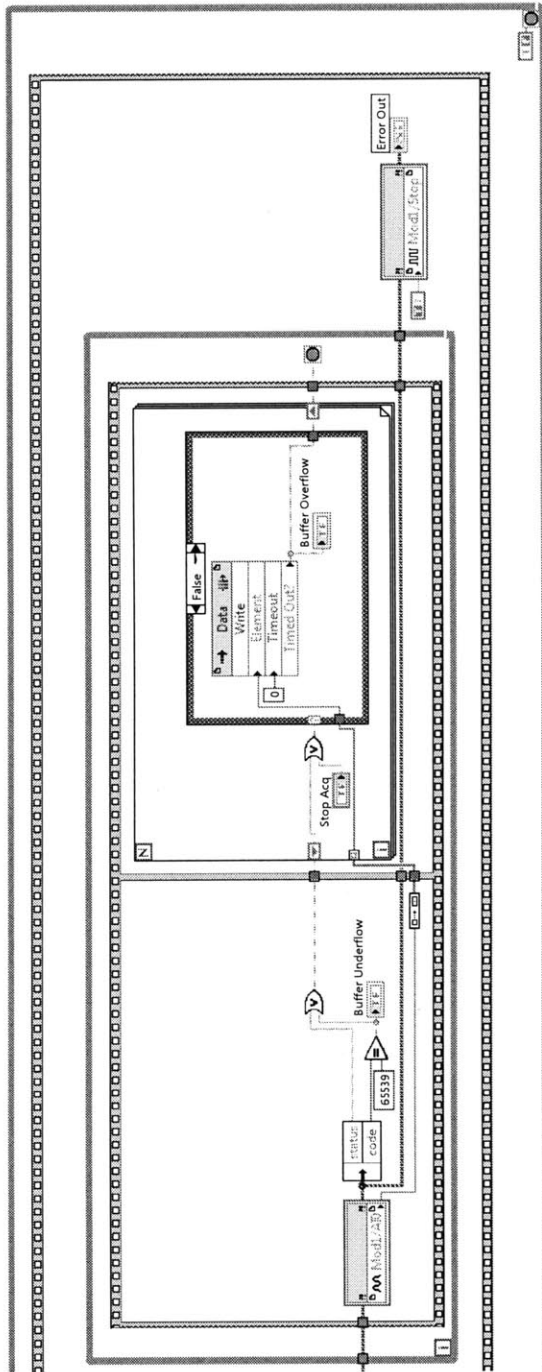


Figure A-7: The second part of the block diagram of the LabVIEW vi on the FPGA. Notice that this part is connected to the first part shown in Fig. A-6.



# Appendix B

## MATLAB Code - Signal Postprocessing

This appendix presents the MATLAB code developed for signal postprocessing. The comments in the code provide all the required information for the user.

```

1 %%%%%%%%%%%%%%%%%%%%%%%%%%%%%%%%%%%%%%%%%%%%%%%%%%%%%%%%%%%%%%%%%%%%%%%%%
2 %%%%%%%%%%%%%%%%%%%%%%%%%%%%%%%%%%%%%%%%%%%%%%%%%%%%%%%%%%%%%%%%%%%%%%%%%
3 %%% This m.file is used for creating the FFT of a series of signals %%%
4 %%% (*.bin files) and calculate corresponding power %%%
5 %%%%%%%%%%%%%%%%%%%%%%%%%%%%%%%%%%%%%%%%%%%%%%%%%%%%%%%%%%%%%%%%%%%%%%%%%
6 %%%%%%%%%%%%%%%%%%%%%%%%%%%%%%%%%%%%%%%%%%%%%%%%%%%%%%%%%%%%%%%%%%%%%%%%%
7
8 clc; clear all; close all;
9
10 %% User specified values %%%%%%%%%%%%%%%%%%%%%%%%%%%%%%%%%%%%%%%%%%%%%%%%%%%%%%%%%%%%%%%%%%%%%%%%%
11 fs = 51.2e3; % %User specifies the sampling frequency
12
13 name = ['hydrophone_at_leak_10lpm_flow_10lpm_leak']; %User specifies the
14                                     ...name of the *.bin file
15
16 filteron = 1; %User specifies if he wants data to be filtered or not(1=yes)
17 filtername = ['FIR_band_20_2000hz']; %User specifies the name of the filter
18                                     ...to be loaded
19
20 timeplot = 1; %User specifies if he wants plot of the time series (1=yes)
21 psd = 0; %User specifies if he wants plot of the psd of signal (1=yes)
22
23 f1 = 0; %User specifies the minimum frequency of interest [Hz]
24 f2 = 2000; %User specifies the maximum frequency of interest [Hz]
25
26 t_ymin = -0.1; %User specifies the min y-amplitude for plot of time signal
27 t_ymax = 0.1; %User specifies the max y-amplitude for plot of time signal
28 t_xmin = 0; %User specifies the min x-amplitude for plot of time signal
29 t_xmax = 1; %User specifies the min x-amplitude for plot of time signal
30 f_ymin = 0; %User specifies the min y-amplitude for plot of FFT
31 f_ymax = 0.002; %User specifies the max y-amplitude for plot of FFT
32
33 smth = 1; %User specifies the size of the moothing window
34                                     ...(1 means no smoothing)
35
36 %% Read data %%%%%%%%%%%%%%%%%%%%%%%%%%%%%%%%%%%%%%%%%%%%%%%%%%%%%%%%%%%%%%%%%%%%%%%%%

```



```

37 fid = fopen([name, '.bin'], 'r'); %Open *.bin file
38 y = fread(fid, 'double'); %Read y-values
39
40 fcl = fclose(fid); %Close the *.bin file
41
42     if ~fcl
43         disp('File Close Successful');
44         disp(['# of data points: ', num2str(length(y))]);
45     else
46         disp('File Close Fail');
47         beep;
48     end
49
50 %%%%%%%%%%%%%%%%%%%%%%%%%%%%%%%%%%%%%%%%%%%%%%%%%%%%%%%%%%%%%%%%%%%%%%%%%
51 %% Post-process time-signal %%%%%%%%%%%%%%%%%%%%%%%%%%%%%%%%%%%%%%%%%%%%%%%%%%%%%%%%%%%%%%%%%%%%%%%%%
52 y = detrend (y, 'linear');
53
54 if (filteron)
55     load(filtername)
56     y = filter(Num,1,y);
57     y= y((length(Num)+1):end);
58 end
59
60 %%%%%%%%%%%%%%%%%%%%%%%%%%%%%%%%%%%%%%%%%%%%%%%%%%%%%%%%%%%%%%%%%%%%%%%%%
61 %% Generate time vector %%%%%%%%%%%%%%%%%%%%%%%%%%%%%%%%%%%%%%%%%%%%%%%%%%%%%%%%%%%%%%%%%%%%%%%%%
62     dt = 1/fs;
63     l = length(y);
64     t = (0:l-1)/fs;
65     disp(['Time taken to measure: ', num2str(t(end))]);
66
67 %%%%%%%%%%%%%%%%%%%%%%%%%%%%%%%%%%%%%%%%%%%%%%%%%%%%%%%%%%%%%%%%%%%%%%%%%
68 %% Calculate Time-Signal Mean Power
69 pow_y = (sum(y.^2)) / t(end);
70 disp(['Time Signal Power: ', num2str(pow_y)]);
71
72 %%%%%%%%%%%%%%%%%%%%%%%%%%%%%%%%%%%%%%%%%%%%%%%%%%%%%%%%%%%%%%%%%%%%%%%%%

```

```

73 %% FFT of the signal %%%%%%%%%%%%%%%%%%%%%%%%%%%%%%%%%%%%%%%%%%%%%%%%%%%%%%%%%%%%%%%%%%%%%%%%%
74
75     nFFT = 2^(nextpow2(l)-1); % Next power of 2 from length of y
76     yFFT = fft(y(1:nFFT), nFFT)/nFFT;
77     f = fs/2*linspace(0, 1, nFFT/2+1);
78     ym = 2*abs(yFFT(1:nFFT/2+1));
79
80     % Calculate maximum peak and frequency
81     [ymax, imax] = max(ym);
82     f_maxPeak = f(imax);
83     disp(['Max Peak Freq: ', num2str(f_maxPeak)]);
84     disp(['Max Peak Ampl: ', num2str(ymax)]);
85
86     name = regexp(name, '_', ' ');
87
88 %%%%%%%%%%%%%%%%%%%%%%%%%%%%%%%%%%%%%%%%%%%%%%%%%%%%%%%%%%%%%%%%%%%%%%%%%
89 %% Calculate the Integral of the Frequency Spectrum from f1 to f2
90 df = f(2)-f(1);
91 elem1 = ceil(f1 / df) + 1;
92 elem2 = floor(f2 / df) - 1;
93
94 Spectral_Energy = trapz(f(elem1:elem2),ym(elem1:elem2));
95 disp(['Integral of Frequency Spectrum: ', num2str(Spectral_Energy)]);
96
97 %%%%%%%%%%%%%%%%%%%%%%%%%%%%%%%%%%%%%%%%%%%%%%%%%%%%%%%%%%%%%%%%%%%%%%%%%
98 %% Calculate Power Spectral Density and plot PSD
99 PSD = (abs(ym).^2)/(t(end)); %Calculate PSD
100
101     if( psd )
102         figure;
103         plot(f,PSD)
104         grid on;
105         ylim('auto');
106         xlim([f1 f2])
107         title({name});
108         xlabel('Frequency [Hz]');

```

```

109         ylabel('Energy [...]');
110     end
111
112     Pxx = trapz(f,PSD); %1st order integration of PSD
113     disp(['Power Spectral Density: ', num2str(Pxx)]);
114
115     %%%%%%%%%%%%%%%%%%%%%%%%%%%%%%%%%%%%%%%%%%%%%%%%%%%%%%%%%%%%%%%%%%%%%%%%%
116     %% Plot time series
117     figure;
118     if( timeplot )
119         subplot(211);
120         plot(t, y, 'b');
121         grid on;
122         ylim([t_ymmin t_ymax]);
123         xlim([t_xmin t_xmax]);
124         title({name});
125         xlabel('Time [sec]');
126         ylabel('Amplitude [V]');
127     end
128
129     %%%%%%%%%%%%%%%%%%%%%%%%%%%%%%%%%%%%%%%%%%%%%%%%%%%%%%%%%%%%%%%%%%%%%%%%%
130     %% Plot single-sided amplitude spectrum
131     if (timeplot)
132         subplot(212);
133     end
134
135     if (1)
136         ymsmth = smooth(ym, smth, 'lowess'); %Specify Size of Time
137                                             ..Window for Smoothing
138     end
139     plot(f, (abs(ymsmth)), 'r', 'linewidth', 1);
140
141     if (0)
142         hold on
143         plot(f, 20*log10(abs(ym)), 'r--');
144     hold off

```

```
145     end
146     grid on;
147
148     if (timeplot)
149         title('Single-Sided Amplitude Spectrum of y(t)');
150     else
151         title({name});
152     end
153
154     ylabel('|Y(j\omega)|')
155     xlabel('Frequency [Hz]');
156     xlim([f1 f2]);
157     ylim([f_ymin f_ymax]);
```

# Appendix C

## MATLAB Code - Filters

This appendix presents the MATLAB code developed for the creation of the FIR digital filters that were used during signal postprocessing. The comments in the code provide all the required information for the user.

```

1 function Hd = filter
2 %FILTER Returns a discrete-time filter object.
3
4 %
5 % M-File generated by MATLAB(R) 7.8 and the Signal Processing Toolbox 6.11.
6 %
7 % Generated on: 30-Jul-2010 17:12:37
8 %
9
10 % FIR Window Bandpass filter designed using the FIR1 function.
11
12 % All frequency values are in Hz.
13 Fs = 51200; % Sampling Frequency
14
15 Fstop1 = 2; % First Stopband Frequency
16 Fpass1 = 10; % First Passband Frequency
17 Fpass2 = 1800; % Second Passband Frequency
18 Fstop2 = 2000; % Second Stopband Frequency
19 Dstop1 = 0.001; % First Stopband Attenuation
20 Dpass = 0.057501127785; % Passband Ripple
21 Dstop2 = 0.0001; % Second Stopband Attenuation
22 flag = 'scale'; % Sampling Flag
23
24 % Calculate the order from the parameters using KAISERORD.
25 [N,Wn,BETA,TYPE] = kaiserord([Fstop1 Fpass1 Fpass2 Fstop2]/(Fs/2), [0 ...
26 1 0], [Dstop1 Dpass Dstop2]);
27
28 % Calculate the coefficients using the FIR1 function.
29 b = fir1(N, Wn, TYPE, kaiser(N+1, BETA), flag);
30 Hd = dfilt.dffir(b);
31
32 % [EOF]

```

# Bibliography

- [1] A. L. Vickers, “The future of water conservation: Challenges ahead,” *Water Resources Update, Universities Council on Water Resources*, vol. 114, pp. 49–51, 1999.
  
- [2] National Water Research Institute - Meteorological Service of Canada, “Threats to water availability in Canada,” *Environment Canada*, 2004, NWRI Scientific Assessment Report Series No. 3 and ACSD Science Assessment Series No. 1.
  
- [3] Al-Dhowalia, K.H., N.Kh. Shamma, A.A. Quraishi, and F.F. Al-Muttair, “Assessment of leakage in the Riyadh water distribution network,” *First Progress Report, King Abdulaziz City for Science and Technology*, 1989.
  
- [4] L. Mays, *Water Distribution Systems Handbook*. McGraw-Hill, 2000.
  
- [5] O. Hunaidi , W. Chu , A. Wang and W. Guan, “Leak detection method for plastic water distribution pipes,” *Advancing the Science of Water, Fort Lauderdale Technology Transfer Conference, AWWA Research Foundation*, pp. 249–270, 1999.
  
- [6] Georgia Environmental Protection Division, Watershed Protection Branch, *Water Leak Detection and Repair Program*. EPD Guidance Document, 2007.
  
- [7] O. Hunaidi, W. Chu, A. Wang and W. Guan, “Detecting leaks in plastic pipes,” *Journal - American Water Works Association*, vol. 92, no. 2, pp. 82–94, 2000.

- [8] O. Hunaidi, A. Wang, M. Bracken, T. Gambino and C. Fricke, “Acoustic methods for locating leaks in municipal water pipe networks,” *International Conference on Water Demand Management*, pp. 1–14, 2004.
- [9] H. V. Fuchs and R. Riehle, “Ten years of experience with leak detection by acoustic signal analysis,” *Applied Acoustics*, vol. 33, pp. 1–19, 1991.
- [10] D. Covas and H. Ramos, “Hydraulic transients used for leakage detection in water distribution systems,” *4th International Conference on Water Pipeline Systems, BHR Group Water Pipeline Systems*, 2001.
- [11] J. P. Vitkovsky, M. F. Lambert, A. R. Simpson and J. A. Liggett, “Experimental observation and analysis of inverse transients for pipeline leak detection,” *Journal of Water Resource Planning and Management*, vol. 133, no. 6, pp. 519–530, 2007.
- [12] B. Karney, D. Khani, M. R. Halfawy and O. Hunaidi, “A simulation study on using inverse transient analysis for leak detection in water distribution networks,” Computer Science Division, University of California,” Technical Report, 2009, NRCC-50452.
- [13] O. Hunaidi and P. Giamou, “Ground-penetrating radar for detection of leaks in buried plastic water distribution pipes,” *Seventh International Conference on Ground Penetrating Radar (GPR’98)*, pp. 783–786, 1998.
- [14] H. Schempf, E. Mutschler, V. Goltsberg, G. Skoptsov, A. Gavaert and G. Vradis, “Explorer: Untethered real-time gas main assessment robot system,” *Proc. of Int. Workshop on Advances in Service Robotics (ASER)*, 2003.
- [15] Y-S. Kwon, E-J. Jung, H. Lim and B-J. Yi, “Design of a reconfigurable indoors pipeline inspection robot,” *International Conference on Control, Automation and Systems*, pp. 3998–4004, 2007.
- [16] H-R. Choi and S-G Roh, “Differential-drive in-pipe robot for moving inside urban gas pipelines,” *Transactions on Robotics*, vol. 21, no. 1, 2005.



- [17] D. W. Kurtz, "Developments in a free-swimming acoustic leak detection system for water transmission pipelines," *ASCE Conf. Proc.*, vol. 25, no. 211, 2006.
- [18] A. Bond, B. Mergelas and C. Jones, "Pinpointing leaks in water transmission mains," *ASCE Conf. Proc.*, vol. 91, no. 146, 2004.
- [19] O. Hunaidi and W. Chu, "Acoustical characteristics of leak signals in plastic water distribution pipes," *Applied Acoustics*, vol. 58, pp. 235–254, 1999.
- [20] D. Chatzigeorgiou, S. Kumar, A. Khalifa, A. Deshpande, K. Youcef-Toumi, S. Sarma and R. Ben-Mansour, "In-pipe acoustic characterization of leak signals for leak detection in water distribution networks," *AWWA Annual Conference and Exposition*, 2010.
- [21] A. Khalifa, D. Chatzigeorgiou, K. Youcef-Toumi and R. Ben-Mansour, "Quantifying acoustic and pressure sensing for in-pipe leak detection," *ASME 2010 International Mechanical Engineering Congress and Exposition*, 2010.
- [22] D. Chatzigeorgiou, K. Youcef-Toumi and R. Ben-Mansour, "Design and analysis of a system for in-pipe water leak detection," *In preparation*, 2010.